

Aus dem Nationalen Zentrum für Strahlenforschung in der Onkologie - OncoRay  
Arbeitsgruppe: Molekulare und Zelluläre Strahlenbiologie  
Gruppenleiter: Herr Prof. Dr. med. habil. Nils Cordes

---

The intermediate filament synemin promotes non-homologous end joining in an ATM-dependent manner

## Dissertationsschrift

zur Erlangung des akademischen Grades  
Doktor der Biomedizin  
Doctor rerum medicinalium (Dr. rer. medic.)

Vorgelegt

der Medizinischen Fakultät Carl Gustav Carus  
der Technischen Universität Dresden

**Sara Sofia Deville, M.Sc.**

born in Santa Fe, Argentina

Dresden 2019

**1. Gutachter: Prof. Dr. med. habil. Nils Cordes**

**2. Gutachter: Prof. Dr. rer. nat. Georg Breier**

**Tag der mündlichen Prüfung: 27<sup>th</sup> January 2020**

**Vorsitzender der Promotionskommission:**

**(Prof. Dr. med. Axel Roers)**

## Contents

Contents.....	I
Abbreviations .....	V
1 Introduction.....	1
2 Background .....	3
2.1 Extracellular matrix, adhesion mediated radiation resistance and 3D cell culture model .....	3
2.2 Integrins and focal adhesion proteins (FAPs).....	5
2.3 Intermediate filaments (IFs).....	6
2.3.1 Cytoskeleton components .....	6
2.3.2 Structure and assembly.....	7
2.3.3 Family classification .....	7
2.4 Synemin, IV intermediate filament.....	9
2.4.1 Structure .....	9
2.4.2 Physiological role of synemin .....	10
2.4.3 Synemin in cancer.....	11
2.5 Head and Neck squamous cell carcinomas (HNSCC) .....	12
2.5.1 Common therapeutical approaches.....	13
2.5.2 Risk factors .....	13
2.6 Effects of ionizing radiation on cellular level .....	14
2.7 DNA damage response .....	16
2.8 DNA double strand break repair mechanisms .....	17
2.8.1 Non-homologous end joining (NHEJ) .....	19
2.8.2 Homologous recombination (HR) .....	19
2.8.3 Alternative end-joining (Alt-EJ).....	20

3	Hypothesis and Aims .....	21
4	Materials and Methods .....	23
4.1	Materials .....	23
4.1.1	Devices .....	23
4.1.2	Further materials .....	25
4.1.3	esiRNA and siRNA .....	26
4.1.4	Inhibitors and chemotherapeutic agents .....	26
4.1.5	Plasmids .....	26
4.1.6	Primers.....	28
4.1.7	Polymerases, Restriction enzymes and ligases.....	28
4.1.8	Bacterial culture .....	28
4.1.9	Protein and DNA ladders.....	29
4.1.10	Method kits.....	29
4.1.11	Primary antibodies .....	30
4.1.12	Secondary antibodies .....	31
4.1.13	Solutions for cell biological applications.....	32
4.1.14	Solutions for protein-biochemical and molecular-biological applications .....	33
4.1.15	Solutions for immunofluorescence.....	35
4.1.16	Further solutions and chemicals .....	36
4.1.17	PC programs.....	36
4.2	Methods .....	37
4.2.1	Cell culture .....	37
4.2.2	Cell freezing and thawing .....	37
4.2.3	siRNA knockdown .....	38
4.2.4	Inhibitor treatment and chemotherapy .....	38
4.2.5	Radiation exposure .....	39
4.2.6	3D Colony formation assay .....	39
4.2.7	3D high-throughput RNAi-based screening .....	40
4.2.8	Screening development.....	40
4.2.9	3D high-throughput screen using esiRNA (3D HTP-RNAi-S).....	42

4.2.10	Immunofluorescence staining.....	42
4.2.11	Foci assay.....	43
4.2.12	Total protein extracts, SDS-PAGE and Western Blotting.....	44
4.2.13	DRGFP and EJ5GFP-based chromosomal break reporter assay.....	46
4.2.14	Cell Cycle analysis.....	48
4.2.15	Kinome analysis.....	48
4.2.16	Immunoprecipitation.....	49
4.2.17	Chromatin fractionation.....	49
4.2.18	Expression constructs, site-directed mutagenesis and transfection of plasmids . .....	50
4.2.19	2D-Proximity Ligation Assay.....	53
4.2.20	Statistics.....	53
5	Results.....	54
5.1	3D high-throughput RNAi-based screening.....	54
5.1.1	Uncovering novel radioresistance-related focal adhesion proteins.....	54
5.1.2	Synemin modulates radiation sensitivity and DNA double strand break repair in HNSCC.....	58
5.1.3	Analysis of synemin dynamics after irradiation.....	63
5.2	The role of synemin in DNA repair mechanisms in HNSCCs.....	66
5.2.1	The effect of synemin knockdown on NHEJ, HR and Alt-EJ in HNSCCs.....	66
5.2.2	The effect of synemin knockdown on DNA repair kinetics in NHEJ and cell cycle.....	68
5.3	Synemin signaling in head and neck squamous cell carcinoma (HNSCC).....	72
5.3.1	Regulation of kinase activity by synemin.....	72
5.3.2	Synemin as upstream protein of c-Abl and DNA-PKcs.....	76
5.3.3	Synemin forms a complex together with c-Abl and DNA-PKcs.....	78
5.3.4	Synemin function is regulated by ATM kinase activity.....	79
5.3.5	Synemin tail is phosphorylated by ATM kinase and it is essential for synemin function.....	82
6	Discussion.....	86

6.1 The 3DHT-RNAi-S demonstrates as a consistent and robust platform for the identification of novel targets.....	87
6.2 The inhibition of synemin significantly increases DSB numbers and cellular radiosensitivity .....	88
6.3 Synemin expression and dynamics change upon irradiation .....	89
6.4 Synemin affects the NHEJ, but not the HR and Alt-EJ, through the regulation of two key DNA repair proteins: DNA-PKcs and Ku70 .....	90
6.5 Synemin inhibition leads to a deregulated tyrosine kinase activity 24 h post X-ray exposure .....	91
6.6 Synemin regulates c-Abl tyrosine kinase at 6 and 24 h post X-ray exposure .....	92
6.7 Synemin forms a complex with DNA-PKcs and c-Abl in an ATM-dependent manner .....	93
6.8 Synemin's function in DNA repair is limited to the tail domain, more specifically to the Serine located in the 1114 position .....	94
7 Summary .....	96
8 Zusammenfassung .....	98
9 Figure legends.....	100
10 Tables .....	102
11 Bibliography.....	104
12 Acknowledgements .....	123
Curriculum vitae .....	124
Anlage 1 .....	127
Anlage 2 .....	128
Darstellung des Eigenanteils .....	129

**Abbreviations**

14-3-3	Tyrosine 3-monooxygenase
2D	Two dimensional
3D	Three dimensional
3D-HTP-RNAi-S	3D high-throughput RNA interference screen
53BP1	Tumor suppressor p53-binding protein 1
AA	Amino acid
ABL1	Tyrosine-protein kinase c-Abl
AKAP	Kinase A anchoring protein
AKT	Serine/threonine protein kinase B
Alt-EJ	Alternative end-joining
ATF2	Activating transcription factor 2
ATM	Ataxia telangiectasia mutated
ATR	Ataxia telangiectasia and Rad3-related protein
BLK	BLK proto-oncogene, Src family tyrosine kinase
BRCA1	Breast cancer tumor suppressor protein-1
BRCA2	Breast cancer 2 tumor suppressor
CAM-DR	Cell adhesion-mediated drugresistance
CAMK	Calcium and calmodulin-regulated kinases
CAM-RR	Cell adhesion-mediated radioresistance

CDK4/6	Cyclin dependent kinase 4 and 6
cDMEM	Complete Dulbeccos modified medium eagle
CESCC	Cervical squamous cell carcinoma
CMGC	Cyclin dependent kinases
CO <sub>2</sub>	Carbon dioxide
CSRP1	Cysteine and glycine rich protein 1
CtIP	C-terminal binding protein-interacting protein
DAPI	4',6-diamidino-2-phenylindole
ddH <sub>2</sub> O	Double-distilled water
DDR	DNA damage response
DMEM	Dulbeccos modified medium eagle
DMSO	Dimethyl sulfoxide
DNA	Deoxyribonucleic acid
DNA-PKcs	DNA-dependent protein kinase catalytic subunit
DSB	DNA double strand break
EC <sub>50</sub>	Half maximal effective concentration
ECM	Extracellular matrix
EGFR	Epidermal growth factor receptor
ERK	Extracellular signal-regulated kinase 2
esiRNA	Endoribonuclease-prepared small interfering
FAK	Focal adhesion kinase
FAP	Focal adhesion protein
FCS	Fetal calf serum
FHL2	Four and a half LIM domains 2



G418	Geneticin
GFP	Green fluorescent protein
GIST	Gastrointestinal stromal cell tumors
GRB7	Growth factor receptor bound protein 7
Gy	Gray
h	Hour
H2AX	H2A histone family member X
H <sub>2</sub> O	Water
H4	Histone 4
HCl	Hydrochloric acid
HNC	Head and neck cancer
HNSCC	Head and neck squamous cell carcinoma
HP1 $\alpha$	Heterochromatin protein 1- alpha
HPV	Human papillomavirus
HR	Homologous recombination
HTS	High-throughput screen
IF	Intermediate filament
IGF1R	Insulin like growth factor 1 receptor
IgG	Immunglobulin G
ILK	Integrin linked kinase
ISCEI	Intron-encoded endonuclease I-SceI
ITGB3BP	Integrin subunit beta 3 binding protein
kDa	Kilodalton
KEAP1	Kelch like ECH associated protein 1

KU70	X-ray repair cross complementing 6 (XRCC6)
KU80	X-ray repair cross complementing 5 (XRCC5)
LCK	Lymphocyte cell-specific protein-tyrosine kinase
LDB3	LIM domain binding 3
LIG4	Ligase IV
LIMS1	LIM zinc finger domain containing 1
LUSCC	Lung squamous cell carcinoma
LYN	V-Yes-1 Yamaguchi sarcoma viral related oncogene homolog
p38MAPK	Mitogen-activated protein Kkinase
MgCl <sub>2</sub>	Magnesium chloride
Min	Minute
Mre11	Meiotic recombination 11
MRN	Complex consisting of Mre11, Rad50 and Nbs1
NaCl	Sodium chloride
NaOH	Sodium hydroxide
Nbs1	Nijmegen breakage syndrome protein 1
NHEJ	Non-homologous end joining
OSTF1	Osteoclast stimulating factor 1
PARP	Poly ADP ribose polymerase
PCNA	Proliferating cell nuclear antigen
PCR	Polymerase chain reaction
PDGFRA	Platelet derived growth factor receptor alpha
PI3K	Phosphatidylinositol-4,5-bisphosphate 3-kinase
PIKK	Phosphatidylinositol 3-kinase-related kinases

PKA	Protein kinase A
PKC $\delta$	Protein kinase C delta type
PLEKHC1	Pleckstrin homology domain-containing family C member 1
PNK	Polynucleotide kinase 3'-phosphatase
POL $\beta$	DNA polymerase beta
POL $\theta$	DNA polymerase theta
PP2A	Protein phosphatase 2 phosphatase activator
PTK	Protein tyrosine kinases
RAD50	RAD50 double strand break repair protein
RAD51	RAD51 recombinase
RAD52	DNA repair protein RAD52 homolog
RAD54	RAD54 like
RGD	Tripeptide Arg-Gly-Asp
RII	Regulatory subunit type II
RPA	Replication protein A 70 KDa DNA-binding subunit
RT	Room temperature
SCC	Squamous cell carcinoma
SDCBP	Syndecan binding protein
SDS	Sodium dodecyl sulphate
SDS-PAGE	Sodium dodecyl sulphate polyacrylamide gel electrophoresis
Ser	Serine
siRNA	Small interfering RNA
SLC3A2	Solute carrier family 3 member 2
SMC1	Structural maintenance of chromosomes 1A

SORBS2	Sorbin and SH3 domain containing 2
SRC	Proto-oncogene tyrosine-protein kinase Src
SSB	Single strand break
STK	Serine/threonine kinases
SYNM	Synemin, IV intermediate filament
TCGA	The Cancer Genome Atlas
TGF $\beta$	Transforming growth factor beta
TGF $\beta$ 1	Transforming growth factor beta 1
Thr	Threonine
TP53	Tumor protein P53
TRIP6	Thyroid hormone receptor interactor 6
Tyr	Tyrosine
VEGFR	Vascular endothelial growth factor receptor
x g	Relative centrifugal force (RCF)
XLF	XRCC4 like factor-complex
XRCC4	X-ray repair complementing defective repair in Chinese hamster cells 4
YES	V-Yes-1 Yamaguchi sarcoma viral oncogene homolog 1

Additionally, generally accepted abbreviations of the SI-unit system are used.

## 1 Introduction

Cancer is the second leading cause of death in Germany following the cardiovascular system diseases. Head and neck cancers (HNC) account for circa 6% of total cancer incidences in Germany (Koch Institute and Centre for Cancer Registry Data, 2009) and it is the sixth most common cancer worldwide (Curado and Hashibe, 2009; Braakhuis et al., 2010). Head and neck cancers include cancers in oral, nose, and throat cavities as well as in the laryngeal region, and around 90% are squamous cell carcinomas (head and neck squamous cell carcinoma, HNSCC) (Curado and Hashibe, 2009; Koch Institute and Centre for Cancer Registry Data, 2009; Braakhuis et al., 2010). Heavy alcohol consumption and smoking are the primary exogenous factors leading to HNC. Treatment choices of HNSCC primarily depend on the stage of the disease. For high grade HNSCC, tumors are generally treated with multimodal therapies consisting of surgical removal and mostly adjuvant radio(chemo)therapy (Langer, 2008). Due to tumor heterogeneity and intrinsic radiation sensitivity, an advanced tumor stage is often accompanied by therapy resistance, enhanced normal tissue toxicity due to intensified therapies and a higher probability of recurrence. In the last 30 years, despite novel therapeutic approaches and advances in the understanding of genetics and molecular mechanisms underlying HNSCC, overall survival and progression-free survival of patients with HNSCC were only minimally improved (Greenlee et al., 2001; Langer, 2008).

In order to overcome resistance to therapy and to enhance treatment success, it remains urgent to discover new treatment approaches. One possible strategy is the inhibition of new target molecules to sensitize tumors to standard therapies (Cordes et al., 2013; Eke and Cordes, 2015). Prerequisite for this therapeutic approach is the basic understanding of tumor biology and the unique properties that make tumor cells different from non-tumor cells. Hanahan and Weinberg described such unique properties for malignant tumors as "Hallmarks of Cancer" (Hanahan and Weinberg, 2011). These include: (1) maintenance of proliferative signaling pathways; (2) inhibition of growth suppressors; (3) activation of invasion and metastasis; (4) resistance to cell death (e.g. apoptosis); (5) enabling replicative immortality; and (6) genome instability and mutations.

Focal adhesion proteins (FAPs) and extracellular matrices have been recently defined as important modulators of the Hallmarks of Cancer and their significant role in therapy resistance (Ganguly et al., 2013; Glukhova and Streuli, 2013; Marelli et al., 2013; Pickup et al.,

2014; Eke and Cordes, 2015; Dickreuter et al., 2016). By binding to extracellular matrix proteins, FAPs activate intracellular signaling cascades to regulate survival, proliferation, apoptosis, invasion and metastasis (Hynes, 2002; Brakebusch and Fässler, 2005; Hehlhans et al., 2007). A growing number of (pre-)clinical studies reported the importance of FAPs and transmembrane receptors (e.g.  $\beta$ 1 integrin, FAK, AKT, EGFR, VEGFR, etc.) for cell survival through the activation of intracellular signaling pathways. *In vitro* and *in vivo* experiments with HNSCC and breast carcinomas showed the inhibition of FAPs lead to sensitization of the tumors to radiotherapy and chemotherapy by the inactivation of key pro-survival signaling pathways (Cordes et al., 2006; Park et al., 2008; Eke et al., 2012). However, the role of FAPs in the repair of DNA double-strand breaks (DSB) induced by radiation is largely unknown. Dickreuter and colleagues identified  $\beta$ 1 integrin as mediator of DNA repair processes through the regulation of key DNA repair proteins such as Ku70, Ku80 and DNA-PKcs. In addition, accumulating evidences suggested that cytoplasmic FAP signaling is associated with nuclear repair dynamics through interactions between the pro-survival non-receptor tyrosine kinases, such as c-Abl, and components of the DNA repair machinery, including DNA-PKcs, ATM, BRCA1 and RAD51 (Jin et al., 1997; Hantschel and Superti-Furga, 2004; Ren, 2005; Shaul and Ben-Yehoyada, 2005).

In this thesis, the influence of FAP-mediated signaling pathways on the repair of radiation-induced DSB and the underlying molecular mechanisms were investigated.

A 3D high-throughput RNA interference screen (3D-HTP-RNAi-S) of 117 FAPs was performed identifying synemin as the main target. The functions of synemin in HNSCC cell survival and therapy resistance was explored uncovering its molecular mechanism involved in DNA repair. It was discovered that synemin inhibition reduces non-homologous end joining (NHEJ) activity and enhances cellular sensitivity to radiochemotherapy. Mechanistically, synemin affects the phosphorylation status of DNA-PK S2056 and also Ku70 protein levels after irradiation. Furthermore, synemin regulates tyrosine kinases upon X-ray exposure. C-Abl, a key tyrosine kinase involved in many pro-survival mechanisms, is highly dependent on synemin expression. Moreover, the here discovered protein complex formed between DNA-PKcs, c-Abl, and synemin was shown to be dependent on ATM kinase activity and inevitable for cell survival and DNA repair. In conclusion, synemin is required for prosurvival DNA repair signaling and the regulation of NHEJ in an ATM dependent manner. Our study provides evidence of cytoarchitectural elements such as intermediate filaments as key co-regulators of nuclear DNA repair.

## 2 Background

### 2.1 Extracellular matrix, adhesion mediated radiation resistance and 3D cell culture model

The extracellular matrix (ECM) surrounds cells in order to provide structural and biochemical support and organizes multicellular complexes into tissues. It is possible to distinguish two subtypes of ECM: the basement membrane, a condensed 1-layer matrix adjacent to epithelial cells, and the interstitial matrix, which surrounds the cells in the connective tissue (Bosman and Stamenkovic, 2003; Frantz et al., 2010).

The ECM comprises two classes of macromolecules: polysaccharide chains and fibrillar proteins. The polysaccharide chains are covalently bound to transmembrane proteins and together they form proteoglycans. The fibrillar proteins such as collagen, fibronectin, elastin, and laminin have a structural function and additionally serve as ligands for the adhesion molecules of cells. The proteoglycans form a gel-like structure in which the fibrillar proteins are embedded. Mesenchymal cells such as fibroblasts are in charge of producing and secreting ECM proteins (Bosman and Stamenkovic, 2003; Kalluri, 2003; Guo and Giancotti, 2004; Frantz et al., 2010).

The ECM is not static, comprising growth factors, cytokines, or hormones, and it is constantly reorganized. For example, the conformation of the ECM drastically changes during development, aging, and tumor progression. Also, processes such as re-synthesis or the proteolytic degradation by matrix metalloproteinases (MMPs) play an important role in restructuring the ECM (Labat-Robert, 2003; Mott and Werb, 2004).

The ECM not only ensures the stabilization of cells in the tissue but also maintains tissue integrity. Through the adhesion of cells to ECM proteins, different cytoplasmic signaling pathways become activated, leading to regulation of cellular processes such as survival, migration, development, and proliferation (Bosman and Stamenkovic, 2003; Kalluri, 2003; Guo and Giancotti, 2004; Frantz et al., 2010). Integrins are an essential group of the ECM adhesion molecules. Reorganization of the ECM drives changes in the integrin-mediated signaling pathways and thus different cell processes are affected. This modulation of integrin-dependent signaling pathways by the ECM restructuring is, on one hand, required for devel-

opment, but is also fundamental for tumor development and response to chemo- and radiotherapy (WERB and CHIN, 1998; Larsen et al., 2006; Eke and Cordes, 2011b; Eke and Cordes, 2011a).

For instance, it has been demonstrated that cells cultured on matrices containing ECM proteins are more resistant to radiation or/and chemotherapy than the ones cultured on plastic. These mechanisms are referred to as cell adhesion-mediated radioresistance (CAM-RR) and cell adhesion-mediated drug resistance (CAM-DR) (Damiano et al., 1999; Cordes and Meineke, 2003). Both normal cells such as human fibroblasts and keratinocytes, as well as glioblastoma tumor cells, pancreatic carcinomas, bronchial carcinomas, melanomas, and breast cancers, have increased resistance to radiation after growth on fibronectin or laminin in comparison to cells cultured on plastic (Cordes et al., 2003; Cordes and Meineke, 2003).

Prof. Cordes' group was able to show that the cytotoxicity and radiation sensitization of the EGFR (epidermal growth factor receptor) inhibitor cetuximab decreases when cells adhere to fibronectin. Cetuximab treatment leads to activation of p38 MAPK (mitogen-activated protein kinase p38) / ATF2 (cyclic AMP-dependent transcription factor ATF-2) for fibronectin synthesis and secretion (Eke, Schneider et al., 2013; Eke, Storch et al., 2013).

The studies listed above were carried out under 2D monolayer growth conditions coated with ECM proteins. However, 3D models in which the cells are embedded in a laminin-rich ECM reflect better the physiological situation of cells in tissues (Storch et al., 2010; Eke and Cordes, 2011). Various studies provide strong evidence that gene and protein expression as well as survival, proliferation, and differentiation are significantly influenced when cells are grown under 3D conditions (Roskelley et al., 1994; Le Beyec et al., 2007; Lelièvre, 2009; Zschenker et al., 2012). Comparative transcriptome and proteome analyses show that 3D ECM-based cell culture is highly similar to the *in vivo* situation (Fig. 2.1) (Petersen et al., 1992). While cells grown on plastic present a stretched-out actin cytoskeleton and flat morphology, 3D-cultured cells, through the interaction with the ECM, exhibit a rounded morphology similar to cells *in vivo* (Yamada and Cukierman, 2007; Eke and Cordes, 2011). Storch et al. have shown that cells grown under 3D conditions, compared to 2D, express an increased proportion of heterochromatin and as a result present less radiation-induced DSBs, leading to increased radiation resistance (Storch et al., 2010).

Because the 3D ECM-based cell culture models the *in vivo* situation, it is more suitable as a predictive *in vitro* assay to evaluate tumor response to therapy. In addition, novel molecular targets can be more clinically relevant and translational when tested in 3D ECM-based cell cultures. For the investigations carried out in this work on the role of FAPs in radiation-induced DSB repair, cells were cultured under 3D conditions in a laminin-rich ECM also termed IrECM (Matrigel™), which is similar to the ECM underlying the epithelium and thus mimics the *in vivo* situation (Bissell et al., 2005; Storch et al., 2010).



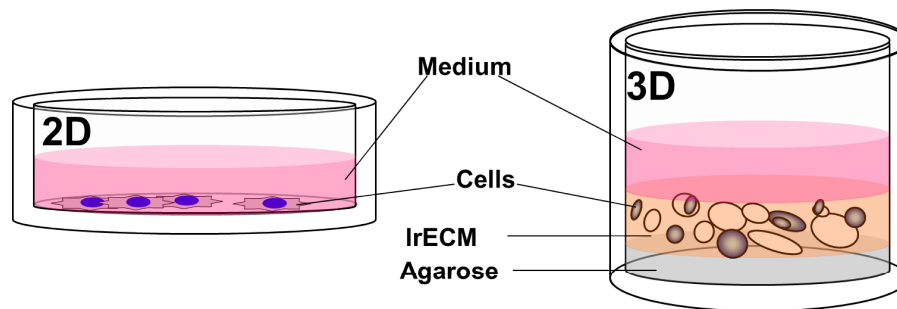


**Figure 2.1: Comparison of 2D and 3D cell culture conditions.** Cells cultivated under 2D conditions show a flat morphology. Cells embedded in a 3D microenvironment exhibit a rounded morphology similar to the *in vivo* situation.

## 2.2 Integrins and focal adhesion proteins (FAPs)

For multicellular structures or tissues to be formed, cells must interact via cell-cell contacts and across adhesion transmembrane receptors, such as integrins, which anchor in the ECM. Integrins, together with large protein complexes, form the focal adhesion (FA) plaques, which anchor on extracellular proteins.

Integrins are heterodimers and consist of an  $\alpha$ - and  $\beta$ -subunit, which are linked by non-covalent bonds. There are 18  $\alpha$ - and 8  $\beta$ -subunits known, from which 24 different integrin receptors can be formed. The combination of the  $\alpha$  and  $\beta$  subunits determines the binding specificity of the integrin (Hynes, 2002). In brief, integrins have one large extracellular ectodomain, a transmembrane domain, and a short cytoplasmic tail. Most integrins are not constitutively active and are located at the cell surface in an inactive state. Integrins are bidirectional signal receptors and can be activated in two ways: inside-out and outside-in stimulation. Both pathways are based on a conformational change in the ectodomain of the integrin. The inside-out activation consists of intracellular regulation of the integrin cytoplasmic domain by proteins such as kindlin or talin. By the conformational changes of integrins, there is an increased binding affinity for extracellular ligands. This activation mechanism controls, among other things, the migration of cells. With the help of outside-in activation, integrins can easily transmit information into the cell. The extracellular binding of a ligand also causes conformational changes of integrins and stimulation of intracellular signaling pathways. Both signaling pathways, inside-out and outside-in, can regulate each other and also lead to CAM-RR (Oxvig et al., 1999; Luo and Springer, 2006; Gahmberg et al., 2009; Shattil et al., 2010; Bouvard et al., 2013; Calderwood et al., 2013).

Intracellular adapter proteins such as paxillin, parvin or talin, members of FAPs complexes, link integrins to the actin cytoskeleton (Fig. 2.2), creating a link between ECM, cell membrane, and cytoskeleton. Although integrins do not possess intrinsic kinase activity, they can recruit and activate a large spectrum of kinases in the cytoplasm. As a result, important cellular processes such as proliferation, apoptosis, differentiation, migration, and cell survival

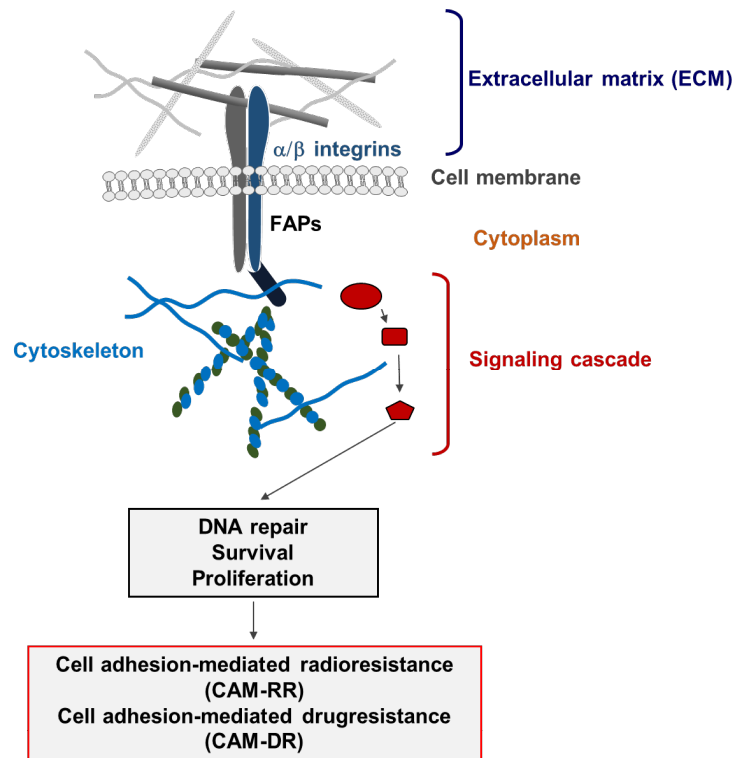


**Figure 2.2: Integrins and FAPs contribute to cancer radio- and drug-resistance by mediating cell adhesion to the extracellular matrix.** Upon cell adhesion to ECM, integrins induce prosurvival signaling cascades and thereby contribute to cell adhesion-mediated radiotherapy- and drug-resistance (CAM-RR and CAM-DR).

are regulated by FAPs (Fig. 2.2) (Miyamoto et al., 1995; Yamada and Miyamoto, 1995; Hehlhans et al., 2007).

Besides integrins, there are thousands of proteins which contribute to the adhesome (Horton, Byron, Janet a. Askari et al., 2015). Some of them are adaptor proteins, actin regulators, kinases, intermediate filament proteins (IFs), GTPases, and phosphatases. In this work, 117 of these FAPs were selected and evaluated in the radiation-induced DSB repair and CAM-RR.

## 2.3 Intermediate filaments (IFs)

### 2.3.1 Cytoskeleton components

The cytoskeleton is an essential component of the cell; it structures the cell shape, anchors main cellular components (such as organelles), and generates roads for transportation (Fletcher and Dyché Mullins, n.d.). The cytoskeleton comprises three major constituents: i. microfilaments (formed by polymerized actins), ii. microtubules (linear polymers formed by alpha and beta tubulins) and iii. intermediate filaments (IFs). Microfilaments are well known to be a flexible component of the cell; they are the main component involved in cytokinesis and changes in cell morphology. Microtubules have several functions: they form complex structures such as in cilia, flagella, and centromeres and they are also, similarly to microfila-

ments, involved in cell cytokinesis. Moreover, microtubules are the transport roads for vesicles, granules, organelles, and chromosomes via the well-known motor proteins kinesin and dynein. IFs, in contrast to the other two cytoskeletal components, are not involved in cell motility; instead, they mechanically support the plasma membrane of the cells during cell-cell interaction or cell-extracellular matrix interaction (Leube et al., 2015; Lowery et al., 2015). In fact, IFs have often been identified as active participators of focal adhesion proteins, such as vimentin, keratins, vinculin, and synemin. Still, many functions of IFs are unclear, also due to the collection of diversities between the IF superfamily members.

### **2.3.2 Structure and assembly**

IFs are composed of conserved domains that can be found in almost all members of the superfamily. The major building block of IFs is the  $\alpha$ -helical rod domain, which contains four different coil structures (Coil 1A, Coil 1B, Coil 2A, and Coil 2B) (Herrmann and Aebi, 2016). These structures are firmly held together by linker domains (L1, L12, and L2). The rod domain contains high amounts of charged amino acids (AAs), leading to high levels of acidity (Herrmann and Aebi, 2016). The head domain balances the acidity from the rod because it is highly basic. Depending on the head, rod length, and charge, the assembly of the filaments may differ. The third common component of the IFs is the tail domain, which is typically not necessary for filament formation, but it contains important information, such as the nuclear localization sequence for lamins and regulates the filament width. IFs form heteropolymer structures that are quite stable over time, differently from microtubules and microfilaments, which are more dynamic.

### **2.3.3 Family classification**

IFs are classified into six different families, depending on various factors such as tissue of origin and compartmental distribution. The IF protein family shows a high degree of diversity due to differences in sequences, sizes, and functionality (Table 2.1). Type I and II are keratins, which can be defined as acidic or basic; these two keratins associate together to form heterodimers and altogether assemble into keratin filaments (Coulombe et al., 2001; Lowery et al., 2015; Anon 2017). Type I and II are composed in total of 33 keratins, 20 being epithelial keratins and 13 being trichocytic keratins (components of hair, nails, etc.). Type III comprises just four proteins: desmin (mainly identified in sarcomeres), glial fibrillary acidic protein (found in astrocytes and glia), peripherin (which arranges in the peripheral neurons), with the last protein being vimentin (Coulombe et al., 2001; Lowery et al., 2015; Anon 2017). Vimentin is one of the major components of IFs that can be found in many tissues and cells. It has important functions such as anchoring of organelles and also in signaling transduction from the membrane to the nucleus of the cell. Type IV IFs are found mainly along the axons

of neurons, for example neurofilaments form part of this category (Coulombe et al., 2001; Lowery et al., 2015; Anon 2017). Other members of this family are: internexin (a component of small interneurons and cerebellar granule cells), synemin (found in sarcomere but also in neurons), and sincoilin (a muscle-specific intermediate filament). There are still two other proteins classified as non-standard subtype IV of the superfamily; these proteins are mainly present in differentiated lens fiber cells referred to as filensin and phakinin. Type V IFs are found in the nuclear lamina of the cells and are called nuclear lamins (Coulombe et al., 2001; Anon 2017). There are two different lamins. A is expressed in differentiated cells. Due to alternative splicing, there are two different isoforms of lamin A: A and C. The second one is lamin B, which is present in every cell and also has two important isoforms: B1 and B2. The last class of IFs is Type VI, which has only one component termed nestin. This IF is present in nerve cells and has a role in the radial growth of axons.

**Table 2.1: IF superfamily classification.** IFs can be categorized depending on the tissue of origin or intracellular localization. To date, there are six different classified groups (adapted from Coulombe et al., 2001).

Type	IF	MW (kDa)	Tissue	Cell location
I	Acidic Keratins (circa 15 proteins)	40-68	Epithelia	Cytoskeleton, cytosol
II	Basic Keratins (circa 15 proteins)	40-69	Epithelia	Cytoskeleton, cytosol
III	Desmin	54	Muscle	Perinuclear region, cytoskeleton
	Glial fibrillary acidic protein	50	Glial cells and astrocytes	Cytoskeleton, cytosol
	Peripherin	54	Peripheral and central neurons	Cell membrane, cytoskeleton, extracellular exosome
	Vimentin	54	Mesenchyme, all cell types	Cytoskeleton, cytosol
IV	NF-L	62	Mature neurons	Cytoskeleton, cytosol
	NF-M	60-102	Mature neurons	Cytoskeleton
	NF-H	106-112	Mature neurons	Cytosol
	Internexin	55	Developing central nervous system	Cytoskeleton, nucleus, extracellular exosome
	Synemin	170-210	Neurons and sarcomere	Cell membrane, cytoplasm, cytoskeleton
	Syncoilin	55	Sarcomere	Perinuclear region
<b>Non standard type IV</b>	Filensin	58-75	Lens fiber cells	Cytoskeleton, cytosol
	Phakinin	46	Lens fiber cells	Cytoskeleton, cytosol
V	Lamin A	65-70	All cell types	Nucleus
	Lamin B	66	All cell types	Nucleus
	Lamin C	65-70	All cell types	Nucleus
VI	Nestin	177	Nerve cells	Cytoskeleton, cytoplasm

## 2.4 Synemin, IV intermediate filament

### 2.4.1 Structure

Synemin was identified as a novel 230 kDa intermediate filament (IF) by Granger and Lazarides in 1980. Synemin was co-purified together with desmin and vimentin filaments from smooth muscle; these filaments gave synemin its name — the Greek word synemin means  $\delta$  υν (with) and νη μν (filament).

Synemin is classified as a IV intermediate filament and it was identified to be genetically evolved from neuro-filament protein genes (Gu ette et al., 2007). In fact, a typical characteristic of these IF, apart from the  $\alpha$ -helical domain, is the long tail domain, which encompasses 75% of the total size of synemin.

Synemin cannot homopolymerize and form filaments itself due to its structure, but it can copolymerize efficiently with type III IFs. Synemin, as other IFs, contains three main domains: the head (1–10 AAs), the intermediate rod (11–300 AAs), and the long tail (301–1,565 AAs) as shown in Figure 2.3. The rod itself is formed of three different coiled coils (1A, 1B, and 2) separated by short variable linkers. The reason why synemin cannot form filaments was well described by Khanamiryan et al. They show that synemin's inability to form filaments is linked to the short head domain. The IF head is typically formed of positively charged residues interacting with the rod domain, which is negatively charged at neutral pH. Due to the short length of synemin's head (just ten AAs), it cannot produce the positive and negative balance necessary for dimer-dimer interaction. In the same publication, the authors also mention that synemin is missing two conserved motifs in the 2A and 2B coiled coil subdomains, both TAAL and TYRKLLEGEE motifs respectively necessary for filament formation (Khanamiryan et al., 2008).

Moreover, synemin C-terminal tail function appears to be fundamental for the formation of cross bridges in filaments and binds to many other FA and cytoskeletal components, such as  $\alpha$ -actinin, dystrophin, talin, vinculin/metavinculin, plectin, utrophin, and zyxin (Geisler and Leube, 2016). There are three different synemin isoforms produced by alternative splicing:  $\alpha$ ,  $\beta$ , and L, and they vary mainly in length. For instance,  $\alpha$ -synemin is the longest isoform with 1,565 AAs;  $\beta$ -synemin is slightly shorter and contains 1,251 AAs. The shorter isoform is L-synemin, which contains 339 AAs and it is composed only of the head and the rod domain (Fig. 2.4). Instead,  $\beta$ -synemin is more similar to  $\alpha$ -synemin because they only differ in the second part of synemin's tail domain between AAs 1,153 to 1,251 located in the last two exons in the long C-terminal tail (Fig. 2.4).

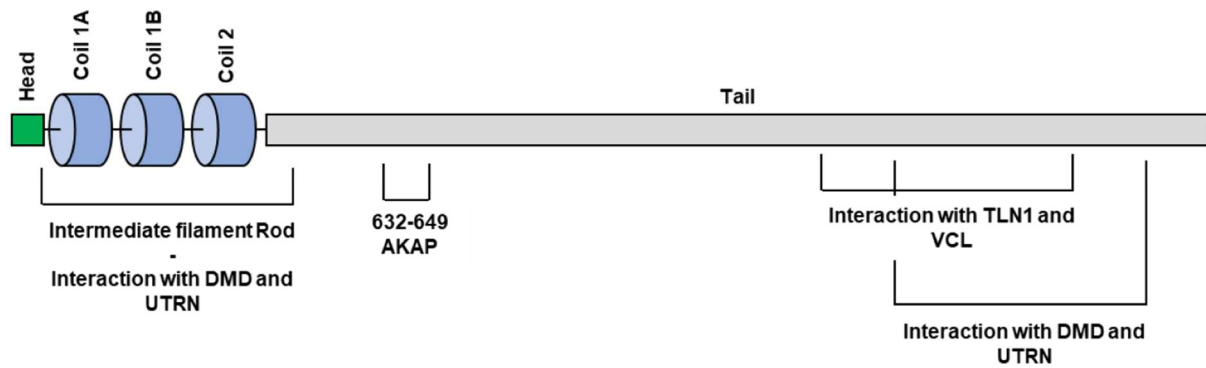


**Figure 2.3: Synemin structure and interaction sites.** Synemin comprises three main building blocks: the head (AAs 1–10), the coil-linker domain (AAs 11–300), and the tail (AAs 31–1,565). Data taken from UniProt.

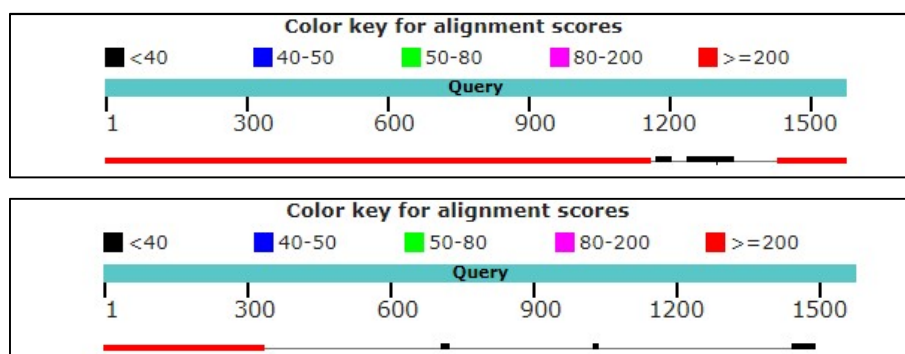


**Figure 2.4: Synemin isoforms.** Synemin is composed of three isoforms:  $\alpha$ ,  $\beta$ , and L. A Blast alignment tool (<https://blast.ncbi.nlm.nih.gov/Blast.cgi>) was used to compare the AA sequences of  $\beta$  and L synemin isoforms to  $\alpha$ -synemin. In the first case ( $\alpha$  vs  $\beta$ ), the similarity between the two proteins is evident, except for some AAs at the distal tail. In the second case ( $\alpha$  vs L), it is observable that the L isoform lacks almost the full-length tail.

## 2.4.2 Physiological role of synemin

Synemin was originally identified from avian smooth muscles as an intermediate filament due to its interactions with desmin and vimentin (B.L Granger and E. Lazarides, 1980). Despite having evolved from neurofilament protein genes (Guérette et al., 2007), synemin expression is not confined to brain tissue. As mentioned previously, synemin can be found in myocytes but also in hepatic stellate, endothelial, and lens cells (Pitre et al., 2012). Depending on the tissue of origin, synemin seems to have different functions and interaction partners. For instance, synemin is involved in the assembly of focal adhesions together with desmin/vimentin, forming hetero-polymeric filaments in muscle cells (Jing et al., 2005; Sun et al., 2010). Typically, synemin localizes in actin-rich regions such as lamellipodia (Bellin et al., 1999). Synemin is considered to be a kinase anchoring protein (AKAP) with scaffold functions regulating the anchoring ability of protein kinase A (PKA) in heart tissue (Russell et al., 2006) through the interaction with the PKA regulatory subunit type II (RII) binding site. PKA is a family of enzymes which function as kinases regulated by cyclic AMP levels. This kinase is

mainly involved in cell metabolism, and deregulation may lead to muscular atrophy. In line with these observations, the Bloch group has determined that absence of synemin causes structural and functional abnormalities in the heart (García-Pelagio et al., 2018). That group reported that synemin silencing leads to left ventricular systolic dysfunction and hypertrophy accompanied by dilatation. Synemin deficient cardio-myocytes showed alterations in calcium handling and in several signaling proteins (PKA-RII, ERK, and p70S6K) which are critical to cardiomyocyte function (García-Pelagio et al., 2018). Furthermore, the Bloch team has demonstrated that synemin silencing not only affects cardiac muscle but also skeletal muscle functionality, leading to a decreased bone density also known as osteopenia (García-Pelagio et al., 2019). Since the discovery of synemin, few groups have been working in order to understand synemin molecular mechanisms and its physiological role. Still, synemin function has not been clearly understood and may differ from tissue to tissue.

### **2.4.3 Synemin in cancer**

The molecular function of synemin in cancer can differ depending on the tumor entity. In glioma cells, synemin is overexpressed and is associated with enhanced cancer cell proliferation and survival (Pitre et al., 2012). Likewise, synemin promotes proliferation and motility of astrocytoma cells (Pan et al., 2008; Skalli et al., 2013). Furthermore, synemin has been identified in several sarcomas, including leiomyosarcomas and gastrointestinal stromal cell tumors (GIST). Synemin was described as a good diagnostic marker for GIST because it was found in proto-oncogene tyrosine kinase receptor CD117<sup>+</sup> positive cells (Criswell et al., 2018; Criswell et al., 2019). In the present study, synemin expression was observed in all applied head and neck squamous cell carcinoma (HNSCC) cell lines, similar to gliomas and astrocytomas. Interestingly, in many squamous cell carcinomas, such as lung (LUSC), cervical (CESC), and HNSCC, the DNA copy number of the SYNEM gene was amplified (Network, 2015). In contrast, a study in breast cancer cells demonstrated that the SYNEM gene can be hypermethylated, leading to down-regulation of synemin expression (Noetzel et al., 2010). When this down-regulation occurs, the breast cancer cells acquire a more migrating phenotype, leading to an increased level of lymph node metastasis.

Skalli's group reported that the malignant role of synemin in glioblastoma is indirectly associated with the regulation of Akt activity. Synemin was characterized as a regulator of protein phosphatase 2 A (PP2A) (Pitre et al., 2012). As a result of synemin depletion, an increased PP2A phosphatase activity down-regulated Akt activity, attenuating the pro-survival mechanism of glioma cells. Besides the direct interaction with Akt, PP2A modulates the DNA DSB repair mechanism by dephosphorylating  $\gamma$ H2AX after DNA repair has been completed. The authors reported the direct interaction between synemin and PP2A located solely inside the nucleus, but the authors did not further investigate the underlying mechanisms.

## 2.5 Head and Neck squamous cell carcinomas (HNSCC)

Head and neck cancers (HNCs) encompass a heterogeneous group of malignant tumors that arise in the upper oral cavity including the pharynx (nasopharynx, oropharynx and hypopharynx), larynx, and oral/nasal cavity. Other common areas where this tumor can develop are the tongue, salivary glands, and paranasal sinuses. Approximately 90% of HNCs are squamous cell carcinomas (HNSCCs). Worldwide, more than 300,000 new cases of HNSCC and about 150,000 deaths per year were estimated (Ferlay et al., 2015). In Germany, HNCs more often affect the male population and around 8% of men die from it every year (Fig. 2.5) (Koch Institute and Centre for Cancer Registry Data, 2009). Although HNSCC represents only a small proportion of the overall cancer incidence, the prognosis of patients with HNSCC remains poor, with a 5-year overall survival rate of 50%.

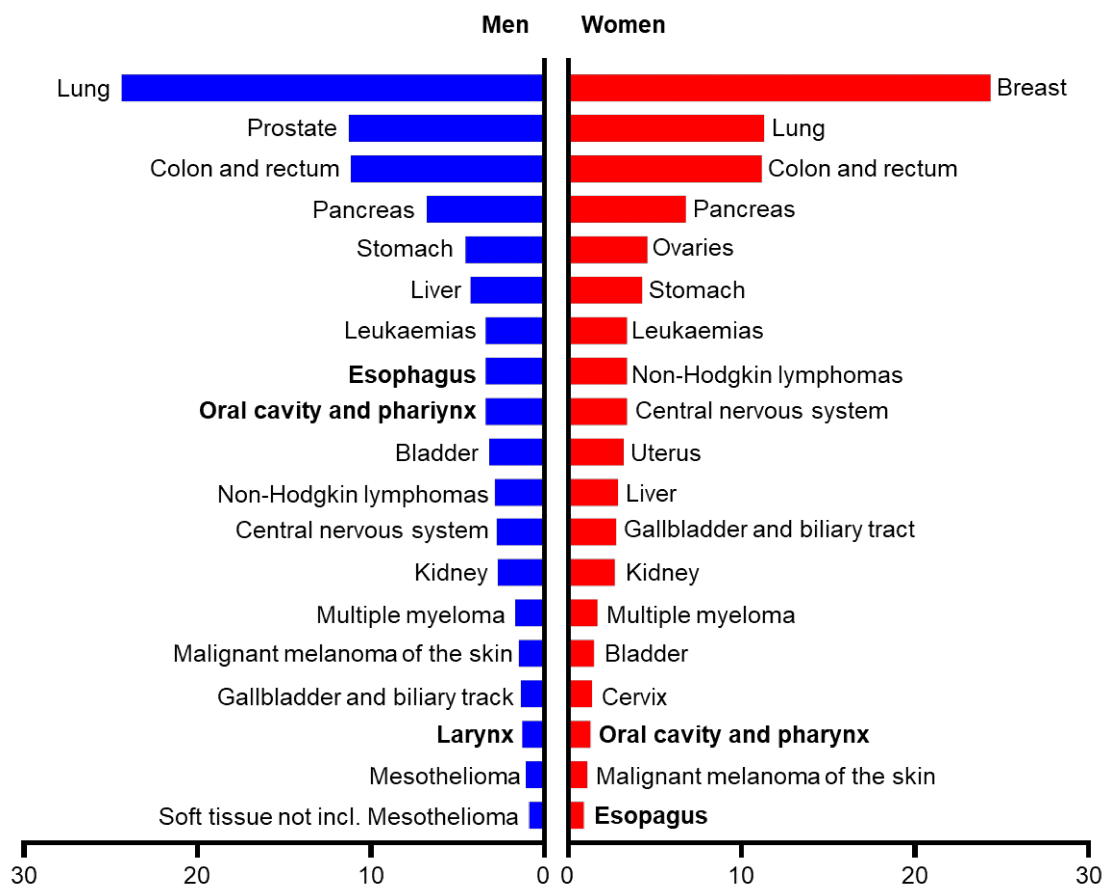


**Figure 2.5: Percentage of the most frequent tumor sites when cancer was the leading cause of death in Germany (2014).** Estimated percentage of tumor incidence and tumor as cause of death in different areas of the body in men and women living in Germany. Different components of HNCs tumors are shown in bold: Esophagus, oral cavity, pharynx, and larynx (Modified from Cancer in Germany, 2013/2014).



### 2.5.1 Common therapeutical approaches

Radiotherapy remains an indispensable element for the curative care of HNSCC. Treatment choice for early stage HNSCC is either surgery or radiotherapy as a single modality, whereas multimodal treatment is important for treating patients with locally advanced HNSCC in stages T3 or T4 (Colevas et al., 2018). Recent developments of curative treatment of HNSCC include: a) optimization of fractionation schedules, b) the use of high-precision radiotherapy modules (i.e., proton therapy and intensity-modulated radiation therapy), and c) implementation of chemotherapeutics or immunotherapeutics in treatment plans (Haddad and Shin, 2008; Santuray et al., 2018). Commonly used drugs are for example cisplatin, bleomycin, cetuximab, docetaxel, hydroxyurea, and many others depending on the tumor characteristics and stages (<https://www.cancer.gov/about-cancer/treatment/drugs/head-neck>).

### 2.5.2 Risk factors

The most common risk factors for HNSCC development are excessive and long-term consumption of alcohol and tobacco in the older population (Kuriakose et al., 1992; Llewellyn et al., 2001; Schmidt et al., 2015). However, recent studies showed an increasing number of young subjects with oral squamous cell carcinoma (SCC), despite low consumption of these substances (Kuriakose et al., 1992; Schmidt et al., 2015). In these cases, the pathogenesis of HNSCC in young people is attributed to genetic and other behavioral factors (Schmidt et al., 2015). Genetic factors include genetic predisposition to cancer (i.e. factors related to DNA instability such as DNA ploidy or chromosomal fragility and rearrangement). Genetic instability can lead to gain and loss of chromosome regions, resulting in mutations that will affect cell cycle progression checkpoints and activation of proto-oncogenes (Kuriakose et al., 1992; Kaminagakura et al., 2011). There is also a so-called familial risk, which involves an increased probability of developing cancer if a first-degree family member has suffered from HNSCC (Schmidt et al., 2015).

Other risk factors are immuno-deficiencies, such as chronic syndromes (Bloom syndrome, Wiskott-Aldrich syndrome) or anemia (Patterson Kelly/ Plummer Vinson syndrome, Fanconi anemia) (Toner and O'Regan, 2009; Schmidt et al., 2015). In Fanconi anemia for example, the DNA repair machinery is partly impaired, leading to an increased probability of developing cancer. In fact, a subject suffering from Fanconi anemia has a 40% risk to develop HNC (Toner and O'Regan, 2009; Schmidt et al., 2015).

Last but not least viral infections, such as the human papillomavirus (HPV), are a common risk factor. There are two different subtypes of HPV viruses depending on low and high risk of leading to cancer development (Chaturvedi and Chocolatewala, 2009). For example, HPV-16 and HPV-18 are high-risk viruses. Viral DNA produces onco-proteins, known as E6 and E7, affecting the infected cell's normal behavior (Schmidt et al., 2015), leading to

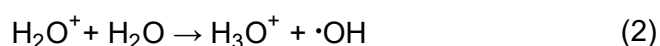
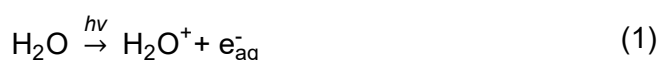
genomic instability and cell immortalization. However, it is well known that HPV-positive head and neck tumors are associated with a more favorable outcome (Ganci et al., 2015) and better response to standard therapy.

## 2.6 Effects of ionizing radiation on cellular level

Radiation therapy is a standard treatment for cancer, and it is typically applied in combination with chemotherapy and/or surgical removal of the tumor bulk. By its genotoxic property, radiation damages the DNA to the degree that cancer cell survival and proliferation is reduced. For this reason, approximately 50–60% of all cancers are treated with irradiation (Koch Institute and Centre for Cancer Registry Data, 2009; Begg et al., 2011; Moding et al., 2013). Irradiation can be classified into two groups: the first one is particulate irradiation (electrons, neutrons,  $\alpha$ -particles, protons, or heavy ions), and the second one is electromagnetic or photon irradiation (X- and  $\gamma$ -rays). X-rays are prevalent for cancer therapy treatment (Hall and Giaccia, 2012).

Ionizing radiation is defined as radiation with sufficient energy to eject an electron out of the atom orbital of a target molecule such as water or intracellular macromolecules. Radiation can be classified into a) directly ionizing and b) indirectly ionizing radiation. In contrast to direct ionization where the energy is directly deposited on target molecules, indirect ionization does not directly cause damage to target molecules but rather ionizes other molecules (e.g. water or intracellular macromolecules) which in turn damage/ionize target molecules. An example of frequent ionized molecules by X-ray are water molecules in solution (radiolysis of water (Breen and Murphy, 1995)).

Upon ionization of water molecules, an aqueous electron ( $e_{\text{aq}}^-$ ) and oxygen (1+) dihydride ( $\text{H}_2\text{O}^+$ ) (Eq. 1) are generated. The oxygen (1+)dihydride then reacts with a nearby water molecule (Eq. 2) forming a hydronium ion ( $\text{H}_3\text{O}^+$ ) and a hydroxyl radical ( $\cdot\text{OH}$ ), both of which can cause further damage to surrounding molecules.



Because cells are composed of 80% water, it is likely that most damage occurs due to indirect ionization upon irradiation of biological materials.

During ionizing radiation, multiple reactive oxygen species are generated. These species react with several biological elements such as proteins (Kumta and Tappel, 1961),

membrane lipids (Konings, 1987), and DNA molecules (Schulte-Frohlinde and Bothe, 1991), generating damage and disrupting their functions.

The major target of ionizing radiation is DNA. Inducing damage to DNA can lead to cell death, mutagenesis, and carcinogenesis. In figure 2.6, the direct and indirect damage on DNA induced by ionizing radiation is illustrated. The energy generated from X-ray is typically distributed along the tracks of the charged particles, also defined as spurs. Interestingly, spurs composed of three ion pairs have a diameter of 4 nm, which is twice the size of the DNA helix size (2 nm), implying that if the spurs overlap the DNA, multiple radical attacks can occur and damage can be induced (Hall and Giaccia, 2012).

Irradiation induces different forms of damage in DNA, such as: change, modification, or loss of bases; single strand breaks (SSBs) and double strand breaks (DSBs). A single dose of 1 Gy irradiation can induce up to 1,000 SSBs and 20–40 DSBs. Additionally, SSBs on both strands in close proximity can lead to the formation of a DSB. It is widely recognized that the most lethal form of damage for cells relates to DSBs. In fact, if left unrepaired or incorrectly repaired, DSBs can lead to abnormal chromosome rearrangements (translocations, deletions) and cell death (Kinner et al., 2008; Galluzzi et al., 2012). Chromosome rearrangements can lead to cell transformation or increase the risk of cancer development (Hall and Giaccia, 2012).

To overcome their fate after DNA damage induction, cells have developed defensive mechanisms, such as DNA damage response and repair. After correct repair, cells regain their functionality and the ability to reproduce.

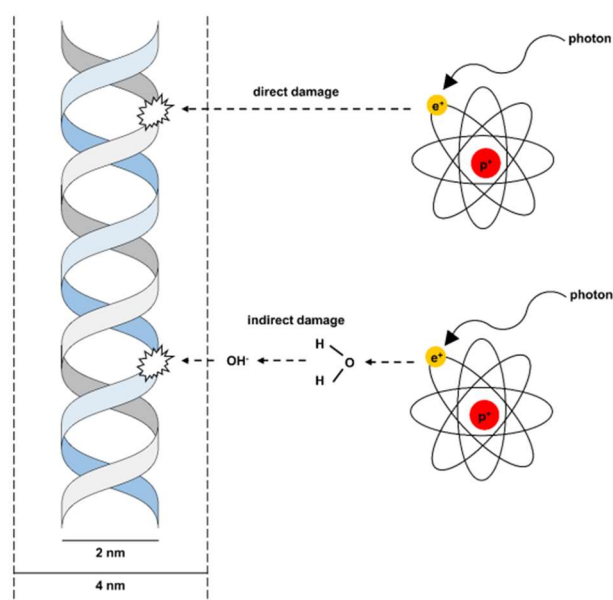


**Figure 2.6: Ionizing radiation induces damage to macromolecules.** Direct damage to DNA and other macromolecules is induced by ionization of the molecules and disruption of their chemical bonds. Damage can be indirectly inflicted by ionization of surrounding water molecules, producing free radicals, which in turn cause damage to the biomolecules. Source: Hall and Giaccia, 2012.

## 2.7 DNA damage response

DNA damage is not only caused by irradiation. In fact, circa 70,000 endogenous lesions occur daily under natural circumstances. Twenty of these lesions are DNA DSBs, serving as a source of spontaneous mutations (Tubbs and Nussenzweig, 2017). To repair DNA damage, eukaryotic cells have developed a signaling network termed DNA damage response (DDR), which can trigger cell cycle arrest, DNA repair, and apoptosis (Ciccia and Elledge, 2010). After the activation of the DDR, the main DNA repair machinery is activated consisting of: non-homologous end joining (NHEJ), homologous recombination, (HR) and in some cases alternative end joining (alt-EJ) (Fig. 2.7) (Willers et al., 2004; Chang et al., 2017).

Commonly, the MRN complex consisting of meiotic recombination 11 (Mre11), Rad50 and Nijmegen breakage syndrome protein 1 (Nbs1) recognizes the DNA DSB. After recognition, the Mre11 mediates DNA end resection due to its endonuclease and exonuclease activities (Hopfner et al., 2001). Rad50 protein is instead responsible for DNA binding and possesses ATPase and adenylate activity (Paull and Gellert, 1999). Nbs1 is simply responsible for nuclear localization of the MRN complex (Williams et al., 2010). Once the MRN complex is located at the damage site, it facilitates the recruitment of three main kinases: ataxia telangiectasia mutated (ATM), ataxia telangiectasia and Rad3 related (ATR), and DNA-dependent protein kinase catalytic subunit (DNA-PKcs) (Bristow and Hill, 2008).

ATM, a serine/threonine kinase, is probably the main player in damage recognition (Roos and Kaina, 2013). ATM is named after the human autosomal recessive disorder ataxia telangiectasia mutated caused by mutations in the ATM gene (Savitsky et al., 1995) and is a key protein of the phosphatidylinositol 3-kinase-related kinase pathway (PIKK) (Uziel et al., 2003). ATM phosphorylates several DDR proteins such as H2AX, p53, checkpoint kinase 2 (Chk2), Nbs1, breast cancer tumor suppressor protein-1 (BRCA1) and structural maintenance of chromosomes 1 (SMC1) after its own activation (Fig. 2.8).

After damage recognition and recruitment of the MRN complex, histone H2AX phosphorylation results in the formation of  $\gamma$ H2AX in the DSB vicinity in less than ten minutes after the damage induction. Besides the MRN complex, the activation of ATM is also mediated by a feedback loop, regulated by  $\gamma$ H2AX and 53BP1 (p53-binding protein 1) foci formation (Uziel et al., 2003). The immunological detection of 53BP1 and  $\gamma$ H2AX is used for visualization and quantification of radiation-induced DSBs (Löbrich et al., 2010). The DSBs are described as foci which disappear after DNA damage repair, while unrepaired foci remain stable and are manifested as residual foci at 24 h post irradiation (Banáth et al., 2004).

DNA damage sensing factors and DNA damage repair proteins involved in HR and NHEJ are subsequently recruited (Bristow and Hill, 2008). The competition of NHEJ and HR as DNA DSB repair pathways is partly controlled by 53BP1 and BRCA1 (Fig. 2.7).

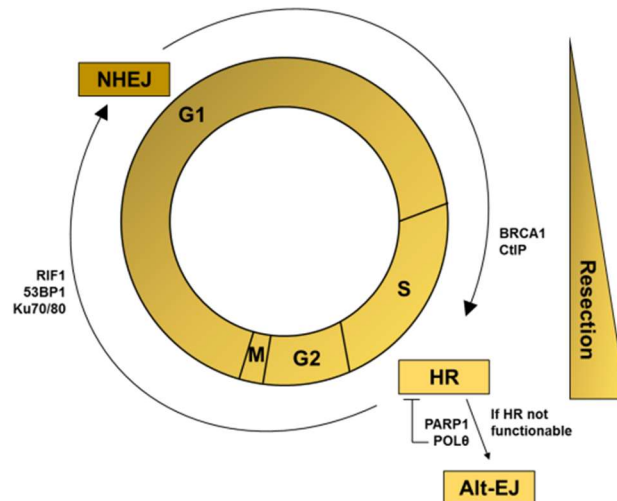


**Figure 2.7: DNA repair mechanism distributed in the cell cycle.** NHEJ is active during the entire cell cycle and is characterized by low resection of the damaged DNA. Instead, HR and Alt-EJ are mainly functional during late S and G2 phase, and DNA resection is necessary for these machineries.

53BP1, another ATM kinase substrate, dismisses the end resection mediated by MRN complex to favor NHEJ. Conversely, BRCA1, a tumor suppressor gene, promotes end resection and removes 53BP1 from DSB to initiate HR (Daley and Sung, 2014). A defect in one of the DNA DSB recognition and repair pathways is strongly associated with extensive genomic instability and high radiosensitivity (Pollard and Gatti, 2009).

## 2.8 DNA double strand break repair mechanisms

As described previously, eukaryotic cells have developed two main mechanisms for repair of DSB: HR and NHEJ. However, Alt-EJ also plays an important role in cancer treatment. In addition to 53BP1 and BRCA1, the decision of which mechanism will be implemented for the repair of DNA damage depends on the cell cycle phase (Fig. 2.7 and Fig. 2.8). NHEJ mainly takes place during G1- and early S phase, but it is active during the entire cell cycle. Because NHEJ does not require a template for DSB repair, this mechanism of damage repair can be error prone (Goodarzi and Jeggo, 2013). Instead, the HR operates only in dividing cells during late S- and G2-phase. HR is a high-fidelity repair mechanism due to the fact that it uses an intact homologue sister chromatid as a template for correct DSB repair (Iyama and Wilson, 2013). In cancer, when HR is not working appropriately, end resection that generates 3' single strands still occurs during G2/S phase and in this case, Alt-EJ repairs the DNA DSBs. Similarly to HR, this mechanism takes place during late S- and G2-phase but unlike HR, Alt-EJ does not use the sister chromatid as a template, leading to erroneous repair introducing mutations. Furthermore, this mechanism is commonly highly slow (Ceccaldi et al., 2016).

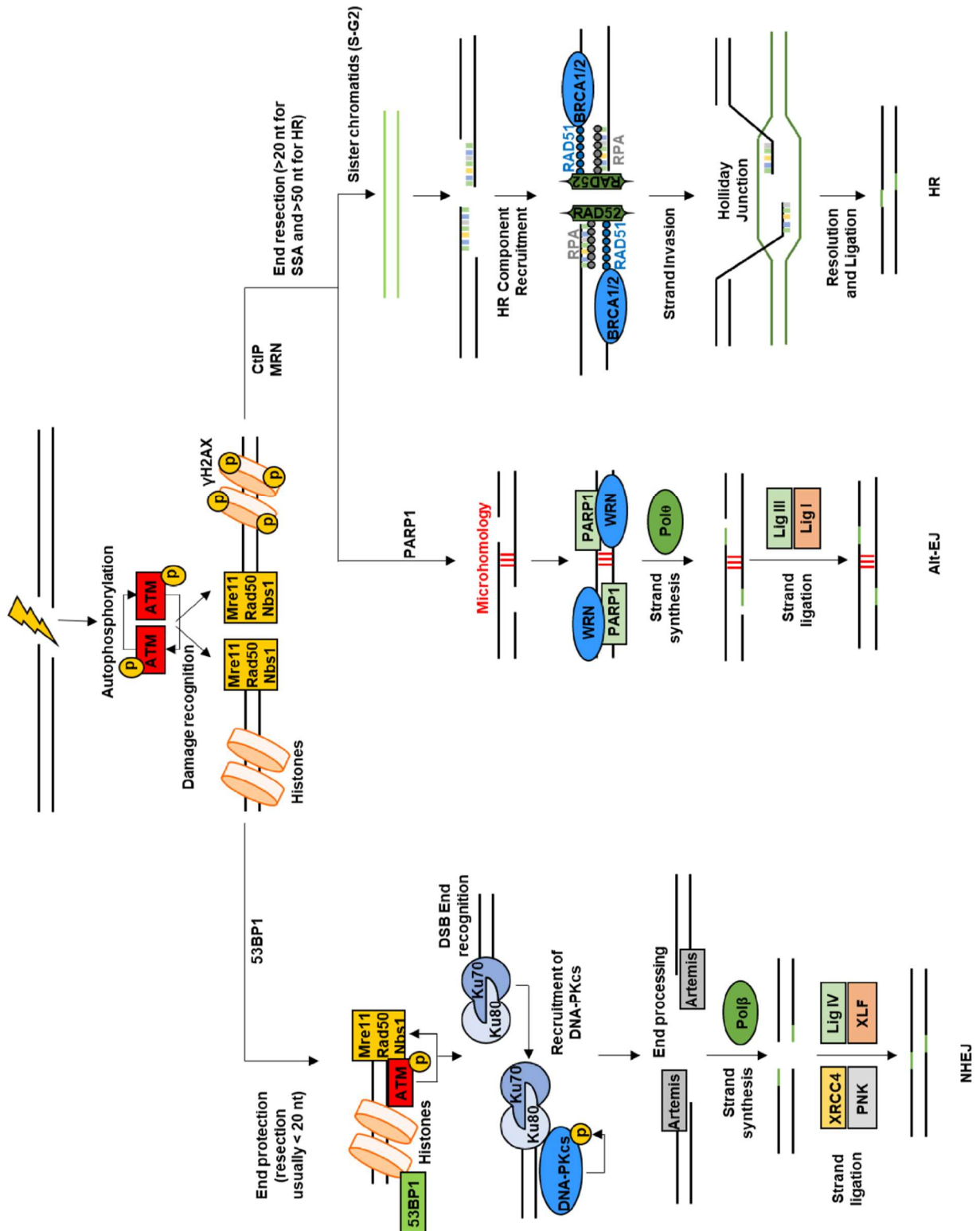


**Figure 2.8: DSB DNA repair mechanisms.** The main DSB DNA repair mechanisms are NHEJ, HR, and Alt-EJ. NHEJ is highly dependent on 53BP1 and the Ku complex which will recruit DNA-PKcs kinase. Instead, HR and Alt-EJ depend on CtIP and the MRN complex which will lead to end resection and the formation of a single stranded DNA, which will be repaired using the sister chromatid in the case of HR or by micro-homology in the case of Alt-EJ (Ceccaldi et al., 2016).

### 2.8.1 Non-homologous end joining (NHEJ)

The NHEJ is based on the direct ligation of two ends and is the major repair pathway in higher eukaryotes (Lieber, 2010). NHEJ is initiated by the recognition of the DSB and binding of the Ku heterodimer complex (Ku70-Ku80) to both ends of the break, thereby preventing extensive DNA end resection (Fig. 2.8). Subsequently, the Ku heterodimer recruits DNA-PKcs to DSB sites forming the Ku/DNA-PKcs complex. The complex formation stimulates the kinase activity of DNA-PKcs, stabilizing and aligning the DNA ends (Rathmell and Chu, 1994; Mladenov et al., 2016). To achieve end-processing of the DNA ends and to remove non-ligable parts, the endonuclease Artemis is phosphorylated and recruited to DSB sites by DNA-PKcs. Artemis then recruits polymerase  $\beta$  (Pol $\beta$ ) to modify the DNA ends and produce appropriate strands for ligation (Löbrich and Jeggo, 2005). Ligation is necessary to terminate the repair; during this final step of NHEJ, Ligase IV (LIG4) together with X-ray repair cross complementing 4 (XRCC4), XRCC4-like factor (XLF), and Polynucleotide kinase 3'-phosphatase (PNK) are recruited and collectively join the processed DNA strands (Koch et al., 2004).

As previously mentioned, NHEJ is considered to be an error-prone mechanism, in which two ends of a DSB break are rejoined without the use of homology. This process is fast but less accurate, thereby causing small deletions or insertions. Despite the enhanced risk of error, gene coding and regulatory regions account for only a minimal fraction of the total genome (ENCODE Project Consortium, 2012), minimizing the probability of damage occurring at protein coding regions. Thereby, the consequence of minor deletions or insertions caused by NHEJ are minimal or non-essential (Joiner and van der Kogel, 2009). Moreover, NHEJ is active throughout the entire cell cycle, providing a flexible repair mechanism and increasing the survival chance of damaged cells (Mladenov et al., 2016).

### 2.8.2 Homologous recombination (HR)

In contrast to NHEJ, the HR mechanism requires an intact sister chromatid as a template for correct repair. Firstly, ATM phosphorylates BRCA1, which is subsequently recruited to DNA DSB ends (Fig. 2.8). The MRN complex associates with the C-terminal binding protein-interacting protein (CtIP). CtIP initiates 5'-3' resection and generates 3' single-strand overhangs (Sartori et al., 2007), which are immediately coated by replication protein A (RPA) to stabilize the exposed ssDNA. RAD52 and BRCA2 promote the replacement of RPA by RAD51, resulting in nucleoprotein filaments. RAD52 is attracted to RAD51-coated nucleoprotein filaments to prevent exonucleolytic degradation. RAD51 supports the invasion of the 3' overhang of the intact homologous DNA region (Kass and Jasin, 2010), leading to the formation of a holiday junction. Finally, supported by RAD54 protein, the DNA polymerase ex-

tends the missing parts and the holiday junction is resolved with the support of ligases connecting the remaining DNA breaks, thereby closing the gap (Goodarzi and Jeggo, 2013).

HR is a slower process compared to NHEJ and requires circa 6 h to conclude the damage. This time is therefore important because it provides cells with an accurate DSB repair mechanism. Germline or somatic mutations of HR repair genes are strongly associated with hereditary diseases and tumorigenesis. For instance, BRCA1/2-mutated genes likely dictate the risk of breast cancer, prostate cancer, and ovarian cancer development (Levy-Lahad and Friedman, 2007). Moreover, patients with hereditary diseases such as Fanconi anemia, Bloom disease, and Werner disease, all of which are caused by defects in HR genes, are reported to have an extremely high radiation sensitivity (Pollard and Gatti, 2009; Krejci et al., 2012).

### **2.8.3 Alternative end-joining (Alt-EJ)**

The term alternative end-joining (alt-EJ) is derived from NHEJ because it was believed to be activated during a deficiency of NHEJ. However, it is still an open question whether alt-EJ is a stand-alone pathway or it is only involved in several processes relying on NHEJ, such as replication and DSB repair (Chang et al., 2017). Alt-EJ is well known for using microhomology sequences between the two DNA single strands to perform ligation and repair. Alt-EJ is highly dependent on four components: poly(ADP-ribose) polymerase I (PARP1), Pol  $\theta$ , CtIP, and MRN complex. At the DNA DSB site, PARP1 is recruited and competes with the Ku complex for access to the damage (Chang et al., 2017). At the same time, PARP1 may be involved in the recruitment of MRN complex to the damage and, in the absence of Ku stabilizing the strand, Mre11 can start with strand processing (Fig. 2.8). When the processed ends present more than 2 bp of homology, Pol  $\theta$  becomes activated and using the annealed partner template, it inserts templated insertions, leading to erroneous repair. The Alt-EJ repair mechanism is slower and more mutagenic compared to NHEJ and HR (Ray Chaudhuri and Nussenzweig, 2017).

In the clinic, PARP1 inhibitors are widely used for patients whose tumors present with BRCA1 deficiency. In fact, during the S/G2 phase, HR is active and end resection is more likely to occur. However, in BRCA1-deficient cells, HR cannot take place and as a surrogate, alt-EJ repairs the damage (Ray Chaudhuri and Nussenzweig, 2017).



### 3 Hypothesis and Aims

Various factors such as the microenvironment of tumors, gene mutations and epigenetic changes have a decisive influence on the success of cancer therapy and can lead to the development of therapy resistance. As a further source of therapy resistance, tumor cells attach to neighboring cells and to ECM, events shown as key drivers of resistance. While adhesion to neighboring cells and the extracellular matrix (ECM), including focal adhesion formation, is not limited to the large family of integrin receptors, inevitable proteins of these processes are FAPs. Cell adhesion molecules together with FAPs facilitate the linkage between ECM, intracellular cytoskeleton and nuclear membrane as well as other mechanisms such as cell-matrix communication.

Despite of all our current knowledge about pro-survival signaling via focal adhesions, it is unclear whether and how FAPs can influence the survival of cells through the regulation of radiation-induced DNA damage repair. Consequently, we hypothesized in the present study that FAPs fundamentally impact on HNSCC cell survival upon radiochemotherapy through the regulation of DNA repair mechanisms.

The aim of this study was to identify the mechanisms of radiation-induced DNA double strand break (DSB) repair as a function of specific FAPs in HNSCC cell lines. To systematically search for novel FAP candidates driving the cancer therapy resistome by linking extracellular cues to intracellular DNA repair decisions, a high-throughput RNA interference screen (3D-HTPS-RNAi-S) combined with X-ray irradiation of HNSCC cultures grown in 3D ECM laminin-rich ECM was established. This 3D ECM system has been previously shown to resemble *in vivo* growth conditions. After the screen, synemin resulted as one of the key targets controlling radiosensitivity and DNA damage repair. Synemin knockdown was used for silencing the protein and DSB were induced by X-rays. In order to investigate an association between synemin and DSB repair and to identify the molecular interaction, residual DSB rate, clonogenic survival, NHEJ activity, protein expression, phosphorylation and localization, kinase activity, protein-protein interactions and complex formation were determined. Since the connection between ECM, FAPs, actin cytoskeleton and nucleus plays an important role in nuclear organization and influences the DNA repair machinery, the role of synemin as linker protein was analyzed.

The results of this work show how synemin regulates the repair of radiation-induced DSB and, thus, contributes to our molecular understanding of synemin-mediated survival signaling. Further, these findings add important facets to our knowledge about cytoarchitectural elements such as intermediate filaments and their function as key co-regulators of nuclear DNA repair.

## 4 Materials and Methods

### 4.1 Materials

#### 4.1.1 Devices

**Table 4.1.** Devices used for the biochemical, molecular-biological and cell culture experiments.

Device	Type	Company
Autoclave	V-65	Systec, Wetztenberg, D
Barometer		Conrad Electronics, Hirschau, D
Binocular, incl. light source	Stemi2000	Carl Zeiss, Jena, D
Bio Imaging System	Genius Syngene	Syngene, Cambridge, GB
Centrifuge	5415R (for 15, 50 ml reaction tubes)	Eppendorf, Hamburg, D
Centrifuge	S415R (for 1,5 ml Safe-Lock reaction tubes)	Eppendorf, Hamburg, D
Dosimeter	PTW Unidos	PTW, Freiburg, D
Cytometers	FACs Canto™ II FACs Celesta	BD, Heidelberg, D
Film welding tool	Dual Electronic	Jencons-PLS, London, GB
Freezer, -20 °C	KX1011	Liebherr, Ochsenhausen, D
Freezer, -80/ -150 °C		Heraeus Holding GmbH, Hanau, D
Fridge		Liebherr, Ochsenhausen, D
Gel electrophoresis-System for LDH-Analysis	Paragon® Electrophoresis System	Beckmann Instruments, Fullerton, USA
Hand drill	Xenox Nail 35k	Xenox, Föhren, D
Ice machine	AT-10	Scotsman, London, GB
Incubator bacteria		Memmert, Schwabach, D
Incubator cell culture	HeraCel	Heraeus Holding GmbH, Hanau, D
Incubator for liquids		Heraeus Holding GmbH, Hanau, D

## Materials and Methods

<b>Device</b>	<b>Type</b>	<b>Company</b>
Inverted Microscope	Axiovert 25	Carl Zeiss, Jena, D
Laser Scanning Microscope (LSM)	Axiovert 200M, LSM 510 Meta	Carl Zeiss, Jena, D
Microwave		Sharp Electronics (Europe) GmbH, Hamburg, D
PCR cycler	Mastercycler epgradient	Eppendorf, Hamburg, D
pH-meter	ph Level 1	inoLab, Weilheim, D
Power Supply	EPS601	Amersham, Freiburg, D
Precision scale	LE244S-0CE	Sartorius, Göttingen, D
Rotary shaker	CERTOMAT®IS	B. Braun Melsungen AG, Melsungen, D
Scale	BL 1500S	Sartorius, Göttingen, D
Semi Dry Blotter	TE77	Amersham, Freiburg, D
Shaker	Polymax 1040, 2040	Heidolph, Schwabach, D
Shaker	KS260 basic	IKA, Staufen, D
Spectrophotometer	Nano-Drop-1000	PEQLAB Biotechnologie GmbH, Erlangen, D
Stirrer, incl. heating	MR3001	Heidolph, Schwabach, D
Sterile work bench	Clean Air	Heraeus Holding GmbH, Hanau, D
Stereotactic instrument	Just for Mouse Stereotaxic Instrument STO-51730	Stoelting Co., Wood Dale, IL
Tecan Microplate-Reader	Genios Pro	Tecan, Crailsheim, D
Thermomixer	comfort 1,5 ml	Eppendorf, Hamburg, D
Vacuum pump	Vacunsafe comfort	VacuSafe IBS Integra Bioscience, Chur, CH
Vertical gel-electrophoresis chamber incl. accessory parts	SE250	Hoefer, San Francisco, USA
Vortex mixer	Reax control	VWR, Darmstadt, D
Water bath	SW22	Julabo Labortechnik GmbH, Seelbach, D
X-ray device	Y.TU320	Yxlon International GmbH, Hamburg, D

### 4.1.2 Further materials

**Table 4.2.** Materials used for the biochemical, molecular-biological and cell culture experiments.

<b>Material</b>	<b>Company</b>
Cell culture flasks; T-25, T-75, T-175 cm <sup>2</sup>	Corning Life Science, Wiesbaden, D
Cell culture plates, 96-Well, flat bottom	Corning Life Science, Wiesbaden, D
Cell culture plates; 6-, 12-, 24-Well	BD, Heidelberg, D
Cell culture plates; 60 mm, 100 mm	BD, Heidelberg, D
Cell scraper; 40 cm	BD, Heidelberg, D
Centrifuge tubes; 15 ml, 50 ml	Greiner Bio-one GmbH, Frickenhausen, D
Coverslips, 12 mm, round	Glaswarenfabrik Karl Hecht KG, Sondheim, D
Cryo vials	Biochrom, Berlin, D
Glass pasteurpipets	Brand GmbH u. Co. KG, Wertheim, D
Hamilton-Syringe, 100 µl	Hamilton Bonaduz AG, Bonaduz, CH
Hamilton-Syringe, 10 µl	Hamilton Bonaduz AG, Bonaduz, CH
Hyper <sup>TM</sup> ECL-films	Amersham, Freiburg, D
Instrument case	Roth, Karlsruhe, D
Insulin syringe, 0,3 mm x 12 mm	Braun, Melsungen, D
Laboratory bottles	Schott AG, Mainz, D
Nitrocellulose membrane Protran; 0,2 µm	Schleicher & Schuell, Dassel, D
Microscopy slides, Superfrost	Roth, Karlsruhe, D
Pipette tips with filter, sterile; 10-1000 µl	Sarstedt, D
Pipettes; 1, 5, 10, 25 ml	BD, Heidelberg, D
Pipette controller, accu jet pro	Brand, Herrenberg, D
Protein A/G beads, 50% slurry	Alpha Diagnostics, Paramus, USA
Reaction tube, Safe Lock; 1,5 ml, 2 ml	Eppendorf, Hamburg, D
Reaction tube rack	Rotilab, Roth, Karlsruhe, D
Whatman filterpaper; 3 mm	Bender-Hobein, Zürich, CH

### 4.1.3 esiRNA and siRNA

**Table 4.3.** Endoribonuclease-prepared small interfering (esi)RNAs or small interfering (si)RNAs used to silence the indicated genes. Corresponding sequences are shown.

RNAi	Sequence (Sense)	Company
esiRLUC	5'- ATTTATTAATTATTATGATCAGAAAAACATGCAGA AAATGCTGTTATTTTTTTAC-3'	Eupheria Biotech
esiSYNM	5'- AAACAGACCAGAAACCATCCGAACAAA- GCCAGAA-GAGAAAATGTTCGATTCTAA-3'	Eupheria Biotech
siCTRL#1	5'- AAAACAGUUGCGCAGCCUGAAAtt-3'	MWG Eurofins, Ebersberg, D
siSYNM#1	5'- GCCGAUUAGUCUAGAAGUAtt -3'	MWG Eurofins, Ebersberg, D
siSYNM#2	5'-CGGUGAAUUUCAUGCCGAAtt-3'	MWG Eurofins, Ebersberg, D
siSYNM#3	5'-GCCUUACCAUGCAUUUCCGtt-3'	MWG Eurofins, Ebersberg, D
si-c-Abl	5'-GGCCAUCAACAAACUGGAGtt-3'	MWG Eurofins, Ebersberg, D
siDNA-PKcs	5'-GGCAAUUCGUCCUCAGAUUtt-3'	MWG Eurofins, Ebersberg, D

### 4.1.4 Inhibitors and chemotherapeutic agents

**Table 4.4.** Inhibitors and chemotherapeutics used for *in vitro* experiments.

Inhibitor	Target	Company
Cisplatin Teva®	DNA intercalator	Teva GmbH
Imatinib	c-Abl	Selleckchem
NU7026	DNA-PKcs	Selleckchem
KU55933	ATM	Calbiochem

### 4.1.5 Plasmids

Applied plasmids are described in Table 4.5. The mCherry-Synemin plasmid expressing a red fluorescent synemin fusion protein was a gift from R. J. Bloch (University of Maryland, USA). The plasmid was further validated by sequencing and used for the generation of different synemin constructs (mCherry-Synemin  $\Delta$ Linker-Tail, mCherry-Synemin  $\Delta$ Head-Linker, mCherry-Synemin- $\Delta$ Head-Linker-Tail1, mCherry-Synemin  $\Delta$ Head-Linker-Tail2, mCherry-Synemin  $\Delta$ Head-Linker-S1114A and mCherry-Synemin  $\Delta$ Head-Linker-S1159A) by PCR as described in 4.2.18.1 Corresponding empty vectors were used as control. Vector pEGFP-N1

and ISCEI endonuclease were gifts from K. Borgmann (Medical Center Hamburg-Eppendorf, Germany) (Pierce et al., 1999; Krajewska et al., 2013).

**Table 4.5.** Plasmids used for cloning, overexpression, flow cytometry, fluorescence microscopy and immunoprecipitation.

Plasmid	Resistance	Specification	Supplier
pmCherry-C1	<i>Kan<sup>R</sup>, Neo<sup>R</sup></i>	Expression vector for generation of fusion proteins; high copy number; <i>CMV</i> -Promotor	Clontech
pmCherry-Synemin	<i>Kan<sup>R</sup>, Neo<sup>R</sup></i>	mCherry, high copy number; <i>CMV</i> -Promotor; b-Expression vector expressing $\alpha$ Synemin isoform	R. J. Bloch (University of Maryland, USA)
mCherry-Synemin $\Delta$ Linker-Tail	<i>Kan<sup>R</sup>, Neo<sup>R</sup></i>	mCherry, high copy number; <i>CMV</i> -Promotor; b-Expression vector expressing Synemin Head domain	N. Cordes (TU Dresden, Germany)
mCherry-Synemin $\Delta$ Head-Linker	<i>Kan<sup>R</sup>, Neo<sup>R</sup></i>	mCherry, high copy number; <i>CMV</i> -Promotor; b-Expression vector expressing Synemin Tail domain	N. Cordes (TU Dresden, Germany)
mCherry-Synemin $\Delta$ Head-Linker-Tail2	<i>Kan<sup>R</sup>, Neo<sup>R</sup></i>	mCherry, high copy number; <i>CMV</i> -Promotor; b-Expression vector expressing Synemin first part of the Tail domain (from 301 to 961 AAs)	N. Cordes (TU Dresden, Germany)
mCherry-Synemin $\Delta$ Head-Linker-Tail1	<i>Kan<sup>R</sup>, Neo<sup>R</sup></i>	mCherry, high copy number; <i>CMV</i> -Promotor; b-Expression vector expressing Synemin second part of the Tail domain (from 962 to 1565 AAs)	N. Cordes (TU Dresden, Germany)
mCherry-Synemin $\Delta$ Head-Linker-S1114	<i>Kan<sup>R</sup>, Neo<sup>R</sup></i>	mCherry, high copy number; <i>CMV</i> -Promotor; b-Expression vector expressing Synemin Tail domain with S1114A AA. mutated	N. Cordes (TU Dresden, Germany)
mCherry-Synemin $\Delta$ Head-Linker-S1159	<i>Kan<sup>R</sup>, Neo<sup>R</sup></i>	mCherry, high copy number; <i>CMV</i> -Promotor; b-Expression vector expressing Synemin Tail domain with S1159G AA. mutated	N. Cordes (TU Dresden, Germany)
pcDNA3-Myc-NLS-ISceI	<i>Amp<sup>R</sup>, Neo<sup>R</sup></i>	Expression vector expressing a nuclear localization sequence b-Endonuclease for DSB induction; high copy number; <i>CMV</i> -Promotor	K. Borgmann (Medical Center Hamburg-Eppendorf, Germany).
pEGFP-N1	<i>Kan<sup>R</sup>, Neo<sup>R</sup></i>	Expression vector for generation of fusion proteins; high copy number; <i>CMV</i> -Promotor	Invitrogen

#### 4.1.6 Primers

**Table 4.6.** Primers used for the amplification and flanking of SYNM (synemin gene) with the indicated restriction sites. Respective sequences are shown.

Primer	Sequence (Sense)	Company
Synemin $\Delta$ Linker-Tail-F	5'-AGCTTcgATGCTGTCCTGGCGGCTGCAGACGGCCCCG-3'	MWG Eurofins, Ebersberg, D
Synemin $\Delta$ Linker-Tail-R	5'-AgcTACGACAGGACCGCCGAC-GTCTGCCCGGGGCCTAG-3'	MWG Eurofins, Ebersberg, D
Synemin $\Delta$ Head-Linker-F	5'-cccAAGCTTcg-GTGAAGACCGGCCTCAGTCTGG-3'	MWG Eurofins, Ebersberg, D
Synemin $\Delta$ Head-Linker-R	5'-cgcGGATCC-TTAAAACCAATGCCCATCATTCTC-3'	MWG Eurofins, Ebersberg, D
Synemin_301-961-F	cccAAGCTTcg-GTGAAGACCGGCCTCAGTCTGG	MWG Eurofins, Ebersberg, D
Synemin_301-961-R	cgcGGATCC-CTCCCTCATGCGCTCGGGAAG	MWG Eurofins, Ebersberg, D
Synemin_962-1565-F	cccAAGCTTcg-CTTCCCGAGCGCATGAGGGAGG	MWG Eurofins, Ebersberg, D
Synemin_962-1565-R	cgcGGATCC-TTAAAACCAATGCCCATCATTCTC	MWG Eurofins, Ebersberg, D
Synemin_S1114A-F	CCACAGGCTTTGCCCAGTCACAGGTGCTG-GAGGATG-F	MWG Eurofins, Ebersberg, D
Synemin_S1114A-R	CCACAGGCTTTGCCCAGGCACAGGTGCTG-GAGGATG-R	MWG Eurofins, Ebersberg, D
Synemin_S1159A-F	GCGGGAGGTGAC-CTAGCTCAGGCAGCGAGCCCGACC-F	MWG Eurofins, Ebersberg, D
Synemin_S1159A-R	GGTCGGGCTCGCTGCCTGAGCTAGGTAC-CTCCCGC-R	MWG Eurofins, Ebersberg, D

#### 4.1.7 Polymerases, Restriction enzymes and ligases

HotStar Plus Polymerase with the corresponding 10x PCR Buffer was used for PCR (Quiagen, Hilden, D). High fidelity restriction enzymes (Hind III for forward and Bam HI for reverse), T4 DNA ligase and appropriate buffers were purchased from NEB (Frankfurt a.M).

#### 4.1.8 Bacterial culture

Competent DH5 $\alpha$  *E.coli* (NEB, Frankfurt a.M., D) were cultured on LB agar plates for clone selection or in LB medium for bacteria growth (Table 4.7). The successful and correct PCR amplification and ligation into the target-vector was ensured by sequencing (Eurofins) and agarose-gel electrophoresis.



**Table 4.7.** Composition of media used to culture bacteria.

Medium	Composition	Company
LB medium	10 g Tryptone	AppliChem GmbH, Darmstadt, D
	5 g Yeast extract	AppliChem GmbH, Darmstadt, D
	Ad 1 l H <sub>2</sub> O	
	pH adjusted to 7.0 using 10 M NaOH	AppliChem GmbH, Darmstadt, D
SOC	20 g Tryptone	AppliChem GmbH, Darmstadt, D
	5 g Yeast extract	AppliChem GmbH, Darmstadt, D
	0.5 g NaCl	AppliChem GmbH, Darmstadt, D
	2.5 ml 1 M KCl	AppliChem GmbH, Darmstadt, D
	20 ml sterile 1 M glucose	AppliChem GmbH, Darmstadt, D

To prepare agar plates, 1 l of LB medium was mixed with 15 g Agar (AppliChem GmbH, Darmstadt, D). Then the mixture was autoclaved and supplemented with selection antibiotics ampicillin (AppliChem GmbH, Darmstadt, D) or kanamycin (AppliChem GmbH, Darmstadt, D) at concentrations 100 µg/mL and 30 µg/mL respectively.

#### 4.1.9 Protein and DNA ladders

Protein ladder used for SDS gel electrophoresis:

- PageRuler Unstained (ThermoFisher Scientific, Erlangen, D);
- HiMark™ Pre-Sained Protein Standard (Novex®, ThermoFisher Scientific, Erlangen, D).

DNA ladder for agarose gel electrophoresis: 1 kb DNA ladder (NEB, Frankfurt a.M., D).

#### 4.1.10 Method kits

**Table 4.8.** Method kits used for biochemical applications.

Kit	Application	Company
BCA Protein Assay Kit	Determination of protein concentration	Pierce, Bonn, D
ECL Western Blotting Detection Reagents	Western blot detection	Amersham, Freiburg, D
Proximity Ligation Assay Kit Duolink®	Protein-Protein interaction	Sigma Aldrich, Taufkirchen, D
QuikChange II Site-Directed Mutagenesis Kit	Site directed mutagenesis	Agilent, Waldbronn, D
NucleoSpin® Gel and PCR cleanup kit	Cleanup of PCR products or vectors after enzymatic digestion	Macherey & Nagel, Düren, D

### 4.1.11 Primary antibodies

**Table 4.9.** Primary antibodies used for Western blot, immunoprecipitation and immunofluorescence.

Antibody	Application	Dilution	Company
ATM, rabbit, monoclonal	Western blot	1:1000	Abcam, Cambridge, UK
	Immunoprecipitation	10 $\mu$ l	
ATM S1981, mouse, monoclonal	Western blot	1:500	Rockland, Pennsylvania, USA
$\beta$ -Actin, Klon AC-15, mouse, monoclonal	Western blot	1:10000	Sigma Aldrich, Taufkirchen, D
DNA-PKcs, rabbit, polyclonal	Western blot	1:1000	Cell Signaling, Frankfurt a. M., D
	Immunoprecipitation	10 $\mu$ l	
DNA-PKcs S2056, rabbit, polyclonal	Western blot	1:500	Abcam, Cambridge, UK
	Immunofluorescence	1:200	
	PLA	1:100	
c-Abl, rabbit, polyclonal	Western blot	1:1000	Cell Signaling, Frankfurt a. M., D
	immunoprecipitation	10 $\mu$ l	
c-Abl T715, rabbit, polyclonal	Western blot	1:500	Cell Signaling, Frankfurt a. M., D
c-Abl Y412, rabbit, polyclonal	Western blot	1:1000	Cell Signaling, Frankfurt a. M., D
	Immunoprecipitation	10 $\mu$ l	
Ku70, mouse, monoclonal	Western blot	1:1000	Abcam, Cambridge, UK
$\gamma$ H2AX S139, mouse, monoclonal	Western blot	1:1000	Millipore, Massachusetts, USA
	Immunofluorescence	1:200	
53BP1, rabbit, polyclonal	Immunofluorescence	1:200	Novus Biologicals, Colorado, USA
Desmuslin, mouse, monoclonal	Western blot	1:500	Abcam, Cambridge, UK
	PLA	1:100	
Desmuslin, rabbit, polyclonal	Western blot	1:500	Abcam, Cambridge, UK
Desmuslin, mouse, monoclonal	Immunoprecipitation	3.5 $\mu$ g	Santa Cruz, Dallas, USA
	Immunofluorescence	1:100	
BrdU, mouse, monoclonal	FACs Analysis	1:50	BD, Heidelberg, D
PARP1, rabbit, polyclonal	Western blot	1:1000	Cell Signaling, Frankfurt a. M., D
HP1 $\alpha$ , rabbit, polyclonal	Western blot	1:1000	Cell Signaling, Frankfurt a. M., D
	Immunofluorescence	1:200	
MEK1/2, rabbit, polyclonal	Western blot	1:1000	Cell Signaling, Frankfurt a. M., D

#### 4.1.12 Secondary antibodies

**Table 4.10.** Secondary antibodies used for Western blot, immunoprecipitation, immunofluorescence or immunohistochemical applications.

<b>Antibody</b>	<b>Application</b>	<b>Dilution</b>	<b>Company</b>
Anti-mouse IgG, HRP conjugated	Western blot	1:5000	Pierce, Bonn, D
Anti-rabbit IgG, HRP conjugated	Western blot	1:5000	Pierce, Bonn, D
Anti-mouse IgG, HRP conjugated	Immunoprecipitation	1:1000	GeneTex, Irvine, USA
Anti-rabbit IgG, HRP conjugated	Immunoprecipitation	1:1000	GeneTex, Irvine, USA
Alexa Fluor®488 Anti-mouse IgG	Immunofluorescence	1:200	Life Technologies GmbH, Darmstadt, D
Alexa Fluor®488 Anti-rabbit IgG	Immunofluorescence	1:200	Life Technologies GmbH, Darmstadt, D
Alexa Fluor®594 Anti-mouse IgG	Immunofluorescence	1:200	Life Technologies GmbH, Darmstadt, D
Alexa Fluor®594 Anti-rabbit IgG	Immunofluorescence	1:200	Life Technologies GmbH, Darmstadt, D
Alexa Fluor®594 Phalloidin	Immunofluorescence	1:800	Life Technologies GmbH, Darmstadt, D

#### 4.1.13 Solutions for cell biological applications

**Table 4.11.** Solutions used for cell biological applications. The detailed composition for each solution is shown.

Substance	Composition	Company
1x PBS	RT	Sigma Aldrich, Taufkirchen, D
1x Trypsin/EDTA	(4 °C)	Sigma Aldrich, Taufkirchen, D
1% Agarose	1 g Agarose <i>ad</i> 100 ml ddH <sub>2</sub> O	Sigma Aldrich, Taufkirchen, D
10 nM Non-Essential Amino Acid Solution (NEAA)	(4 °C)	Sigma Aldrich, Taufkirchen, D
80% Ethanol	800 ml Ethanol, denatured, 99% <i>ad</i> 1 l ddH <sub>2</sub> O	Berkel, Berlin, D
Cell culture medium	DMEM with GlutaMAX™ (supplemented with 10% FCS, 1% NEAA)	Life Technologies, Karlsruhe, D
Matrigel™ Basement Membrane High Concentration, Laminin rich Extracellular Matrix	20 mg/ml (-20 °C) 10 mg/ml, in DMEM (4 °C) 5 mg/ml, in Komplettmedium (4 °C)	BD, Heidelberg, D
Coomassie stain	100 ml Methanol 37,5 ml Acidic acid 0,25 g Coomassie G250 <i>ad</i> 500 ml ddH <sub>2</sub> O	Roth, Karlsruhe, D Merck, Darmstadt, D Merck, Darmstadt, D
Fetal Calf Serum (FCS)	Heat inactivated prior to use: 30 min at 56 °C (-20 °C)	PAA Laboratories GmbH, Cölbe, D
HEPES solution 1M		Sigma Aldrich, Taufkirchen, D
Lipofectamine2000	(4 °C)	Life Technologies, Karlsruhe, D
Oligofectamine	(4 °C)	Life Technologies, Karlsruhe, D
OptiMEM	with GlutaMAX™ (4 °C)	Life Technologies, Karlsruhe, D

#### 4.1.14 Solutions for protein-biochemical and molecular-biological applications

**Table 4.12.** Solutions used for protein-biochemical and molecular-biological applications. The composition for each solution is shown.

<b>Substance</b>	<b>Composition</b>	<b>Company</b>
10% Ammonium persulfate (APS)	1 g APS <i>ad</i> 10 ml ddH <sub>2</sub> O (-20 °C)	AppliChem GmbH, Darmstadt, D
10x Blotting buffer (Maniatis-SDS)	29 g Glycine 58 g Tris <i>ad</i> 1 l ddH <sub>2</sub> O	Roth, Karlsruhe, D Roth, Karlsruhe, D
1x Blotting buffer	100 ml 10x Blotting buffer 200 ml Methanol <i>ad</i> 1 l ddH <sub>2</sub> O	Roth, Karlsruhe, D
5% BSA solution	0,5 g Bovine Serum Albumin <i>ad</i> 10 ml PBST (4°C)	Serva, Heidelberg, D
1x Cell Lysis Buffer	1 ml 10x Cell Lysis Buffer 40 µl Complete™ protease inhibitor cocktail <i>ad</i> 9 ml ddH <sub>2</sub> O	Cell Signaling, Frankfurt a. M., D
25x Complete™ protease inhibitor cocktail	1 Tablet <i>ad</i> 2 ml ddH <sub>2</sub> O (-20 °C)	Roche Diagnostics GmbH, Mannheim, D
GBX-Developer-Kodak	250 ml Developer <i>ad</i> 1 l ddH <sub>2</sub> O	Kodak, Stuttgart, D
GBX-Fixer-Kodak	250 ml Fixer <i>ad</i> 1 l ddH <sub>2</sub> O	Kodak, Stuttgart, D
10x Loading dye	250 mg Bromphenol blue 33 ml 150 mM Tris (pH 7,6) 60 ml Glycerol <i>ad</i> 100 ml ddH <sub>2</sub> O (4°C)	AppliChem GmbH, Darmstadt, D Roth, Karlsruhe, D Roth, Karlsruhe, D
5% Milk powder	5 g skimmed milk powder <i>ad</i> 100 ml 1x PBS (4 °C)	AppliChem GmbH, Darmstadt, D
Modified RIPA lysis buffer	951 µl RIPA buffer 40 µl 25x Complete™ protease inhibitor cocktail 5 µl 200 mM Na <sub>3</sub> VO <sub>4</sub> 4 µl 500 mM NaF	
200 mM Na <sub>3</sub> VO <sub>4</sub>	3,678 g Na <sub>3</sub> VO <sub>4</sub> <i>ad</i> 100 ml ddH <sub>2</sub> O (-20 °C)	Sigma Aldrich, Taufkirchen, D
500 mM NaF	2,1 g NaF <i>ad</i> 100 ml ddH <sub>2</sub> O (-20 °C)	Sigma Aldrich, Taufkirchen, D

<b>Substance</b>	<b>Composition</b>	<b>Company</b>
20x PBS (pH 7,4)	160 g NaCl	Merck, Darmstadt, D
	4 g KCl	Merck, Darmstadt, D
	36 g Na <sub>2</sub> HPO <sub>4</sub>	Merck, Darmstadt, D
	4,8 g KH <sub>2</sub> PO <sub>4</sub> <i>ad 1 l ddH<sub>2</sub>O</i>	Merck, Darmstadt, D
1x PBS	50 ml 20x PBS <i>ad 1 l ddH<sub>2</sub>O</i>	
PBS/0,05% Tween 20 (PBST)	0,5 ml Tween 20 <i>ad 1 l 1x PBS</i>	Serva, Heidelberg, D
6x Laemmli SDS sample buffer	50 ml 6x sample	Alfa Aesar, ThermoFisher Scientific, Erlangen, D AppliChem GmbH, Darmstadt, D
RIPA buffer	12,5 ml Tris-HCl (pH 7,4)	AppliChem GmbH, Darmstadt, D
	2,5 ml NP-40	Fluka, München, D
	6,25 ml 10% Sodium deoxycholate	AppliChem GmbH, Darmstadt, D
	7,5 ml 5 M NaCl	Merck, Darmstadt, D
	0,5 ml 0,5 M EDTA <i>ad 250 ml ddH<sub>2</sub>O</i> (4 °C)	Roth, Karlsruhe, D
10% SDS	100 g SDS <i>ad 1 l ddH<sub>2</sub>O</i>	Roth, Karlsruhe, D
10x SDS running buffer	30,3 g Tris 144,1 g Glycine 10 g SDS <i>ad 1 l ddH<sub>2</sub>O</i>	Roth, Karlsruhe, D Roth, Karlsruhe, D Roth, Karlsruhe, D
1x SDS running buffer	100 ml 10x SDS running buffer <i>ad 1 l ddH<sub>2</sub>O</i>	
10x TBE buffer (pH 8,0)	108 g Tris	Roth, Karlsruhe, D
	55 g Boric acid	Merck, Darmstadt, D
	40 ml 0,5 M Na <sub>2</sub> EDTA	Merck, Darmstadt, D
	<i>ad 1 l ddH<sub>2</sub>O</i>	
0,5 M Tris buffer (pH 6,8)	30,275 g Tris <i>ad 1 l ddH<sub>2</sub>O</i>	Roth, Karlsruhe, D
3 M Tris buffer (pH 8,8)	181,71 g Tris <i>ad 1 l ddH<sub>2</sub>O</i>	Roth, Karlsruhe, D
Buffer I for Chromatin fractionation	0.5 ml 50 mM HEPES, pH 7.5 0.15 ml 150 mM NaCl	

Substance	Composition	Company
	0.01 ml 1 mM EDTA, pH 8.0 25 µl 0.05% Nonidet P40 <i>ad</i> 4.34 ml ddH <sub>2</sub> O before use add protease inhibitors	
Buffer II for Chromatin fractionation	0.5 ml 50 mM HEPES, pH 7.5 0.15 ml 150 mM NaCl 0.01 ml 1 mM EDTA, pH 8.0 25 µl 0.05% Nonidet P40 <i>ad</i> 4.34 ml ddH <sub>2</sub> O before use add protease inhibitors and 10 µl of 100 µg/ml RNAase plus Benzonase	
Buffer III for Chromatin fractionation	0.5 ml 50 mM HEPES, pH 7.5 0.15 ml 150 mM NaCl 0.01 ml 1 mM EDTA, pH 8.0 25 µl 0.05% Nonidet P40 <i>ad</i> 4.34 ml ddH <sub>2</sub> O before use add protease inhibitors	
Buffer IV for Chromatin fractionation	0.5 ml 50 mM HEPES, pH 7.5 0.45 ml 450 mM NaCl 0.01 ml 1 mM EDTA, pH 8.0 50 µl 1% Triton X-100 <i>ad</i> 3.64 ml ddH <sub>2</sub> O before use add protease inhibitors	

#### 4.1.15 Solutions for immunofluorescence

**Table 4.13.** Solutions used for immunofluorescence and immunohistological applications. The composition for each solution is shown.

Substance	Composition	Company
0,25% Triton X-100	125 µl Triton X-100 <i>ad</i> 50 ml 1x PBS	Roth, Karlsruhe, D
1% BSA	0,5 g Bovine serum albumin (BSA) <i>ad</i> 50 ml 1x PBS	Sigma Aldrich, Taufkirchen, D
3% Formaldehyde	1 ml 37% Formaldehyde <i>ad</i> 11 ml 1x PBS	Merck, Darmstadt, D

#### 4.1.16 Further solutions and chemicals

**Table 4.14.** Further solutions and chemicals used for biochemical, molecular-biological or *in vitro* applications.

Substance	Company
30% Acrylamide bis-acrylamide solution (29:1)	Serva, Heidelberg, D
Agarose, <i>electrophoresis grade</i>	Life Technologies, Karlsruhe, D
Agarose, Type-A	Sigma Aldrich, Taufkirchen, D
Dimethyl sulfoxide (DMSO)	AppliChem GmbH, Darmstadt, D
Ethanol, denatured, 99%	Merck, Darmstadt, D
Formaldehyde, 37%	Merck, Darmstadt, D
G418 Sulfat (100 mg/ml in 0,1 M HEPES)	Calbiochem, Bad Soden, D
Isopropyl alcohol	Merck, Darmstadt, D
Ponceau S	Sigma Aldrich, Taufkirchen, D
ProLong Diamant Antifade Mountant	Life Technologies, Karlsruhe, D
ProLong Diamant Antifade Mountant with DAPI	Life Technologies, Karlsruhe, D
Red Safe™ <i>nucleic acid staining solution</i>	iNtRON Biotechnology, Kyungki-Do, Korea
Tetramethylethylene-diamine (TEMED)	Merck, Darmstadt, D

#### 4.1.17 PC programs

**Table 4.15.** PC programs for data analysis and presentation.

Program	Company
GraphPad Prism 7	GraphPad Software Inc., San Diego, USA
Fiji (Schindelin et al., 2012)	National Institutes of Health
Magellan 5.0 Software	Tecan, Crailsheim, D
Microsoft Office 2010	Microsoft Corp., Redmond, WA, USA
Zeiss LSM Image Browser Version 3,5,0,376	Carl Zeiss GmbH Jena, D
Zeiss AxioVision SE64 Rel. 4.9	Carl Zeiss GmbH Jena, D
FlowJo (Version 7.6.2)	FlowJo LLC, Oregon, USA



## 4.2 Methods

### 4.2.1 Cell culture

Mycoplasma-free HNSCC (Cal33, FaDu, HSC4, SAS, UTSCC5, UTSCC8, UTSCC14, UTSCC15, UTSCC45, XF354fl) cell lines were kindly provided by R Grenman (Turku University Central Hospital, Finland). SKX cells were provided by M Krause (TU-Dresden, D). Stably transfected Cal33-pEJ5GFP and Cal33-pGC cells were obtained from K Borgmann (Hamburg, D). Cells were asynchronously cultured in Dulbecco's modified Eagle's medium containing glutamax-I and supplemented with 10 % fetal calf serum and 1 % non-essential AAs at 37 °C in a humidified 8.5 % CO<sub>2</sub> incubator. Cells were grown to 70-80 % confluency, harvested or subcultured every 3-4 days. Splitting ratios were cell line dependent, but mainly 1:10 was used.

**Table 4.16.** HNSCC cells and origin

Cell line	Origin
Cal33	Tongue
FaDu	Hypopharynx
HSC4	Tongue
SAS	Tongue
SKX	Floor of the mouth
UTSCC5	Tongue
UTSCC8	Larynx
UTSCC14	Tongue
UTSCC15	Tongue
UTSCC45	Floor of the mouth
XF354fl	Floor of the mouth

### 4.2.2 Cell freezing and thawing

Adherently growing cells were trypsinized, resuspended in culture medium and centrifuged at 130 x g for 3 min. Following centrifugation, cells were reconstituted in freezing medium (complete DMEM supplemented with 20 % FCS and 0.5 % DMSO), aliquoted into cryovials and transferred into the liquid nitrogen for the long-term storage.

For thawing, cells were rapidly transferred into the tube with the culture medium, centrifuged at 130 x g for 3 min, resuspended in fresh medium, and seeded on the culture flask.

### 4.2.3 siRNA knockdown

In order to specifically inhibit the expression of genes of interest (Table 4.3), RNA interference technique was used (Elbashir et al., 2001; Kim, 2005). Using endoribonuclease-prepared small interfering (esiRNA) or small interfering RNA (siRNA), the expression of the mRNA from the library, as well as synemin, DNA-PKcs and c-Abl were knocked down (Table 4.3). To this end cells were plated in a 6-well plate or 100 mm Petri dish at concentrations  $3 \times 10^5$  cells or  $1.2 \times 10^6$  cell per well/dish respectively. Twenty-four h after the seeding, cells were transfected using 26.6 nM esiRNA or 20 nM siRNA. Nonspecific control RLUC/siRNA (siCTRL) or specific esi- or si-RNA were diluted in OptiMEM (solution A). In parallel, a second dilution composed of Oligofectamine/OptiMEM was prepared in a different reaction tube (solution B) (Table 4.17). Both dilutions were incubated for 10 min. Subsequently, A and B dilutions were mixed together and the final solution was incubated for 20 min. In the meantime, cells were washed with OptiMEM. Finally, 800  $\mu$ l or 4.8 ml OptiMEM were added per 6-well or 100 mm dish, respectively. Transfection of cells was performed using 200  $\mu$ l (6-well) or 1.2 ml (100 mm dish) transfection mix. Following an 8 h incubation period under standard cell culture conditions, OptiMEM supplemented with 20 % FCS was added (1 ml per 6-well or 6 ml per 100 mm dish). Twenty-four h after transfection, cells were used for experiments.

**Table 4.17.** Pipetting scheme for esiRNA and siRNA transfection in 6-well plates and 100 mm dishes.

			esiRNA dilution		Oligofectamine dilution	
	C <sub>siRNA</sub>	C <sub>final</sub>	RNAi	OptiMEM	Oligofectamine	OptiMEM
6-well plate	20 mM	26 nM	1.33 $\mu$ l	179 $\mu$ l	8 $\mu$ l	12 $\mu$ l
100 mm dish	20 mM	26 nM	8 $\mu$ l	1072 $\mu$ l	48 $\mu$ l	72 $\mu$ l
			siRNA dilution		Oligofectamine dilution	
	C <sub>siRNA</sub>	C <sub>final</sub>	RNAi	OptiMEM	Oligofectamine	OptiMEM
6-well plate	20 mM	20 nM	1 $\mu$ l	184 $\mu$ l	4 $\mu$ l	11 $\mu$ l
100 mm dish	20 mM	20 nM	6 $\mu$ l	1104 $\mu$ l	24 $\mu$ l	66 $\mu$ l

### 4.2.4 Inhibitor treatment and chemotherapy

The chemotherapeutic agents cisplatin and imatinib and the inhibitors of ATM and DNA-PKcs were added into the cells as single compounds or in combination 1 h prior to X-ray irradiation. Dilution of all inhibitors was performed in DMSO. Cisplatin was used at effective concentrations EC<sub>10</sub> and EC<sub>50</sub>, which were determined by the colony formation assay. Imatinib, ATMi and DNA-PKcsi were applied at a final concentration of 10  $\mu$ M. Substances were applied 1 h prior to irradiation.

#### 4.2.5 Radiation exposure

Cells were irradiated at RT using single doses of 200 kV X-rays filtered with 0.5 mm Cu (Yxlon Y.TU 320; Yxlon, Hamburg, Germany). The dose-rate was approximately 1.38 Gy/min at 20 mA. The absorbed dose was measured using a Duplex dosimeter (PTW, Freiburg, Germany) considering temperature and atmospheric pressure. Applied doses were ranged from 0 to 6 Gy X-rays.

#### 4.2.6 3D Colony formation assay

The colony formation assay represents a gold standard for the measurement of genotoxic stress effects induced by ionizing radiation or cytotoxic substances. This assay, frequently used in radiobiology, measures the reproductive integrity of cells (Puck and Marcus, 1956). Cells capable to pass through five or more mitoses and being able to form colonies of at least 50 cells are considered clonogenic (van der Kogel, 2009). These cells, despite being subjected to stress, have retained their capacity to divide indefinitely. The plating efficiency (PE) is a parameter which indicates the percentage of seeded cells that grow into colonies and thereby reflects the basal cell survival (Hall and Giaccia, 2012). PE is calculated using this formula:

$$\text{Plating Efficiency} = \frac{\text{Number of colonies}}{\text{Cells seeded}} \times 100$$

Upon irradiation or treatment with cytotoxic substances the fraction of surviving cells (SF) is calculated as follows:

$$\text{Surviving Fraction} = \frac{\text{Colonies counted}}{\text{Cells seeded} \cdot \frac{PE}{100}}$$

Results are presented as dose survival curves showing mean  $\pm$  s.e.m. from three or more independent experiments, with the dose plotted on a linear scale and surviving fraction on a logarithmic scale (Puck and Marcus, 1956).

Measurement of clonogenicity was performed by plating single cells (Table 4.18) embedded in 0.5 mg/ml laminin-rich extracellular matrix (IrECM) in 96-well culture dishes coated with 50  $\mu$ l of 1 % agarose to avoid cell adhesion (Eke et al., 2009)(Storch et al., 2010b). Dependent on the cell line a specific number of cells per-well (Table 4.18) was seeded in 100  $\mu$ l culture medium together with 0.5 mg/ml IrECM. Cells were incubated at standard cell culture conditions (section 4.2.1) for 24 h allowing the matrix to polymerize. The polymerized matrix was covered with 100  $\mu$ l of cDMEM followed by single radiation doses of 2, 4, 6 Gy or left unirradiated (Fig. 4.1). After the cell line specific incubation period (Table 4.18) cells were fixed with 50  $\mu$ l of 9% FA and stored at 4 °C. Colonies with more than 50 cells were counted by using the inverted microscope.

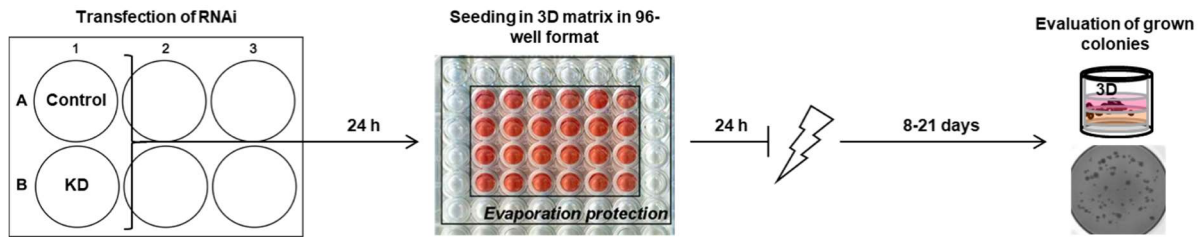


**Figure 4.1: Schematic representation of the 3D colony formation assay workflow.** Cells were transfected with the corresponding RNAi and 24 h after resuspended and reseeded in a 3D IrECM format. Next day cells were irradiated and kept for couple of days at optimal conditions for the colony evaluation later on.

**Table 4.18.** Cell numbers and corresponding incubation periods used for the colony formation assays.

Cell line	Cell numbers [0, 2, 4 and 6 Gy]	Incubation [d]
Cal33	2000	14
FaDu	2000	9
HSC4	2000	8
SAS	2000	8
UTSCC5	2000	14
UTSCC8	3000	21
UTSCC14	1000	8
UTSCC15	1000	8
UTSCC45	1000	8
XF354fl	3000	14

#### 4.2.7 3D high-throughput RNAi-based screening

High-throughput screening (HTS) is a versatile and fast approach to investigate complex biological questions. It is commonly used for the identification of novel drugs, genes or proteins which modulate particular biological mechanism (e.g. survival, apoptosis, DNA repair, metabolism, etc).

#### 4.2.8 Screening development

For the 3D high-throughput RNAi-based screening (3DHT-RNAi-S) development, firstly the library was designed based on the Integrin Adhesome containing all the main focal adhesion (FAPs) proteins present in cells. To do so, 117 FAPs were selectively chosen based on the review from Horton et al., 2015, leaving out receptor tyrosine kinases and transcription factors. On Table 4.19, it is possible to observe all the FAPs that were used for this screen. The library was purchased from Eupheria Biotech.

Once the library was ready, it was necessary to automatize and improve the protocol for 3D colony formation and foci assay. To do so, a special cell line containing pEGFP-53BP1-C1 plasmid was generated for fast quantification of foci. During the generation of the pEGFP-53BP1-UTSCC15 cells, optimization of several parameters was needed:

1. Number of cells to be seeded before transfection (7500, 10000 and 15000 cells per 96-well)
2. Amount of trypsin needed (10, 20, 30 or 50  $\mu$ l per 96-well plate)
3. Amount of needed medium for resuspension after trypsinization (100, 150, 170 or 200  $\mu$ l per 96-well)
4. Number of cells post detachment (evaluation of cell numbers and good detachment)
5. Correct dilution in order to have a homogenous suspension for CFA and residual DSB.

**Table 4.19.** List of focal adhesion proteins selected for the screen library according to the Integrin Adhesome described by Horton et al., 2015.

ACTB	FBLIM1	ITGA9	KIF11	PARVA	SSH3BP
ACTN1	FERMT3	ITGAD	KTN1	PARVB	SVIL
ARPC2	FHL2	ITGAE	LASP1	PFN1	SYNM
BCAR1	FLNA	ITGAL	LDB3	PKD1	TENC1
C20orf42	GAB1	ITGAM	LIMS1	PLEKHC1	TES
CALR	GNB2L1	ITGAV	LIMS2	PPFIA1	TGFB1I1
CASS4	GRB2	ITGAX	LPP	PVR	THY1
CAV1	GRB7	ITGB1	LPXN	PXN	TLN1
CD151	HAX1	ITGB1BP1	LRP1	RDX	TNS1
CD47	IRS1	ITGB2	MSN	RLUC	TRIP6
CEACAM1	ITGA1	ITGB3	NCK2	SDC4	TRPM7
CFL1	ITGA10	ITGB3BP	NDEL1	SDCBP	VASP
CORO1B	ITGA11	ITGB4	NEDD9	SH2B1	VCL
CORO2A	ITGA2	ITGB5	NEXN	SH3KBP1	VIL2
CRK	ITGA3	ITGB6	NF2	SHC1	ZFYVE21
CRKL	ITGA4	ITGB7	NRP1	SLC3A2	ZYX
CSRP1	ITGA5	ITGB8	NRP2	SMPX	
CTTN	ITGA6	JUB	NUDT16L1	SORBS1	
ENAH	ITGA7	KCNH2	OSTF1	SORBS2	
ENG	ITGA8	KEAP1	PALLD	SORBS3	

Once all the parameters were optimized, the workflow of the 3DHT-RNAi-S (Fig. 5.1) consisted of the evaluation of CFA and residual DSB after FAPs knockdown in combination of 0 or 6 Gy X-rays.

#### 4.2.9 3D high-throughput screen using esiRNA (3D HTP-RNAi-S)

Subsequent to the variables optimization, the extended protocol included the following steps.

In the first day, 15000 UTSCC15 cells, stably expressing pEGFP-53BP1-C1, were seeded per 96-well. Twenty-four h after, transfection was performed using a master-mix composed by 18.6  $\mu$ l of OptiMEM, 1  $\mu$ l of esiRNA (with a final concentration of 10 ng) and 0.4  $\mu$ l of Oligofectamine per well. Before adding the solution, cells were washed with OptiMEM and subsequently, 30  $\mu$ l of OptiMEM was added. After that, 20  $\mu$ l of the master-mix was added. Eight h post incubation, 50  $\mu$ l of OptiMEM containing 10% FCS was added to the cells. Next day, cells were trypsinized with 30  $\mu$ l of trypsin and resuspended with 170  $\mu$ l of cDMEM. From this suspension, 50  $\mu$ l were used for the CFA (plus 50  $\mu$ l matrigel (5 mg/ml, with a final concentration of 0.5 mg/ml) and 400  $\mu$ l cDMEM) and 75  $\mu$ l was used for the residual DSB evaluation (plus 30  $\mu$ l matrigel (5 mg/ml, with a final concentration of 0.5 mg/ml) and 195  $\mu$ l cDMEM). Everything was well mixed in 96 deep-well plates.

From the master-mix, 100  $\mu$ l were then transferred in 96-well plates pre-coated with 1% agarose. Next day cells were irradiated with 6 Gy X-rays or left untreated. The residual number of foci was evaluated 24 h post irradiation, while clonogenic survival was measured after 8 d of incubation as published in (Dickreuter et al., 2016b). Cell colonies (>50 cells) were counted.

#### 4.2.10 Immunofluorescence staining

Immunofluorescence is a technique to visualize the localization of proteins of interest based on the specificity of antibody-antigen interactions. A primary antibody is used to specifically bind a protein of interest and a fluorophore-coupled secondary antibody directed against the primary antibody is used for detection. Using a fluorescence microscope or a laser scanning microscope the localization of the protein can be visualised.

To analyze endogenous localization of synemin in HNSCC cell lines,  $40 \times 10^5$  HNSCC cells were grown on glass coverslips. Twenty-four h after the seeding cells were fixed with 3 % Formaldehyde. Following fixation step, coverslips were washed 3 times with ice cold 1x PBS and permeabilized with 0.25% Triton-X-100/PBS for 10 min at RT. After that the washing step cells were blocked with 1 % BSA/PBST for 1 h at RT and incubated with specific primary antibody overnight at 4 °C. Subsequently, fluorophore-coupled secondary antibodies or fluorophore-coupled-Phalloidin (for F-actin staining) were applied for 1 h at RT. Finally, cells were washed three times with 1x PBS and mounted using ProLong Diamant Antifade Mountant with DAPI. Images were acquired using LSM510meta (Zeiss).

#### 4.2.11 Foci assay

To analyze DNA damage, we performed immunofluorescent staining for  $\gamma$ H2AX, 53BP1 and DNA-PKcs S2056. Previously it has been shown that 53BP1, phosphorylated histone H2AX and DNA-PKcs phosphorylated at Serine 2056 are strictly associated with DNA damage and form foci at the DSB sites (Fig. 4.2) (Kopenhagen et al., 2016). For further determination of DSBs, co-localized foci of  $\gamma$ H2AX and 53BP1 (Löbrich et al., 2010) were analyzed. In the current part of the study, we investigated foci kinetic after 30 min, 1h, 2h, 6h, and 24 h post irradiation. For the evaluation of residual foci (the damages that cannot be repaired) cells were fixed 24 h post irradiation.

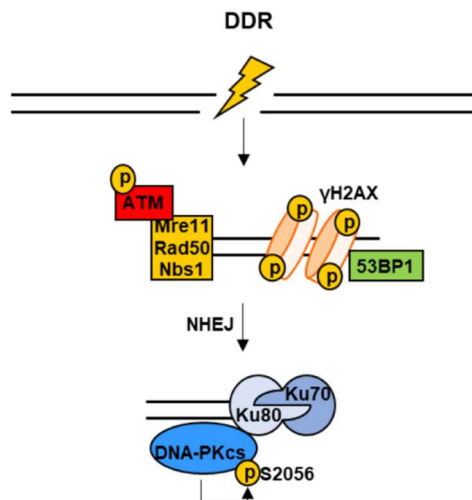


**Figure 4.2: Schematic representation of a DSB marked by  $\gamma$ H2AX and 53BP1.** Phosphorylation of H2AX and binding of 53BP1 to the DNA occurs immediately after the DSB induction. Then, when NHEJ prevails over HR, Ku70/Ku80 complex get recruited at the damage, followed by DNA-PKcs which overactivates itself with a feedback S2056 autophosphorylation.

#### • 2D Foci assay

Cells were seeded and immunostained as described in section 4.2.10. The list of antibodies used for the staining shown in Tables 4.9 and 4.10.

#### • 3D Foci assay

For the 3D culture, 24-well plates were coated with 250  $\mu$ l of 1 % agarose to avoid cell adhesion. For each condition, we seeded  $5 \times 10^4$  cells per well embedded in 0.5 mg/ml of IrECM. After the plating, cells were treated with a single dose of 6 Gy X-rays (non-irradiated cells were used as a control) and fixed 24 h after irradiation (Fig. 4.3). For the fixation procedure, cells were transferred into the 15 ml Falcon tube with PBS, centrifuged at 300 x g, 4 °C for 3 min and incubated with trypsin/EDTA for 10 min at 37 °C in the bacteria shaker. After another centrifugation step (300 x g, 4 °C for 5 min) cells were resuspended and incubated in

3 % formaldehyde for 10 min at RT. Finally, the fixed cells were washed with PBS and permeabilized with 0.25 % Triton X-100 for 10 min at RT. Following the washing step, 1 % BSA blocking solution was applied for 1 h at RT and cells were incubated with the primary anti- $\gamma$ H2AX, -53BP1 or -DNA-PKcs S2056 antibodies overnight at 4 °C. After the incubation cells were washed with PBS and re-probed with secondary antibodies for 1 h at RT in darkness. Thereafter samples were washed with PBS and centrifuged 2 times. Finally, 15  $\mu$ l of cell suspension was mounted on a microscope slide using DAPI-containing Vectashield® mounting medium (Vector Laboratories, California, USA). Nuclei were analyzed using a fluorescence microscope with a 40 x magnification. The number of  $\gamma$ H2AX, 53BP1 and DNA-PKcs S2056 foci were counted in 50 nuclei per condition.

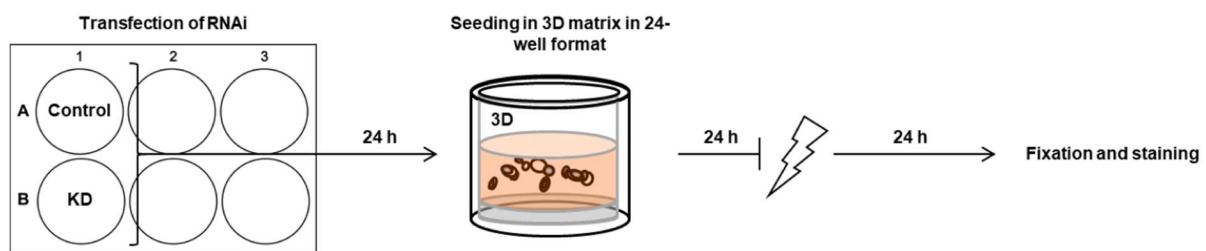


**Figure 4.3: Foci assay workflow.** Cells were transfected with the corresponding RNAi. 24 h after the cells were resuspended and reseeded in a 3D IrECM format. Next day cells were irradiated and 24 h after cells were fixed and stained for foci detection.

## 4.2.12 Total protein extracts, SDS-PAGE and Western Blotting

### 4.2.12.1 Cell lysates

In order to isolate proteins, cells cultured in 2D conditions were washed once with ice cold 1x PBS, lysed in 1xRIPA lysis buffer and detached from the dish using a cell scraper To lyse cells grown in 3D, 3 times concentrated RIPA buffer was applied. For the 3D a condition, 24-well plates were coated with 250  $\mu$ l of 1 % agarose to avoid cell adhesion. For each condition, 1 ml consisting of  $5 \times 10^4$  cells embedded in 0.5 mg/ml were seeded per well. At the proper time point for lysis, 200  $\mu$ l of cells cultivated in IrECM were transferred to a 1.5 ml Eppendorf tube. Rapidly after, cells were lysed with 100  $\mu$ l of 3xRIPA lysis buffer.

For both 2D and 3D cell cultures, cell lysates were incubated on ice for 30 min. and thereafter passed through the insulin syringe in order to break the nuclear membranes. Then, the samples were incubated for 1 h on ice followed by centrifugation for 20 min at 16,000 x g, 4 °C. Finally, the supernatants were transferred to the new 1.5 ml reaction tubes. At this step samples could be stored at -80 °C.

For the 2D samples, protein concentration was determined using the BCA Protein Assay Kit according to the manufacturer's instructions. Using a microplate reader together with



the Magelan 5.0 software, the absorption of standard series and samples were measured and the protein concentration was calculated. For 3D samples, protein concentration was determined through western blot and immunoblotting of  $\beta$ -actin as described in the following section.

#### 4.2.12.2 SDS-Polyacrylamide gel electrophoresis (SDS-PAGE)

SDS-PAGE, developed by Laemmli (1970), is used to separate proteins of a whole cell lysate according to the molecular weight of proteins. Gels for SDS-PAGE were prepared using the Hoefer Mini gel system. Based on the molecular weight of the target proteins, different separation gels with varying acrylamide concentrations (4 %, 8 %, 10 % and 12 %) were prepared (Table 4.20). For all separations, 5 % stacking gels were used.

25  $\mu$ g of protein was mixed with 6x loading dye and incubated at 99 °C for 5 min to denature high order protein structures. Next, samples and protein ladder were loaded into polyacrylamide gels and separated by electrophoresis with a current of 35 mA per gel.

**Table 4.20.** Composition of stacking and separation gels used for SDS PAGE.

Stacking gel	5 % [ml]	Separation gel	4 % [ml]	8 % [ml]	10 % [ml]	12 % [ml]
ddH <sub>2</sub> O	1,63	ddH <sub>2</sub> O	2,83	2,16	1,83	1,5
0,5 M Tris/HCL pH 6,8	0,72	3 M Tris/HCL pH 8,8	1,25	1,25	1,25	1,25
Acryl amide 30 %	0,5	Acryl amide 30 %	0,67	1,33	1,67	2,00
50 % Glycerol	0,06	50 % Glycerol	0,10	0,10	0,10	0,10
10 % SDS	0,03	10 % SDS	0,05	0,05	0,05	0,05
10 % APS	0,06	10 % APS	0,10	0,10	0,10	0,10
TEMED	0,0048	TEMED	0,004	0,004	0,004	0,004

#### 4.2.12.3 Western Blot

The electrophoretically separated proteins were transferred onto a nitrocellulose membrane using a semi dry blotter Hoefer, TE77X at 35mA per gel for 3h. In detail, the stacking gel was removed from the glass and 6 sheets of Whatman paper as well as one sheet nitrocellulose membrane were soaked with 1x blotting buffer. The different components were assembled as shown in Figure 4.4 **Fehler! Ungültiger Eigenverweis auf Textmarke..** Proteins were transferred for 3 h using a current of 35 mA (0.8 mA pro cm<sup>2</sup>) per membrane. Following protein transfer, membranes were incubated with the PonceauS solution, a negatively charged dye, which reversibly binds to the protein AAs. Subsequently, membranes were destained in

1x PBS and blocked for 1 h in 5 % milk powder or 5 % BSA solution according to the instructions of antibody manufacturers.

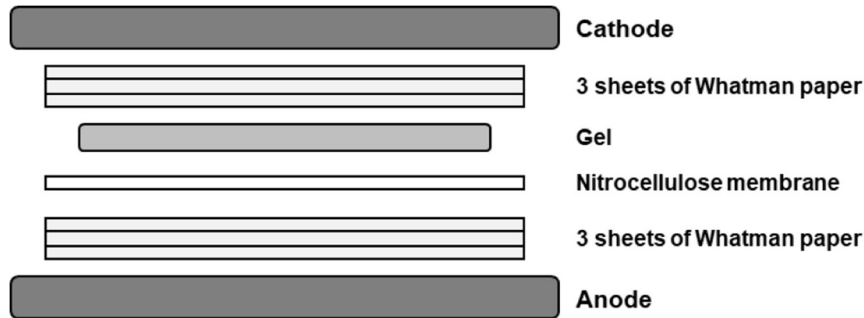


**Figure 4.4: Scheme of the Western blot setup.** Whatman paper and nitrocellulose membrane were soaked with 1x blotting buffer. Three sheets of Whatman paper were placed on the anode and covered with the nitrocellulose membrane followed by the gel. Finally, 3 sheets of Whatman paper and the cathode were placed on top.

Then membranes were treated with primary antibodies overnight at 4 °C under continuous rotation. After the incubation step, membranes were washed 4x for 10 min in PBST and horseradish peroxidase-conjugated (HRP) secondary antibodies were applied for 1.5 h at RT. Finally, membranes were washed in PBST (5 x 10 min) and PBS (1 x 10 min) and incubated for 3 min with the ECL Western Blotting Detection system. Chemiluminescent signals were detected by using X-ray films exposed to the prepared membrane. X-ray films were developed, fixed, washed in water and air-dried. Then the films were scanned and densitometric analysis of western blot bands was performed using the ImageJ Fiji software. Protein band intensity was then normalized to  $\beta$ -actin (for total protein) or total protein expression (for analysis of phosphorylations).

#### 4.2.13 DRGFP and EJ5GFP-based chromosomal break reporter assay

To study the activity of HR and NHEJ, we utilized DRGFP- and pimEJ5GFP-based reporter assays (Bennardo et al., 2008; Krajewska et al., 2013). The reporter pimEJ5GFP plasmid (Fig. 4.5) contains two I-SceI sites in the 5' untranslated region of the GFP transcript and an artificial start codon (ATGart) inserted between both I-SceI sites, which prevents GFP translation. I-SceI cleavage removes the artificial ATG. Subsequent rejoining of the free DNA ends via NHEJ reactivates translation and leads to green fluorescence.

In case of the DRGFP reporter plasmid, the substrate is composed of two differentially mutated GFP genes oriented as direct repeats and separated by puromycin N-acetyltransferase gene (a drug selection marker). One of the GFP genes, SceGFP, is mutated in order to be recognized by the rare-cutting I-SceI endonuclease, which generates DSB upon expression. The second GFP gene is truncated and used to repair SceGFP in case of

HR-mediated DSB repair, which results in the generation of one functional GFP copy detectable by flow cytometry (Fig. 4.5).

HNSCC cell line Cal33 was stably transfected with DRGFP and pimEJ5GFP plasmids as previously published (Pierce et al., 1999). In order to measure HR/NHEJ-mediated repair, control and synemin esiRNA-treated cells were transiently transfected with pcDNA3BMy-NLS-I-SceI plasmid (hereafter designated as I-SceI plasmid) by the use of Lipofectamine 2000 according to the manufacturer's protocol. In parallel with I-SceI, the pEGFP-N1 plasmid (hereafter designated as pN1 plasmid) (Clontech) was introduced to determine transfection rates. Four h after the transfection with I-SceI and pN1 plasmids, cells were trypsinized and embedded into 0.5 mg/ml IrECM. In case of the synemin overexpressing cells (mCherry-Synemin and mCherry-C1), mCherry-Synemin plasmid or control mCherry-C1 plasmid were introduced together with the pN1 and I-SceI plasmids using Lipofectamine 2000 according to manufacturer's instructions. Cal33 cells were then reseeded in 3D, trypsinized at 72 h and subjected to the flow cytometry analysis (BD LSRII flow cytometer; Beckton Dickinson).  $2 \times 10^4$  events were measured per sample. GFP positive cells were normalized to pEGFP-N1-positive cells. Data analysis was performed using FlowJo software (version 7.6.2).

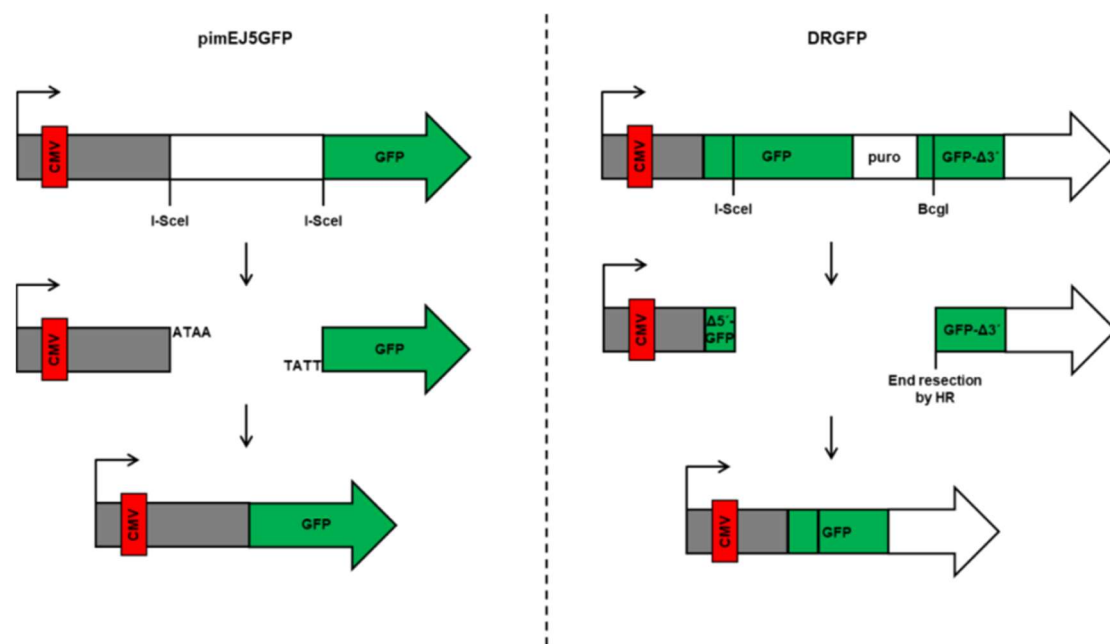


**Figure 4.5: Schematic representation of the EJ5GFP and the pGC reporter plasmid.** EJ5GFP contains two I-SceI sequences inserted into the 5' region that cannot be translated into the GFP transcript. Once the sequence gets excised, the plasmid will get ligated by NHEJ and the GFP sequence will be read and expressed. DRGFP plasmid has two mutated GFP genes oriented as direct repeats and separated by a puromycin gene. One of the GFP mutated genes will get resected by the endonuclease and the second one will be subjected to end resection and repair by HR. The result of both assay will lead to one functional GFP copy. Modified according to Bennardo et al., 2008.

#### 4.2.14 Cell Cycle analysis

Cell cycle analysis was performed using the 5-bromo-2-deoxyuridine (BrdU) incorporation assay. BrdU is a thymidine analog which integrates into DNA of cells during the S-phase of the cell cycle. To determine the number of cells in G1/G0, S and G2 phases control and synemin-deficient SAS cells with and without irradiation were cultured for 24, 48 and 72 h. Then BrdU solution (BD Biosciences) was added into the cells at concentration 10 mM 10 min before cell detachment (1x trypsin/EDTA) and fixation (80 % ice-cold ethanol). Following washing step with cold PBS, cells were incubated for 10 min with 0.01 % RNase A (Sigma-Aldrich), treated with 2 N HCl (Sigma-Aldrich) for 30 min and permeabilized with 0.5 % Triton-X-100/PBS (Carl Roth GmbH). Subsequently, mouse anti-BrdU antibodies and propidium iodide (Sigma-Aldrich) were added to analyze BrdU incorporation and total DNA content. Cell cycle distribution was determined by using FACs Canto™ II with the FlowJo software (version 7.6.2).

#### 4.2.15 Kinome analysis

Kinase activity analysis in cells upon synemin knockdown and irradiation was performed using the phosphotyrosine kinase (PTK) and serine-threonine kinase (STK) microarrays (PamGene). Each array contained 140 (STK) and 144 (PTK) peptides with known phosphorylation sites. For each condition, 12-well plates were coated with 400 µl of 1 % agarose to avoid cell adhesion. After synemin depletion using esiRNA, 1 ml consisting of  $1.5 \times 10^6$  cells embedded in 0.5 mg/ml IrECM, were plated per well. The next day cells were treated with 6-Gy X-ray or left unirradiated. Cells were lysed with 10x kinase buffer (#9802, Cell Signaling), supplemented with HALT phosphatase and protease inhibitor cocktail (#1862495 and #1862209, Thermo Scientific) at 1 and 24 h after 6Gy X-ray treatment (non-irradiated cells were used as a control). Using a 200 µl pipette, cells clusters were collected from the IrECM and transferred to a 1.5 ml Eppendorf tube. Rapidly after, cells were lysed with 100 µl of 3x lysis buffer. The lysate was then resuspended using an insulin syringe and kept on ice for 30 min. After that, they were centrifuged for 20 min at 16,000 x g and 4 °C. The supernatant was removed and transferred to a new 1.5 ml reaction tube. Snap-frozen samples were sent to the Genomics and Proteomics Core Facility Microarray (German Cancer Research Center, Heidelberg) for analysis of kinase activity on a Pamstation 12 System (PamGene). In brief, the arrays were blocked with 2 % BSA in water for 30 cycles and washed 3 times with PK assay buffer. Kinase reactions were performed for 1 h at 30 °C. Phosphorylated peptides were detected using fluorescence labeled antibodies (anti-rabbit-FITC) FITC-labeled arrays were then imaged using a 12-bit CCD camera. BioNavigator software (PamGene International BV) was employed for quantification of the images obtained from the phosphorylated arrays. A list of significantly phosphorylated peptides was generated from the control and

knockdown samples and analyzed with GeneGo, PhosphoSite database and KinMap to predict main down/upregulated kinases. The experiments were performed in triplicate.

### 4.2.16 Immunoprecipitation

Immunoprecipitation is a well-established and widely used technique for the detection and analysis of protein-protein interactions. This method is based on precipitation of the antibody-protein complex out of a cell lysate using protein A/G-beads. Subsequently, protein interactome can be characterized by western blotting or mass spectrometry.

For the analysis of endogenous protein-protein interactions, SAS and SKX cells were harvested using 10x cell lysis buffer (Cell Signaling) diluted in ddH<sub>2</sub>O and supplemented with 40 µl/ml Complete protease inhibitor cocktail. The total protein amount was measured by the BCA assay. Then, cell lysates were pre-cleaned with Protein A/G sepharose slurry (50 % v/v). Briefly, the lysate-bead solution was rotated at 4 °C for 1 h, and centrifuged at 500 x g for 5 min. Next, the supernatant was transferred to a new reaction tube and incubated with primary antibodies (IgG as isotype control) for 1 h at 4 °C under continuous rotation. Subsequently, 100 µl of Protein A/G sepharose slurry (50 % v/v) was added to the samples and rotated overnight at 4 °C. Immunoprecipitates were washed 3 times with cold lysis buffer. Whole cell lysates and immunoprecipitated proteins were boiled in 50 µl sample buffer, separated by SDS-PAGE, transferred, and blotted. Protein precipitates were analyzed with specific primary antibodies as indicated.

### 4.2.17 Chromatin fractionation

This assay is used for the extraction of chromatin-bound proteins that can then be quantified with western blot. The protocol is based on the publication from Cheng et al. published on Nucleic Acid Research in 2011. In brief,  $1.5 \times 10^6$  SAS cells were seeded on 100 mm dishes. One of the dishes was left un-irradiated and the other 2 underwent to 6 X-ray treatment. At the appropriate time point, cells were trypsinized and collected in a 15 ml Falcon tube, centrifuge at 150 x g (at 4 °C for 3 min). After the supernatant was removed, the pellet was resuspended in 200 µl of buffer I and let it incubate for 5 min on ice. Then the sample was centrifuged at 1000 x g for 5 min. The supernatant was transferred in a 1.5 ml labeled reaction tube. Next, the pellet was resuspended in 200 µl of buffer II. After 10 min of incubation at RT, the sample was centrifuged for 5 min at 1000 x g. After removing the supernatant, the pellet was further resuspended in 200 µl of buffer III and left it for 40 min on ice. Next, the sample was centrifuged at 16000 x g for 5 min. Finally, the pellet was resuspended in 200 µl of buffer IV and sonicated two times for 15 seconds. The lysates were then stored in the -80 °C and later used for western blot analysis.

## 4.2.18 Expression constructs, site-directed mutagenesis and transfection of plasmids

### 4.2.18.1 PCR

Fluorescent proteins were generated by PCR amplification (Table 4.5) of synemin gene with the addition of restriction sites, restriction digest of PCR product and desired expression vector (Table 4.22) followed by ligation. List of the primers is provided in Table 4.6. Products were purified using the NucleoSpin® Gel and PCR clean up kit according to the manufacturer's instructions.

**Table 4.21.** PCR protocol used to amplify genes of interest and add flanking restriction sites.

Reagent	Required concentration	Amount per PCR tube
PCR buffer (10x)	1x	5 $\mu$ l
dNTP	10 mM	1 $\mu$ l
ForwardPrimer	10 $\mu$ M	1 $\mu$ l
Reverse Primer	10 $\mu$ M	1 $\mu$ l
MgCl <sub>2</sub>	25 mM	1.25 $\mu$ l
HotStar Plus Polymerase	5 units/ $\mu$ l	0.25 $\mu$ l
cDNA	500 ng/ $\mu$ l	Plasmid dependent
H <sub>2</sub> O		<i>Ad</i> 50 $\mu$ l

Truncated synemin constructs (mCherry-Synemin  $\Delta$ Linker-Tail, mCherry-Synemin  $\Delta$ Head-Linker, mCherry-Synemin<sub>301-961</sub> and mCherry-Synemin<sub>962-1565</sub>) were generated by PCR-based amplification from expression plasmids, with specific primers (Table 4.6). Constructs were flanked with Kpn I and Bam HI restriction sites and inserted into the Kpn I and Bam HI sites of pmCherry-C1.

**Table 4.22.** Protocol for restriction digest of PCR-products flanked with restriction sites and desired expression vectors. High fidelity restriction enzymes (NEB, Frankfurt a.M., D) were applied.

Reagent	Volume
Purified PCR product	30 µl
Vector 10 µg	Vector dependent
CutSmart	10 µl
Enzyme I	3.5 µl
Enzyme II	3.5 µl
ddH <sub>2</sub> O	<i>ad</i> 100 µl

**Table 4.23.** Protocol for ligation of PCR-products flanked with restriction sites and desired expression vectors. The NEB cloner/Ligation calculator was used to calculate the amount of purified PCR product necessary to achieve a vector:insert ratio of 1:3 or 1:5.

Reagent	Self-ligation control	Amount per PCR tube	
		1:3	1:5
Purified Vector	1 µl	1 µl	1 µl
Purified PCR product	0 µl	Dependent on size of PCR product and vector (calculated with NEB cloner)	
Ligation Buffer	2 µl	2 µl	2 µl
T4 DNA Ligase	1 µl	1 µl	1 µl
ddH <sub>2</sub> O	16 µl	<i>ad</i> 20 µl	<i>ad</i> 20 µl

#### 4.2.18.2 Transformation

Plasmid transformation into the competent DH5α *E.coli* (NEB, Frankfurt a.M., D) was performed using the heat shock method. Briefly, 50 µl competent cell suspension was thawed and incubated with 2 µl plasmid DNA for 30 min on ice. Subsequently, bacteria were heated to 45 °C for 42 s followed by 2 min incubation on ice. After transformation, 950 µl SOC medium was added and bacteria were incubated for 2 h at 500 rpm and 37 °C in a thermomixer. Next, 200 µl bacteria suspension were seeded in agar plates containing either Ampicillin or Kanamycin for selection of successfully transformed clones. After 24 h incubation at 37 °C, positive clones were selected and transferred into a 15-ml centrifuge tube containing 5 ml selection medium and incubated for 6 h at 37 °C using a bacterial shaker. Subsequently, 4

ml of the pre-culture were added to 200 ml selection medium and incubated overnight at 37 °C using a rotary shaker. Plasmid DNA was isolated using the NucleoSpin® Plasmid Easy-Pure kit according to the manufacturer’s instructions and correct integration of the insert-DNA into the desired vector was verified by sequencing.

#### 4.2.18.3 Site-directed mutagenesis

Mutation of the putative synemin phosphorylation sites by ATM (S1114 and S1159) predicted by GSP was performed using the QuikChange II Site-Directed Mutagenesis Kit according to manufacturer’s instructions with specific primers listed in Table 4.6. Putative synemin phosphorylation sites were modified by mutation of serine residues to alanine (S1114 and S1159). The presence of mutated sites was confirmed by sequencing.

#### 4.2.18.4 Plasmid transfection

Cal33-pimEJ5GFP and Cal33-DRGFP were transiently transfected with pcDNA3-Myc-NLS-*ISceI* and pEGFP-N1 plasmids. In brief,  $5 \times 10^5$  cells or  $1.5 \times 10^6$  cells were plated on a 6-well plate or 100 mm Petri dish respectively. Twenty-four h after the seeding, cells were transfected using 4 µg or 24 µg of plasmid. The plasmid was diluted in OptiMEM (solution A). In parallel, a second dilution composed of Lipofectamine 2000/ OptiMEM was prepared in a different reaction tube (solution B) (Table 4.24). Both dilutions were incubated for 5 min. Subsequently, A and B dilutions were mixed together (1:1) and the final solution was incubated for 20 min. In the meantime, cells were washed with cDMEM. Finally, 1 ml or 5 ml of cDMEM was added per 6-well or 100 mm dish respectively. Transfection of cells was performed using 500 µl of transfection mix for the 6-well plate well and 3 ml for the 100 mm dish. Following 5 h incubation period, cells were washed and supplemented with normal growth medium. Similarly, SAS cells were transiently transfected using the following plasmids: mCherry-C1, mCherry-Synemin, mCherry-Synemin  $\Delta$ Linker-Tail, mCherry-Synemin  $\Delta$ Head-Linker, mCherry-Synemin\_301-961, mCherry-Synemin\_962-1565, mCherry-Synemin\_S1114A and mCherry-Synemin\_S1159A).

**Table 4.24.** Pipetting scheme for plasmid transfection in 6-well plates and 100 mm dishes.

	DNA dilution		Oligofectamine dilution	
	DNA	OptiMEM	Oligofectamine	OptiMEM
6-well plate	4 µg	250 µl	10 µl	250 µl
100 mm dish	24 µl	1.5 ml	60 µl	1.5 ml



#### 4.2.19 2D-Proximity Ligation Assay

The Proximity Ligation Assay is a well-described method to study protein-protein interactions and to identify their subcellular localization (Fig. 4.6). Briefly,  $4 \times 10^5$  cells were irradiated with 6 Gy X-rays one day after the plating on coverslips. At 1 h post irradiation, cells were fixed with cold methanol for 15 min at  $-20^\circ\text{C}$  and incubated with primary antibodies (Desmuslin, Ab211630 and c-Abl 2862P or Desmuslin, Ab211630 and DNA-PKcs S2056, ab18192) overnight. Thereafter PLA assay was performed according to the manufacturer's protocol using the Duolink® PLA – protein detection kit with PLA PLUS and MINUS Probes for mouse and rabbit (DUO92101-1KT, Sigma-Aldrich®). Samples were analyzed using the Axioimager M1 (Carl Zeiss Inc.) fluorescent microscope with a magnification of 40 x.

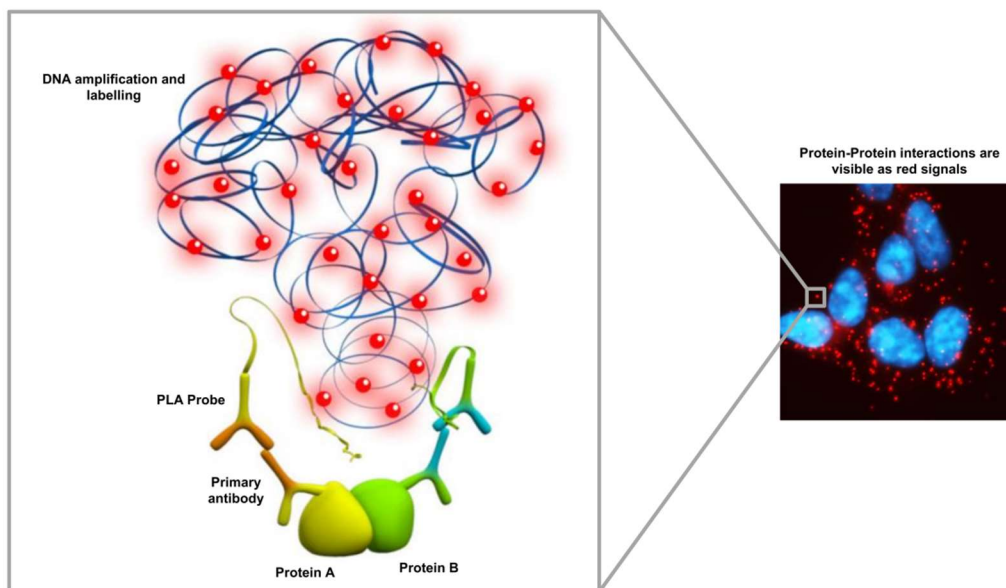


**Figure 4.6: Principle of Proximity Ligation Technique.** Protein A (mouse) and Protein B (rabbit) are recognized by specific primary antibodies. Subsequently, species-specific secondary antibodies (anti-mouse and anti-rabbit) bind to the primary antibodies. Short DNA strands are attached to the PLA samples. If the 2 proteins are in close proximity (<40 nm), the DNA oligonucleotides will be able to hybridize and the enzyme will form a close ligated circle. During amplification, the oligonucleotide sequences are amplified, generating a repeated product. Complementary, fluorescently labeled oligonucleotides can bind and become microscopically detectable at a wavelength of 594 nm. A red signal represents a protein-protein interaction (picture modified from OLINK, Sweden; [www.olin.com](http://www.olin.com), accessed June 2014).

#### 4.2.20 Statistics

The statistical analysis was performed using GraphPad Prism 5 software. All data are presented as a mean  $\pm$  s.e.m. of at least three independent experiments. The significance of data was determined using two-tailed Student's t-test. P-values of less than 0.05 are considered statistically significant.

## 5 Results

### 5.1 3D high-throughput RNAi-based screening

#### 5.1.1 Uncovering novel radioresistance-related focal adhesion proteins

To identify novel FAPs modulating radioresistance and DSB repair in HNSCC, a 3D IrECM high-throughput RNAi-based screen (3DHT-RNAi-S) depleting 117 FAP was designed and performed in UTSCC15 cell line stably expressing EGFP-53BP1 (UTSCC15\_EGFP-53BP1) (Fig. 5.1 and Table 4.19). The screen was carried out under 3D culture system providing a physiological relevant condition compared to 2D cell culture system.

The outcome of 3DHT-RNAi-S provided a consistent and extensive data set (Fig. 5.2a,b and 5.3), allowing to identify several potential protein candidates (Fig. 5.2a,b and 5.3). The association between FAPs, such as  $\beta$ 1 integrin, LIMS1, FAK, and FHL2 and resistance to cancer therapy was previously reported (Eke et al., 2012b; Hehlhans et al., 2012; Rossow et al., 2015; Zienert et al., 2015). In the present study depletion of integrins  $\alpha$ 5,  $\beta$ 3,  $\beta$ 5, as well as TRIP6, OSTF1, ITGB3BP, PLEKHC1 and zyxin in UTSCC15\_EGFP-53BP1 cells remarkably enhanced basal clonogenicity. Interestingly, all integrins which affected the plating efficiency possessed the tripeptide Arg-Gly-Asp (RGD) motif (Takagi, 2004) (Fig. 5.2a and 5.4a). In contrast, a reduction in basal clonogenicity upon knockdown of moesin and KIF-11 was observed (Fig. 5.2a and 5.4a). On the next step, clonogenic survival of UTSCC15\_EGFP-53BP1 cells exposed to 6 Gy X-rays was analyzed, which showed no overlap with the results of the basal survival except for KIF-11 and moesin. These data demonstrated that esiRNA silencing of parvin  $\beta$ , GRB7, vinculin, sorbin and SH3 Domain Containing 2 (SORBS2), and integrin  $\alpha$ 1 significantly enhanced cellular radiosensitivity (Fig. 5.2b and 5.4b), while knockdown in SLC3A2 and CSRP1 mediated remarkable radioresistance (Fig. 5.2b and 5.4b).

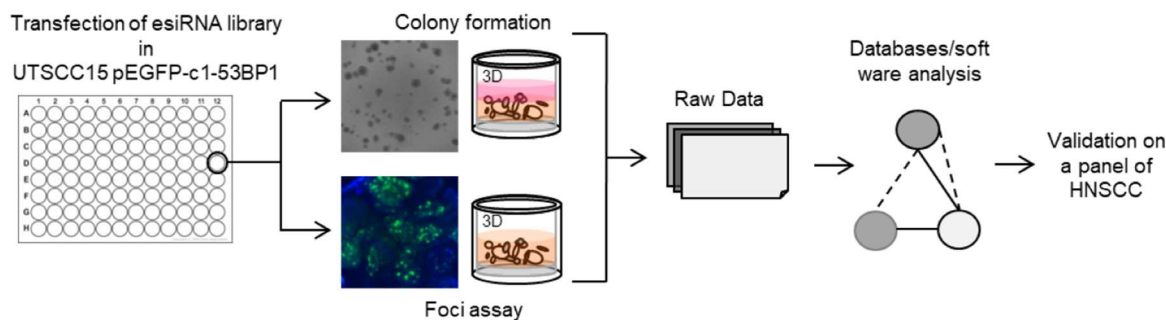


**Figure 5.1: Identification of focal adhesion proteins affecting cell survival, radiosensitivity and DNA repair.** Workflow of 3D high-throughput RNAi screening (3D HTP-RNAi-S).

Residual 53BP1-GFP foci were measured as readout for DSB repair capacity in (un-) irradiated UTSCC15\_EGFP-53BP1 (Fig. 5.3) upon knockdown of the 117 FAPs. Depletion of several FAPs such as integrin  $\alpha$ V,  $\alpha$ 7,  $\alpha$ 8,  $\alpha$ 11, and  $\beta$ 8 subunits as well as kelch like ECH associated protein 1 (KEAP1), LDB3, TGFB1, and SDCBP resulted in a significant increase in the number of 53BP1-GFP foci after irradiation as compared to the control cells (Fig. 5.3 and 5.4c). Remarkably, the numbers of endogenous 53BP1 foci (in non-irradiated cells) remained unaffected (Fig. 5.3). Correlation analysis between the number of 53BP1 foci/cell and clonogenic radiation survival were performed revealing a list of potential FAPs (integrin  $\alpha$ 1 and  $\alpha$ 7, endoglin, SDCBP, KEAP1, synemin, and talin 1) contributing to enhanced radiosensitivity and impaired DSB (Fig. 5.4d). Additionally, depletion of several FAPs (e.g. vinculin, nexin, meosin) led to an enhancement of cellular radiosensitivity without affecting 53BP1 foci/cell. This effect could be associated with alternative pro-survival mechanisms. Altogether, these results imply that a perturbed function in several FAPs significantly affects both radiation survival and DSB repair. Moreover, the 3D-HT-RNAi-S resulted to be a robust screening platform for the identification of the new potential regulators of cellular radiation survival and DSB repair.

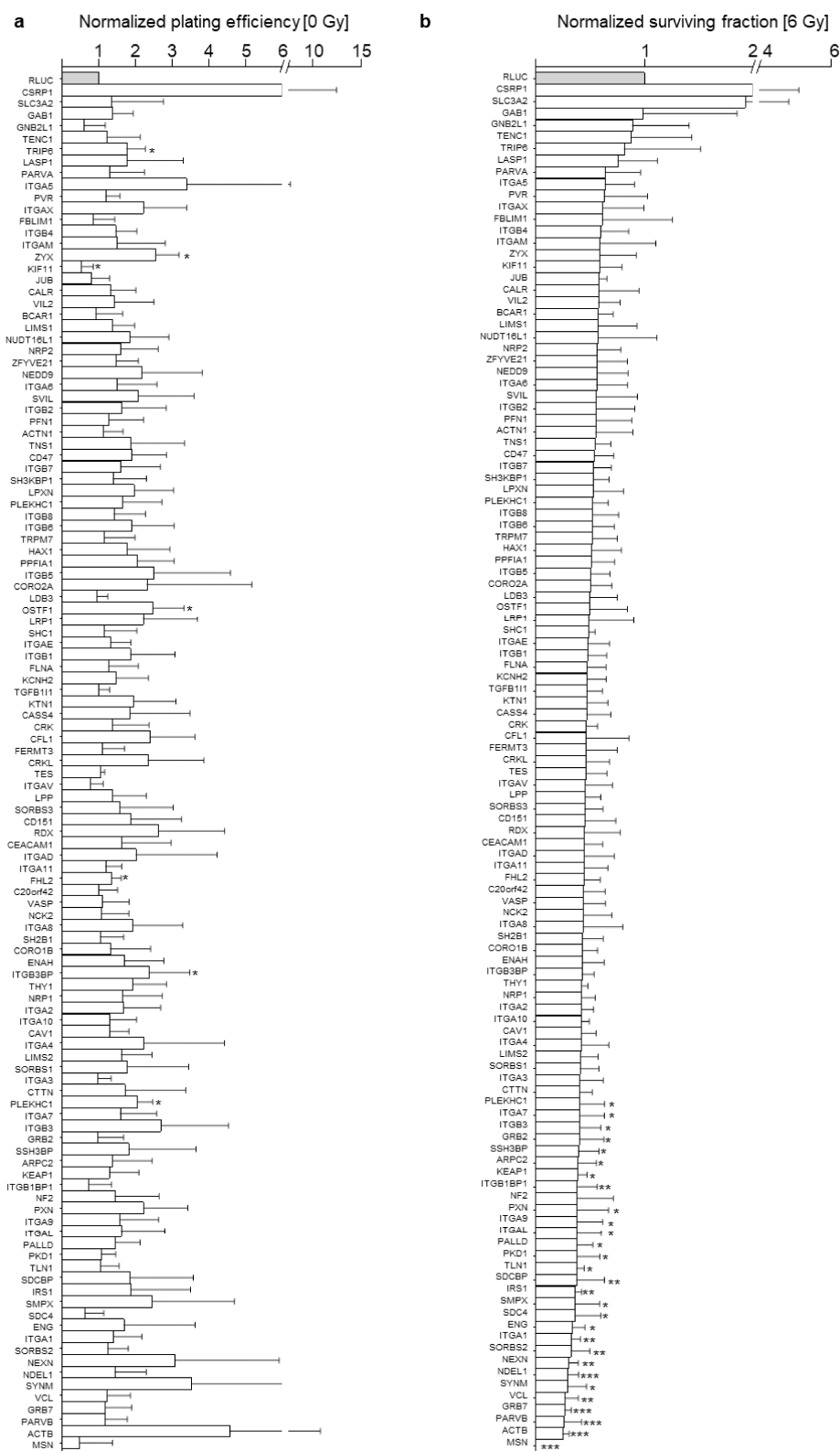


**Figure 5.2: Identification of focal adhesion proteins affecting cell survival and radiosensitivity. a,** Plating efficiency of 3D IrECM cell cultures with indicated knockdown (n = 4). **b,** Surviving fraction of 3D IrECM cell cultures with indicated knockdown and 6 Gy X-rays (n = 4). Data are represented as mean  $\pm$  SD (two-sided t-test; \*P<0.05, \*\*P<0.01, \*\*\*P<0.001).

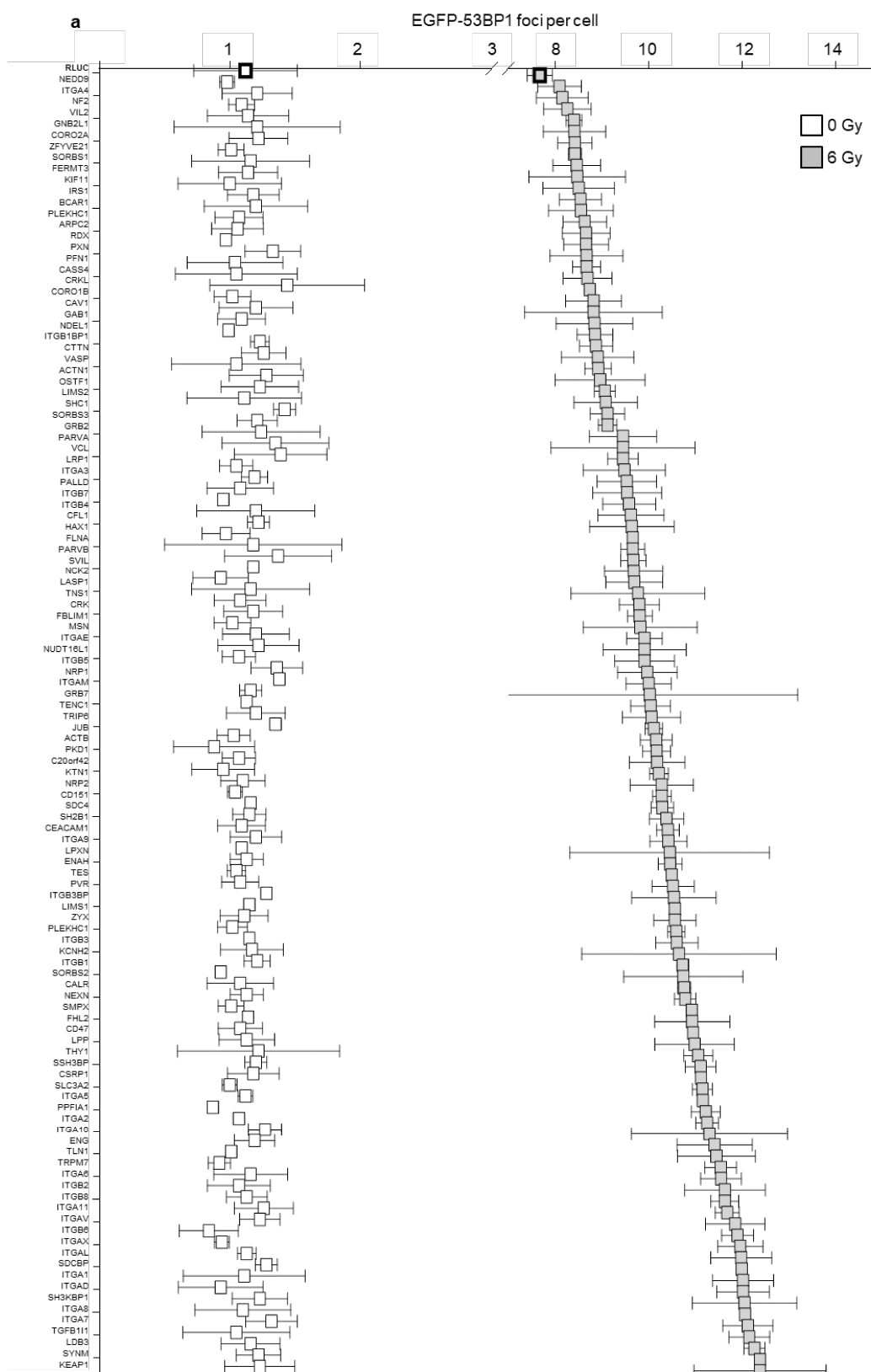


**Figure 5.3: Identification of focal adhesion proteins affecting DNA repair. a,** Residual 53BP1 foci numbers in 6-Gy irradiated, FAPs knockdown cells (grey) and non-irradiated controls (white). Main identified candidates from our screen are outlined in grey area. Data are represented as mean  $\pm$  SD.

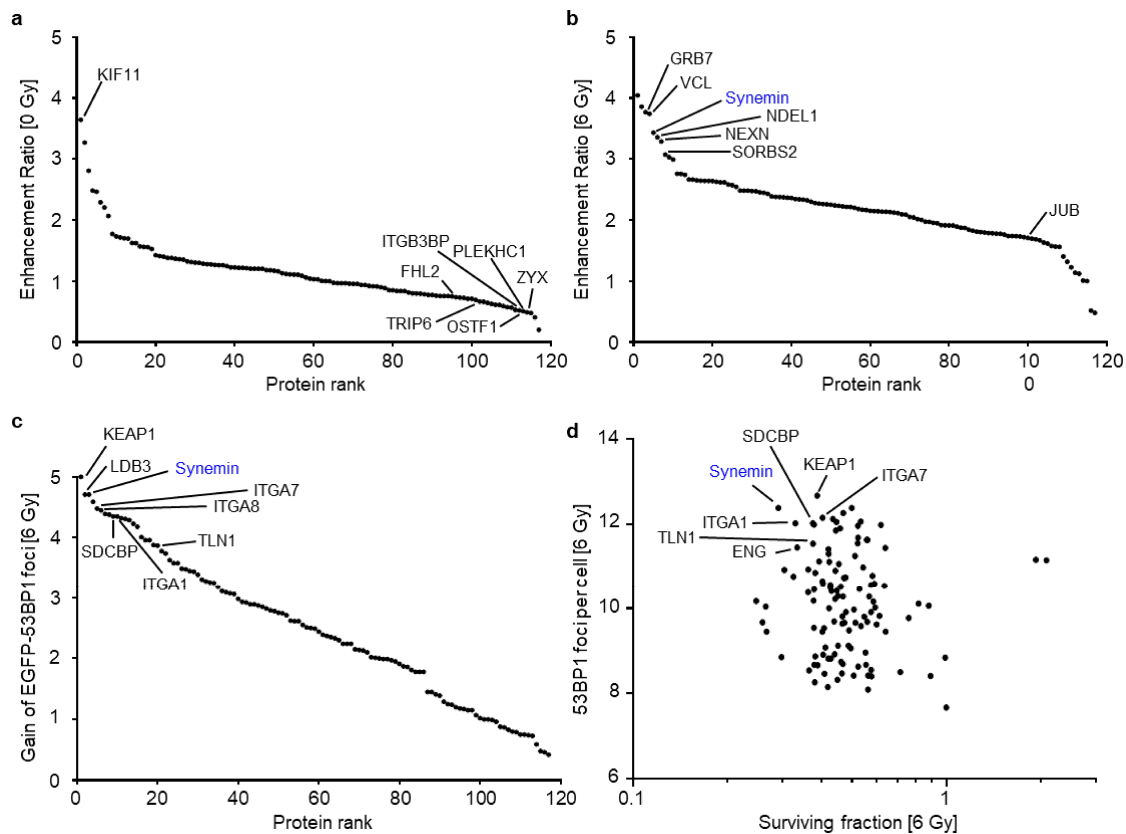


**Figure 5.4: Identification of focal adhesion proteins affecting cell survival, radiosensitivity and DNA repair.** **a**, Enhancement ratios of cell cultures in response to FAP knockdowns (n = 4). **b**, Enhancement ratios of FAP knockdown cell cultures exposed to 6 Gy X-rays (n = 4). **c**, Gain of residual 53BP1 foci number per cell in FAPs knockdown cell cultures irradiated with 6 Gy X-rays (53BP1 foci in controls were subtracted from the total number of foci). **d**, Scatter plot of 53BP1 residual foci/cell against surviving fraction upon FAPs knockdown and 6 Gy irradiation. Main candidates with high foci/cell and low cell survival are shown on the graph.

### 5.1.2 Synemin modulates radiation sensitivity and DNA double strand break repair in HNSCC.

Database- and software-based analyses were performed to filter the targets from the screen. Due to its novelty in HNSCC, synemin was chosen as the main candidate. Based on Oncomine database (<https://www.oncomine.org>), synemin showed an upregulation in different human malignancies including HNSCC compared to the corresponding normal tissues (Fig. 5.5a). In addition, the analysis of the cancer genome atlas dataset demonstrated that synemin was amplified in different types of several squamous cell carcinomas, such as HPV negative HNSCC, lung squamous cell carcinomas (LUSCC) and cervix squamous cell carcinomas (CESCC) (Fig. 5.5b) (Network, 2015).

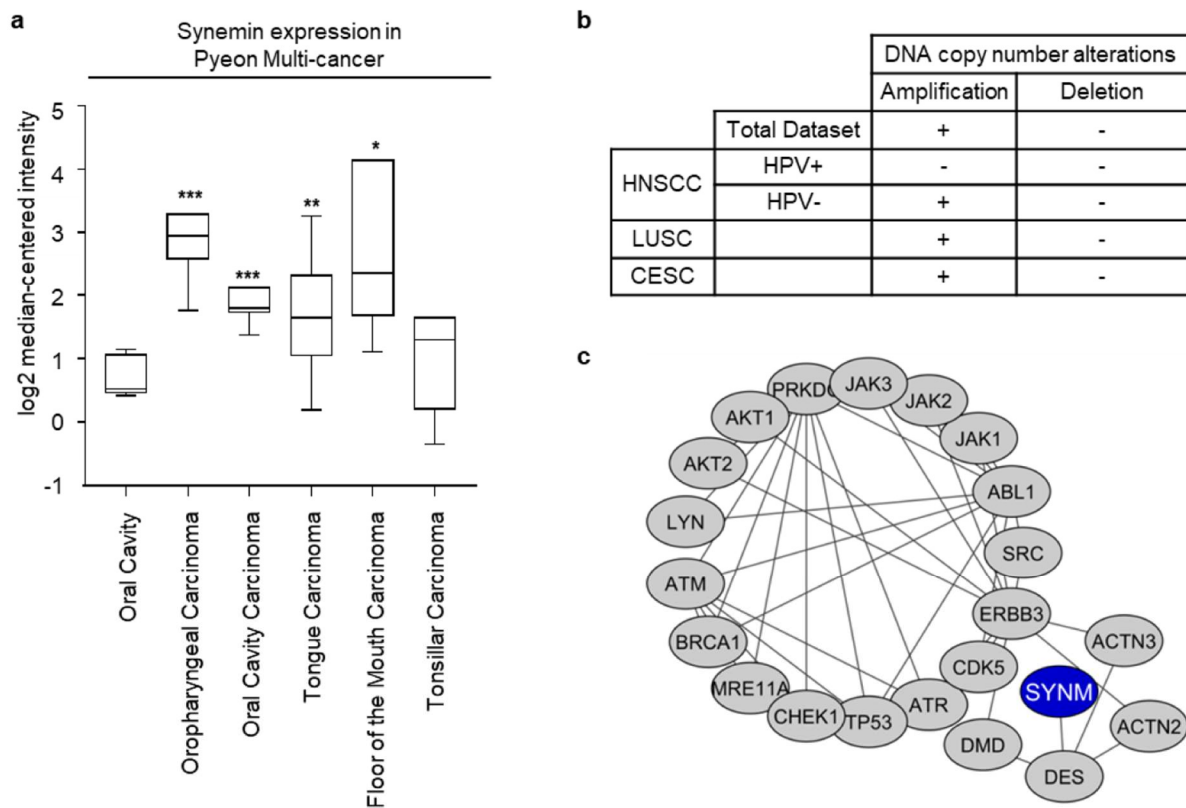


**Figure 5.5: Top focal adhesion protein affecting cell survival.** **a**, To evaluate synemin overexpression of the head and neck carcinomas in comparison to the corresponding normal tissue, the mRNA level was analyzed using Oncomine database (<https://www.oncomine.org>). **b**, DNA copy number alterations from TCGA data (Comprehensive genomic characterization of head and neck squamous cell carcinomas, The Cancer Genome Atlas Network). **c**, Interactome map of synemin using Cytoscape software (<https://cytoscape.org/>) with Reactome plugin. Data are represented as mean  $\pm$  SD (two-sided t-test; \* $P < 0.05$ , \*\* $P < 0.01$ , \*\*\* $P < 0.001$ ).

Interactome prediction of the main candidates in DNA repair response using Cytoscape software (Xue et al., 2008) with Reactome plug-in revealed synemin as a potential interactor of ATM and ATR (Fig. 5.5c).

To validate the function of synemin in DNA damage repair response clonogenic survival and 53BP1 foci assay was carried out in a panel of ten 3D grown HNSCC cell lines upon synemin depletion and X-ray radiation exposure. The basal clonogenic survival, as well as the endogenous 53BP1 foci number, of all tested HNSCC cell lines remained unaltered upon synemin knockdown (Fig. 5.6a-c).

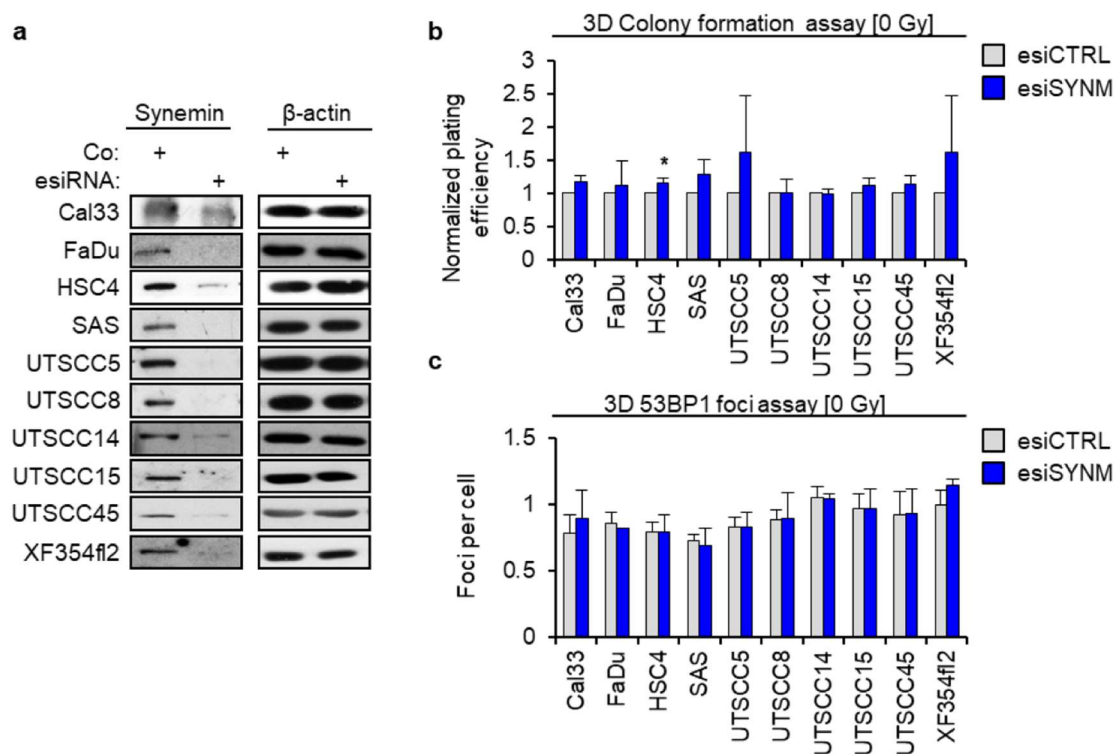


**Figure 5.6: Synemin essentially controls cellular radiosensitivity and DSB repair.** **a**, Immunoblots with knockdown efficiencies in a panel of HNSCCs. **b**, Normalized plating efficiency of a panel of HNSCCs upon synemin inhibition ( $n \geq 3$ ). **c**, Spontaneous foci per cell in a panel of HNSCC upon synemin inhibition ( $n = 3$ ). Data are represented as mean  $\pm$  SD (two-sided t-test; \* $P < 0.05$ ).

Interestingly, synemin depletion led to significant radiosensitization of seven out of ten cell lines relative to controls (Fig. 5.7a,b). Likewise, synemin silencing elicited a significant increase in the number of 53BP1 foci in all HNSCC cell lines after irradiation (Fig. 5.7c,d). To confirm these results, SAS cells were transfected with mCherry-Synemin plasmid inducing overexpression of the protein (Fig. 5.7e,f). Contrary to synemin depletion, SAS cells overexpressing mCherry-Synemin showed a higher clonogenic survival and a reduced residual 53BP1 foci number after irradiation relative to the controls (Fig. 5.7g,h).



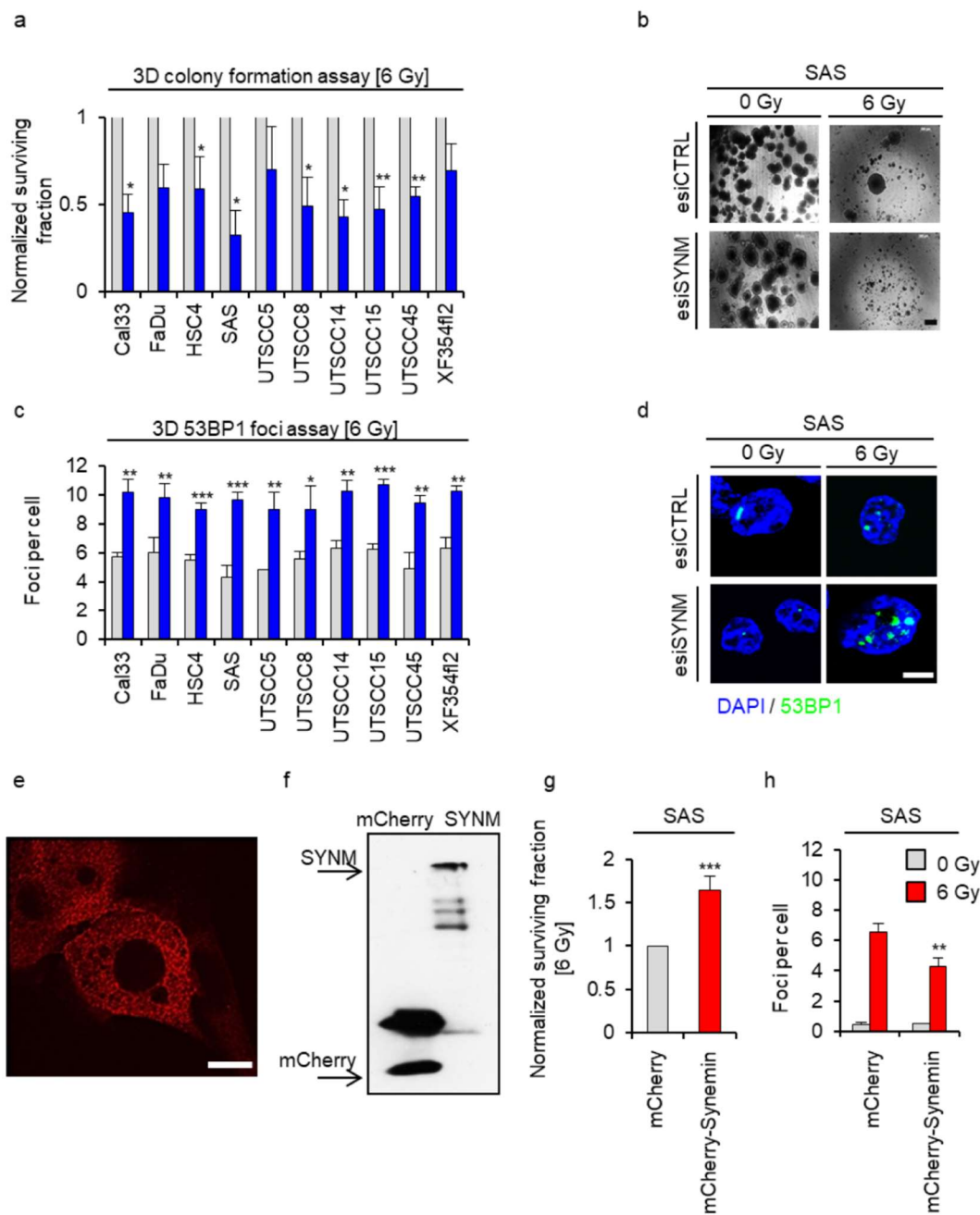


**Figure 5.7: Synemin essentially controls cellular radiosensitivity and DSB repair.** **a**, Clonogenic radiation survival of 6-Gy X-ray irradiated 3D IrECM HNSCC cell cultures after esiRNA-mediated synemin depletion ( $n \geq 3$ ) and **b**, representative phase contrast images of 3D IrECM grown cell cultures (bar, 500  $\mu\text{m}$ ). **c**, Effect of synemin silencing on residual 53BP1 foci in a panel of 6-Gy irradiated 3D IrECM HNSCC cell lines ( $n = 3$ ) and **d**, corresponding representative immunofluorescence images (bar, 10  $\mu\text{m}$ ). **e**, Fluorescence image of mCherry-Synemin positive SAS cell (bar, 10  $\mu\text{m}$ ). **f**, Immunoblotting of the mCherry-Synemin compared to the mCherry empty vector. **g**, Clonogenic radiation survival of mCherry-Synemin transfectants relative to mCherry controls (6 Gy X-rays) ( $n = 3$ ). **h**, Residual 53BP1 foci in mCherry-Synemin transfectants exposed to 6 Gy X-rays ( $n = 3$ ). Data are represented as mean  $\pm$  SD (two-sided t-test; \* $P < 0.05$ , \*\* $P < 0.01$ , \*\*\* $P < 0.001$ ).

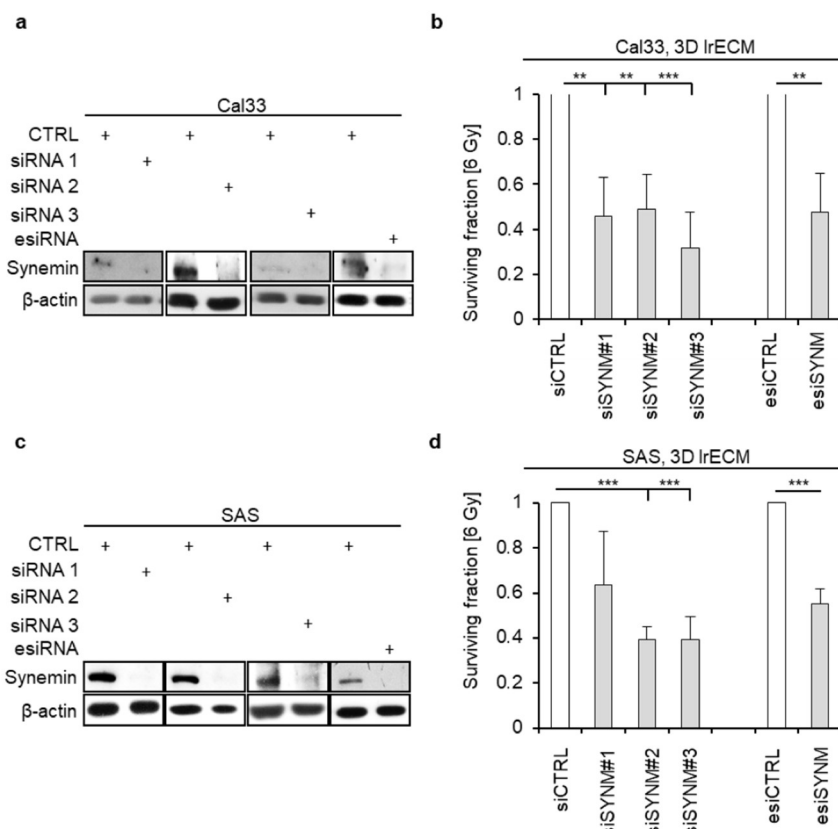


**Figure 5.8: Synemin essentially controls cellular radiosensitivity.** a-d, Knockdown efficiencies using 3 different siRNAs for synemin silencing in Cal33 and SAS cells (a,c) and survival fraction (b,d) (n = 3). Data are represented as mean  $\pm$  SD (two-sided t-test; \*\*P<0.01, \*\*\*P<0.001).

Depletion of synemin by using the different siRNAs, to verify off target effects, were achieved in Cal33 and SAS cells upon synemin knockdown. This experiment revealed that all tested synemin siRNAs, led to enhanced radiosensitivity (Fig. 5.8a-d).

To further delineate the role of synemin in radio(chemo)resistance, a platinum-based genotoxic substance-cisplatin that directly binds to DNA inhibiting its replication (common chemotherapeutical for HNSC patients) was applied in combination with/ without X-rays irradiation under synemin depletion. Upon synemin depletion, cells responded to both treatment approaches showing significantly higher levels of residual 53BP1 foci relative to controls (Fig. 5.9b). In contrast, numbers of residual  $\gamma$ H2AX and 53BP1/ $\gamma$ H2AX colocalized foci did not differ when cisplatin was applied as monotherapy. The combinatorial treatment irradiation/cisplatin, interestingly, significantly induced residual  $\gamma$ H2AX and 53BP1/ $\gamma$ H2AX colocalized foci number (Fig. 5.9b).

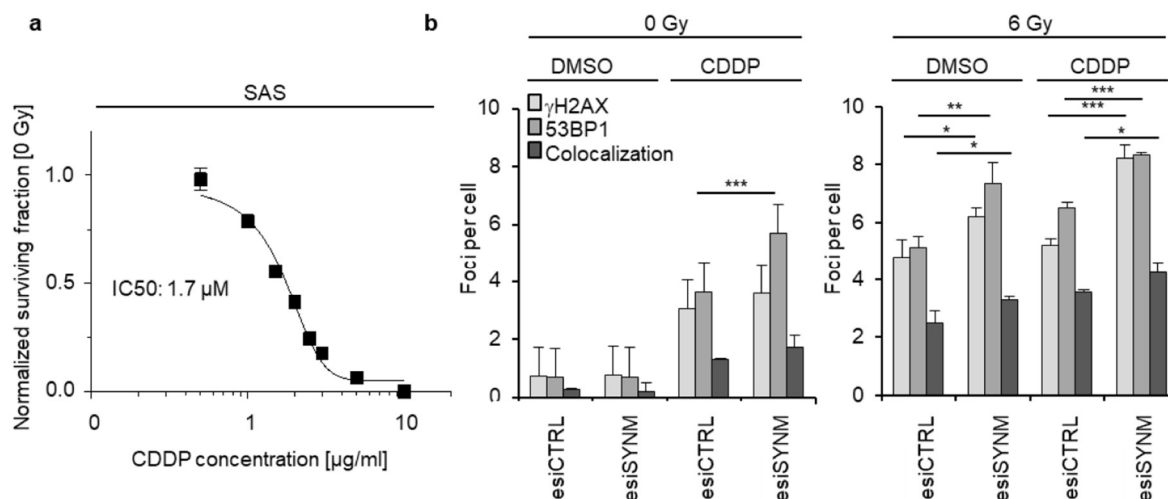


**Figure 5.9: Synemin characterization upon radiochemotherapy.** **a**, Dose-response relationship of SAS cells upon cisplatin (CDDP) exposure ( $n = 3$ ). **b**, Effect of synemin depletion on 53BP1,  $\gamma$ H2AX and colocalized foci numbers upon CDDP treatment in combination with and without irradiation ( $n = 3$ ). Data are represented as mean  $\pm$  SD (two-sided t-test; \* $P < 0.05$ , \*\* $P < 0.01$ , \*\*\* $P < 0.001$ ).

In conclusion, the intermediate filament and focal adhesion protein synemin regulates clonogenic survival of HNSCC through the modulation of DSB repair after irradiation and cisplatin treatment.

### 5.1.3 Analysis of synemin dynamics after irradiation

To characterize synemin expression and its subcellular localization, immunofluorescence staining of synemin was performed in all tested HNSCC cell lines. Synemin was predominantly localized in the cytoplasmic compartment with a slight accumulation in the perinuclear area and the area adjacent to the cell membrane (Fig. 5.10). Remarkably, an exposure of HNSCC cells to X-rays significantly induced synemin expression on the protein level, which peaked at 1 h after irradiation and decreased back to the expression level of non-irradiated cells 24 h later. At the same time, immunofluorescence staining of SAS and Cal33 cell lines demonstrated a presence of filament-like synemin structures within 30 min after irradiation. These structures (Fig. 5.11a,b) further developed into a strong and stable network in the cytoplasm, which persisted within 6 h after X-ray exposure. In contrast, non-irradiated cells did not reveal any complex synemin organization. Nevertheless, it is questionable whether the reorganization of synemin surrounding the nucleus is associated with its scaffold function (Fig. 5.11a-c).

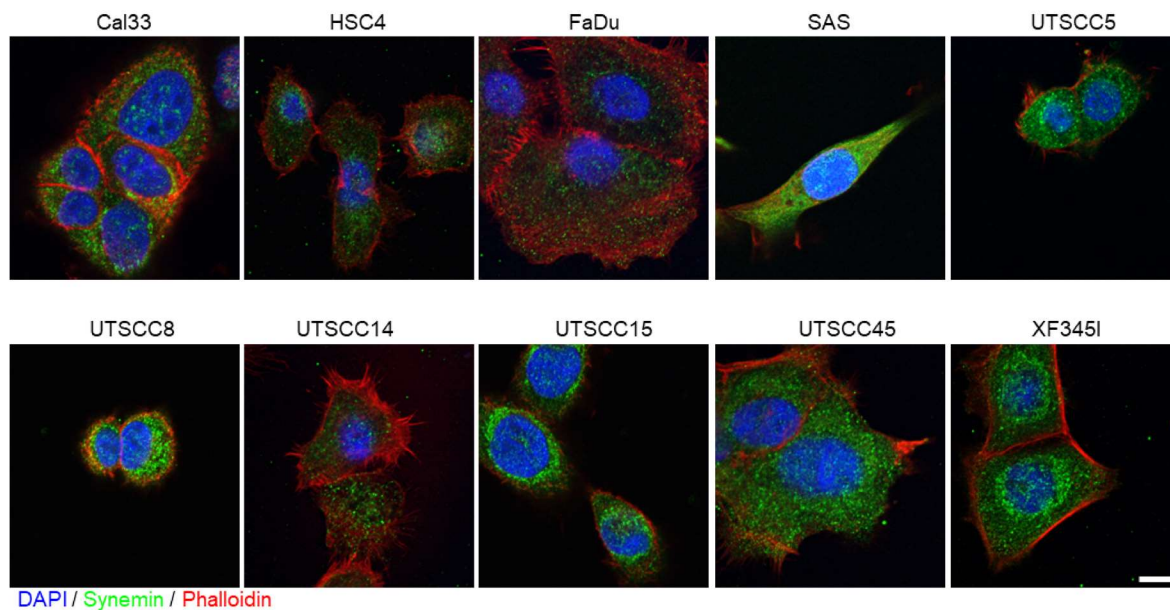


**Figure 5.10: Synemin distribution in a panel of 10 HNSCC cell lines.** Immunofluorescence staining of synemin distribution (green) in a panel of HNSCCs. Cells were counterstained with phalloidin (red) and DAPI (blue) (bar, 20  $\mu$ m).

To further investigate and validate the kinetics of synemin, a chromatin fractionation assay was carried out. Chromatin was fractionated into 4 fractions as followed: fraction I consisted solely of membrane components, fraction II was composed of cytoplasmatic proteins, fraction III contained nuclear protein that loosely bound to chromatin and fraction IV included proteins with a strong affinity to chromatin. The result indicated that synemin was primarily observed in the fractions I and II, with a slight accumulation in the fraction IV under normal condition. Interestingly, synemin increased in fraction III 1 h after irradiation (Fig. 5.11d,e).

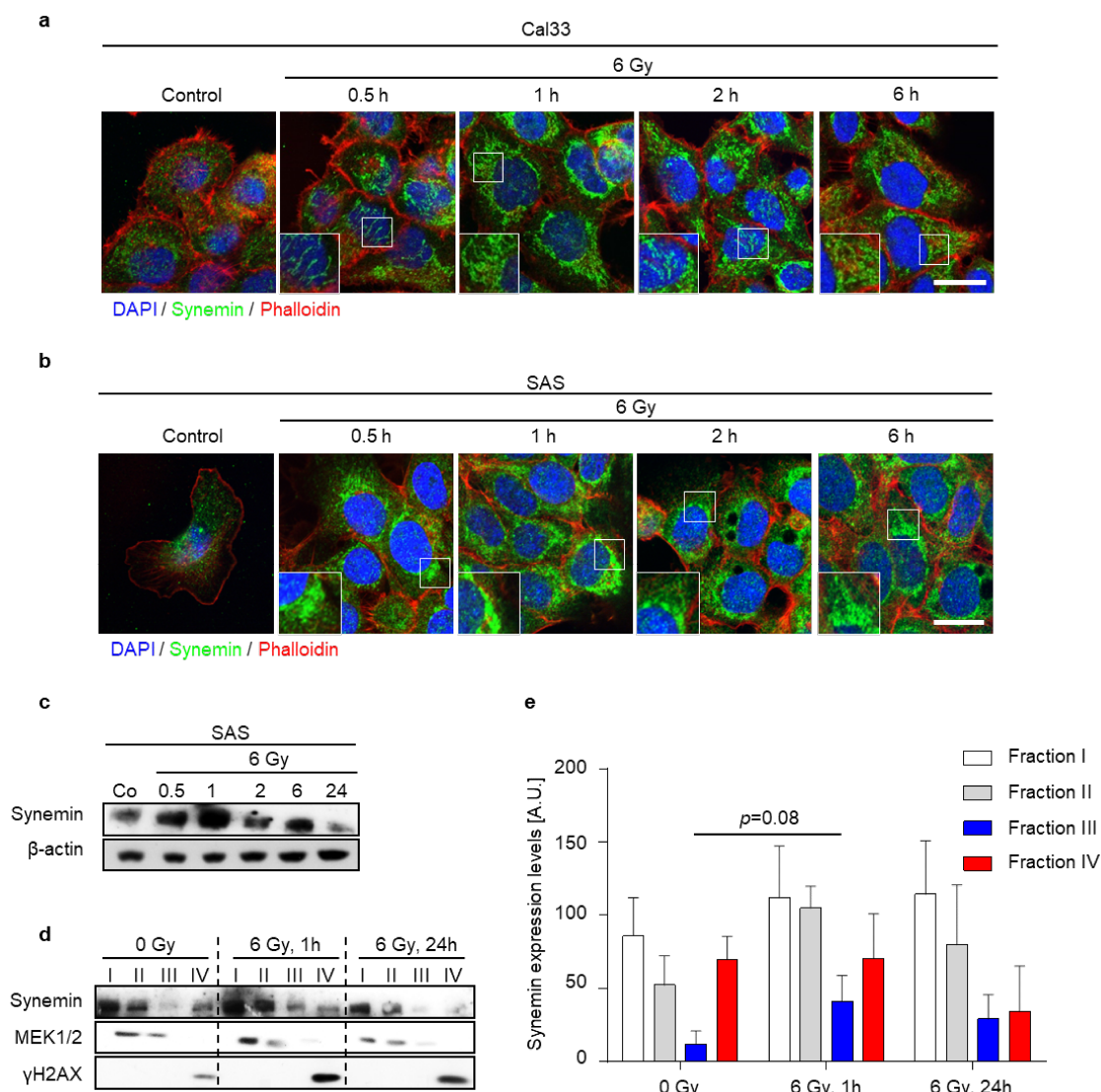


**Figure 5.11: Synemin kinetics upon radiotherapy treatment.** **a**, Subcellular localization of synemin in Cal33 and **b**, in SAS at different time points post 6 Gy X-rays (co-staining with DAPI (nucleus) and phalloidin (actin)) (bar, 20  $\mu$ m). Overview and zoom-in. **c**, Immunoblotting of synemin expression kinetics post 6 Gy irradiation in SAS cells.  $\beta$ -actin served as loading control. **d**, Immunoblots of synemin, MEK1/2 and  $\gamma$ H2AX from the chromatin fractionation (I, II, III and IV fractions) samples after SAS cells were exposed or not to 6 Gy X-ray ( $n = 3$ ). **e**, Densitometries and quantification of synemin protein levels in the different fractions and after the different treatment. Arbitrary units (A.U.). Data are represented as mean  $\pm$  SD.

These data evidence that synemin might have a direct effect on the DNA repair process and are in line with the previous observation showing the accumulation of synemin in the perinuclear area. Collectively, these results suggested that synemin might play an essential role in cell survival after genotoxic injury as well as in the DSB repair.

## 5.2 The role of synemin in DNA repair mechanisms in HNSCCs

### 5.2.1 The effect of synemin knockdown on NHEJ, HR and Alt-EJ in HNSCCs

To investigate the role of synemin in DNA repair mechanisms, DNA repair reporter assays (pGC, pEJ5) were conducted to measure HR and NHEJ activity. While synemin depletion left HR activity unaffected, NHEJ activity was significantly impaired showing a 40% reduction (Fig. 5.12a-c).

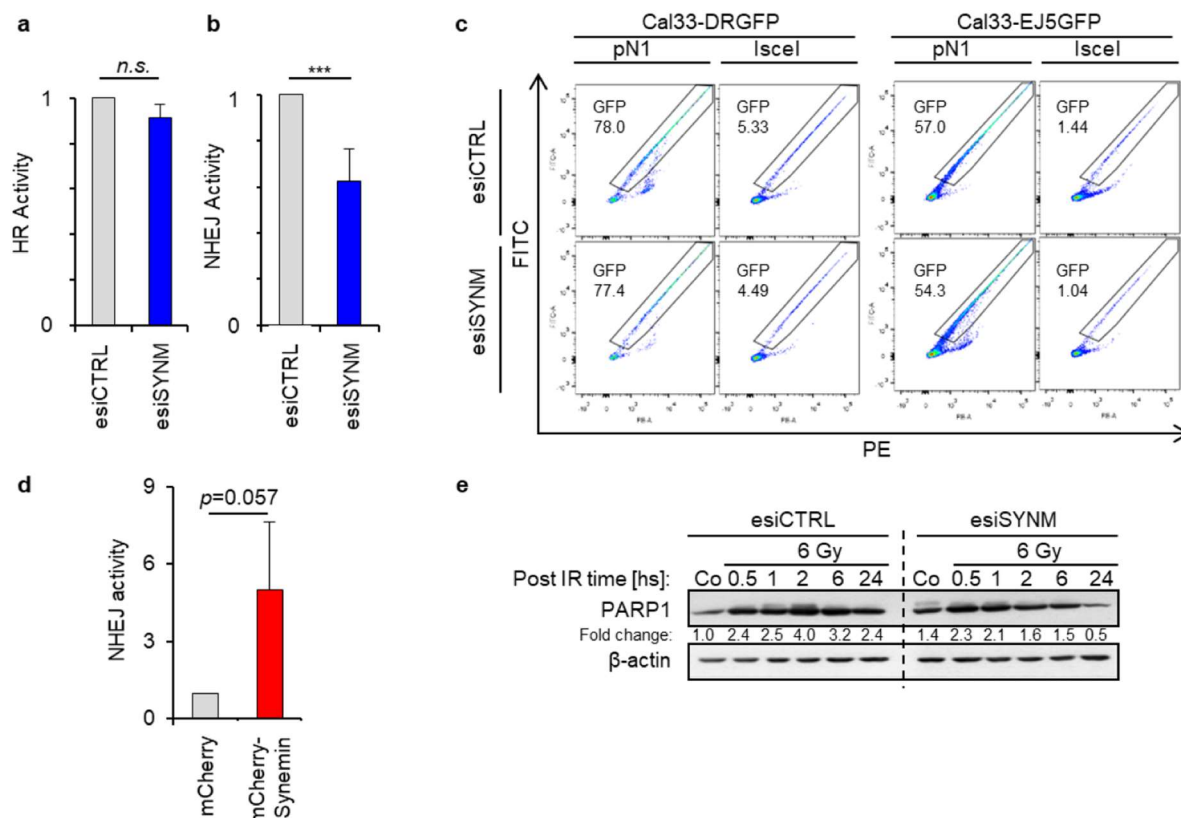


**Figure 5.12: Synemin functions in non-homologous end joining.** **a**, GFP-based reporter assays for HR and **b**, NHEJ. Cal33 cells stably transfected with DRGFP or pimeJ5GFP recombinant plasmids were depleted of synemin ( $n = 3$ ). The number of GFP-positive cells was analyzed by FACS. **c**, Representative figures of DNA repair reporter assay to evaluate homologous recombination (HR) and non-homologous end joining (NHEJ) activity. pN1 is the empty vector (pEGFP-N1) serving as positive control and I-SceI is a plasmid expressing an endonuclease used to generate the DSBs. The cells that have performed DNA repair will express a GFP fluorescent protein. **d**, NHEJ activity in mCherry-Synemin-overexpressing Cal33-pEJ cells ( $n = 3$ ). Analysis performed by FACS as indicated under (a) and (b). **e**, Immunoblots from synemin-depleted and 6-Gy irradiated cells showing total PARP1 levels ( $n = 3$ ).  $\beta$ -actin served as loading control. Fold change quantifications are shown under the respective blot. Data are represented as mean  $\pm$  SD (two-sided t-test; \*\*\* $P < 0.001$ ).

Similarly, synemin overexpression strongly enhanced NHEJ activity of almost three folds compared to the empty vector mCherry-C1 (Fig. 5.12d). Notably and corroborating a specific impact of synemin on NHEJ, neither PARP1 levels (a key protein for Alt-EJ) nor HR showed modifications by synemin silencing in unirradiated and irradiated cells (Fig. 5.12e). To further

demonstrate that synemin is an essential component in the regulation of NHEJ, the expression levels of the main NHEJ associated proteins and their phosphorylated forms were measured i.e. DNA-PKcs, phosphorylated DNA-PKcs at serine 2056 residue (DNA-PKcs S2056), ATM, phosphorylated ATM at serine1891 residue (ATM S1891), and Ku70 (Fig. 5.13 a). Western blot analysis revealed that synemin depletion decreases radiation-induced DNA-PKcs phosphorylation at S2056, especially 1 and 2 h after irradiation. Radiation-induced ATM phosphorylation level at S1891 showed only a trend towards a reduction in synemin deficient cells as compared to the control cells. Strikingly, the level of Ku70 protein was gradually decreased as a function of time due to the synemin deficiency and was undetectable at 2, 6 and 24 h after irradiation (Fig. 5.13a,b). In contrast, synemin overexpression enhanced the expression level of phosphorylated DNA-PKcs at S2056 and Ku70 at the baseline (0 Gy). Altogether, these data suggested that synemin might contribute to the DNA damage repair via NHEJ by modulating DNA-PKcs, ATM and Ku70 functions.

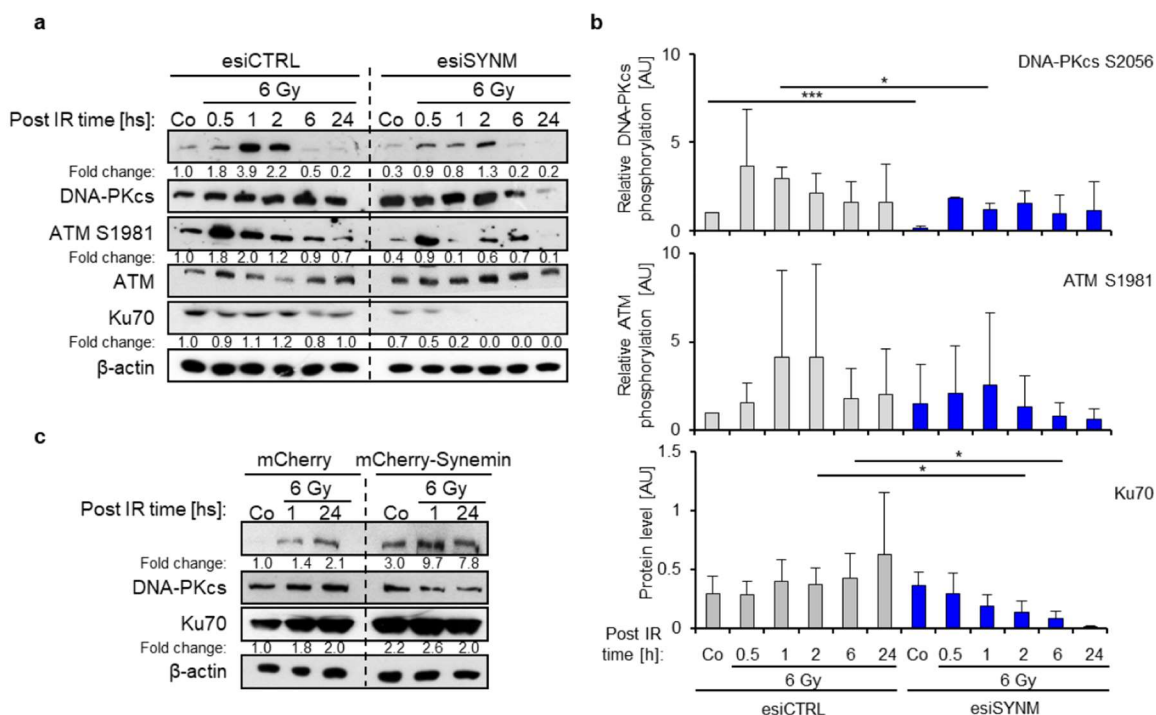


**Figure 5.13: Synemin functions in non-homologous end joining.** **a**, Immunoblots from synemin-depleted and 6-Gy irradiated cells showing total and/or phosphorylation of DNA-Pkcs, ATM and Ku70.  $\beta$ -actin served as loading control. Fold change quantifications are shown under the respective blot. **b**, Densitometries from immunoblots from synemin-depleted and 6-Gy irradiated cells showing phosphorylated or total forms of DNA-PKcs, ATM and Ku70 (n = 4). Phosphorylation levels were calculated relative to the total amount of the respective protein. **c**, Immunoblot of DNA-PKcs and Ku70 from whole cell lysates of 6-Gy X-ray irradiated and mock-treated mCherry-Synemin transfectants (n = 3).  $\beta$ -actin served as loading control. Data are presented as mean  $\pm$  SD (two-sided t-test; \*P<0.05, \*\*\*P<0.001).

### 5.2.2 The effect of synemin knockdown on DNA repair kinetics in NHEJ and cell cycle

As shown above, synemin might be involved in the regulation NHEJ. Therefore, on the next step of this study, foci kinetics of DNA-PKcs S2056 and 53BP1 were determined upon synemin depletion in 1-Gy irradiated cells (Fig. 5.14a-d). Intriguingly and in line with the immunoblotting data, a significant reduction of DNA-PKcs S2056 foci was detected in synemin-depleted cells over 24-h observation period relative to controls (Fig. 5.14a,d). At 30 min post irradiation, a reduction of DNA-PKcs S2056 foci c.a. 3-4 foci/cell was observed, whereas the amount of 53BP1 foci was not altered. An increase in a number of 53BP1 foci in synemin deficient cells was found 1 h after irradiation (Fig. 5.14a,c) which could be related to the presence of unsolved DNA-PKcs S2056 foci at 30 min after X-ray exposure. Similar observations were made for  $\gamma$ H2AX foci (Fig. 5.14b) which presented a lower amount of foci as compared to the respective control at 30 min and 1 h after irradiation. This result might be related to the delayed recruitment of  $\gamma$ H2AX foci in synemin-depleted cells, but the number of  $\gamma$ H2AX foci was then significantly increased 2 h post IR.

Since synemin is indispensable for NHEJ, cell cycle re-distribution could be attributed to the function of synemin. Hence, cell cycle analysis were performed upon synemin silencing in unirradiated and irradiated cells (Fig. 5.15a,b). The result indicated no connections between synemin and cell cycle progression.



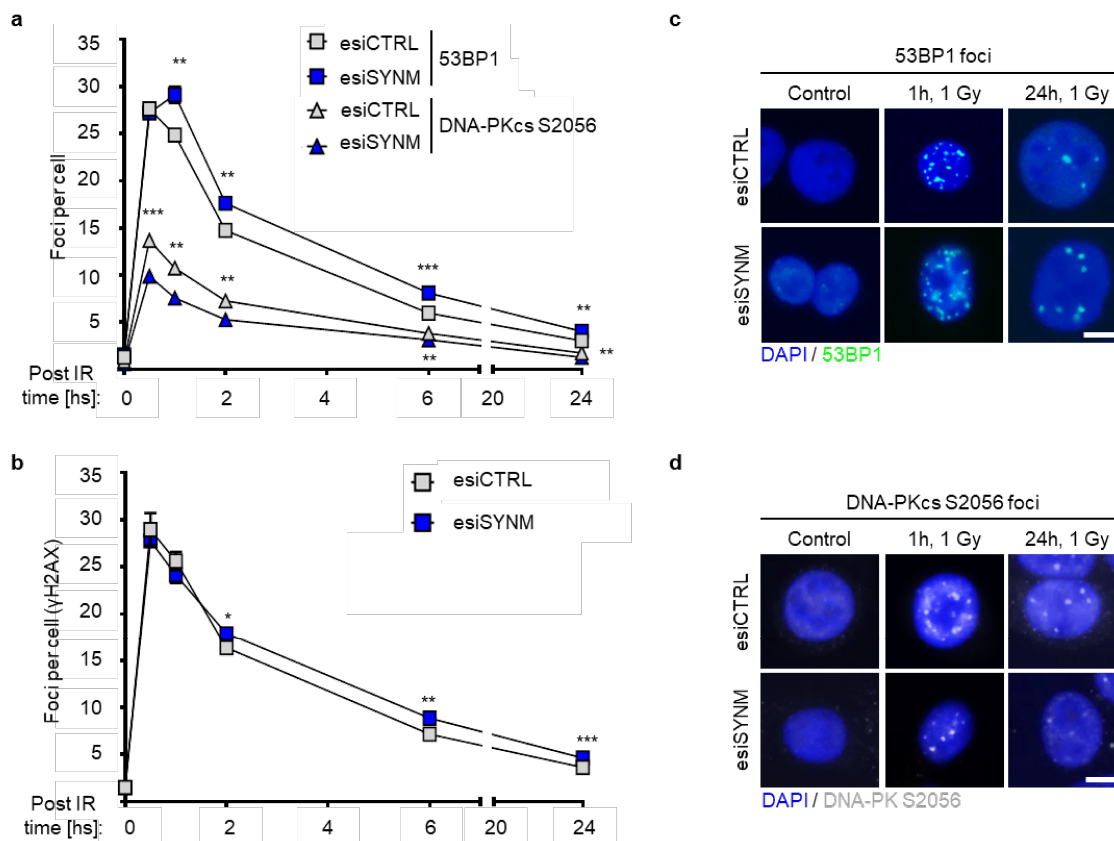


**Figure 5.14: Synemin functions in non-homologous end joining.** **a**, Kinetics of 53BP1, DNA-PKcs S2056 and **b**,  $\gamma$ H2AX foci upon synemin knockdown at different time points post 1 Gy X-rays including immunofluorescence images of residual 53BP1 (**c**) and DNA-PKcs S2056 (**d**) foci of synemin knockdown and control cell cultures 1 h after 1 Gy X-rays (bar, 10  $\mu$ m). Data are presented as mean  $\pm$  SD (n = 3; two-sided t-test; \*P<0.05, \*\*P<0.01, \*\*\*P<0.001).

It was observed that synemin partially interacts with chromatin, by which chromatin modification might be affected by the depletion of synemin. Therefore, an expression level of a crucial chromatin modification factor, termed heterochromatin protein 1- alpha (HP1- $\alpha$ ), was determined upon synemin knockdown. The HP1- $\alpha$  expression level was determined by immunoblotting and immunocytochemical staining. In both analyses, no significant alteration in chromatin condensation upon synemin knockdown was observed, neither in untreated cells nor X-ray exposed cells.

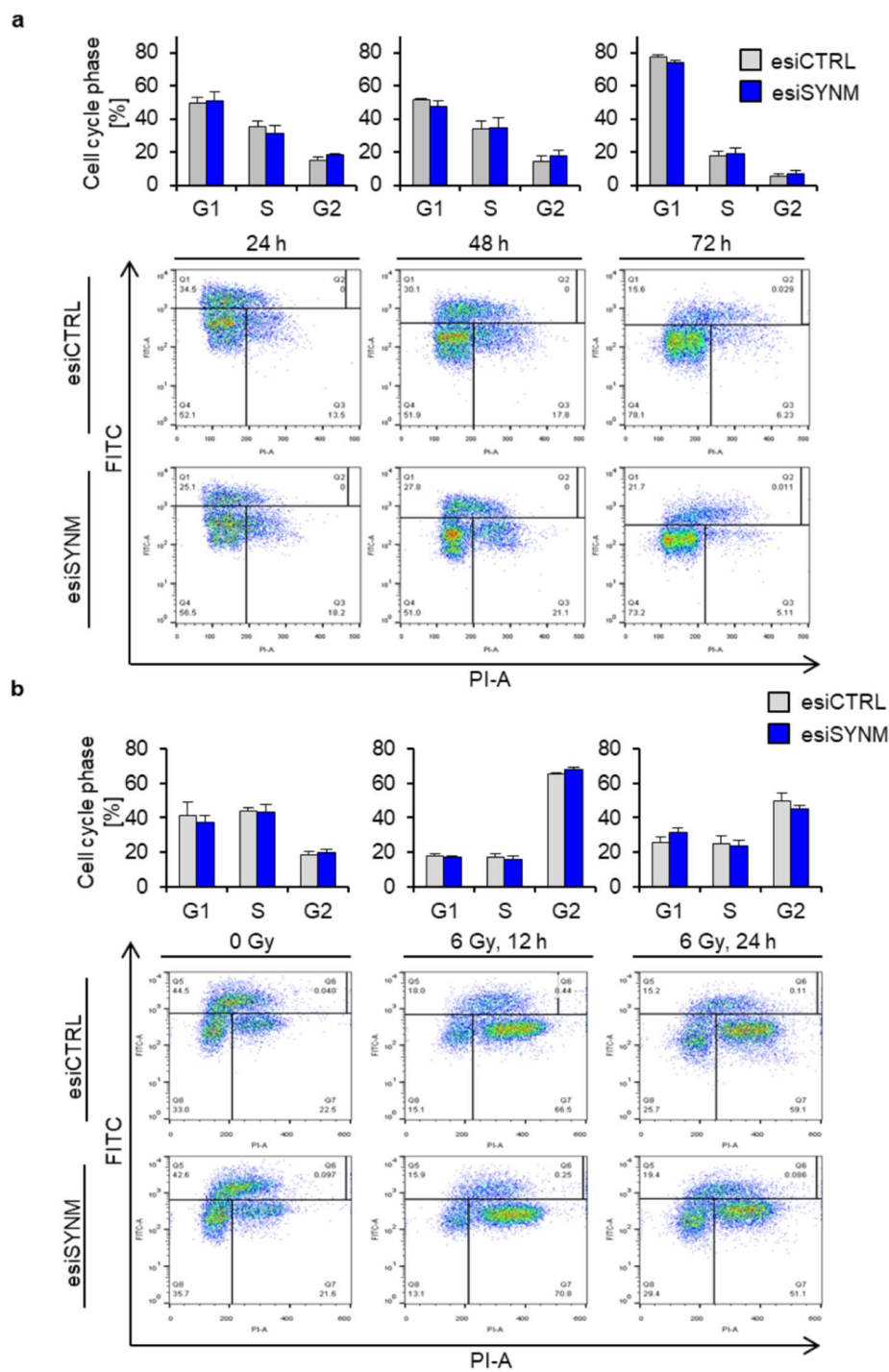


**Figure 5.15: Synemin effects on cell cycle.** **a**, Cell cycle distribution of SAS cells upon synemin knockdown at 24, 48 and 72 h post transfection **b**, and at 12 and 24 h post 6 Gy X-ray irradiation. Data are represented as mean  $\pm$  SD (n = 3; two-sided t-test).

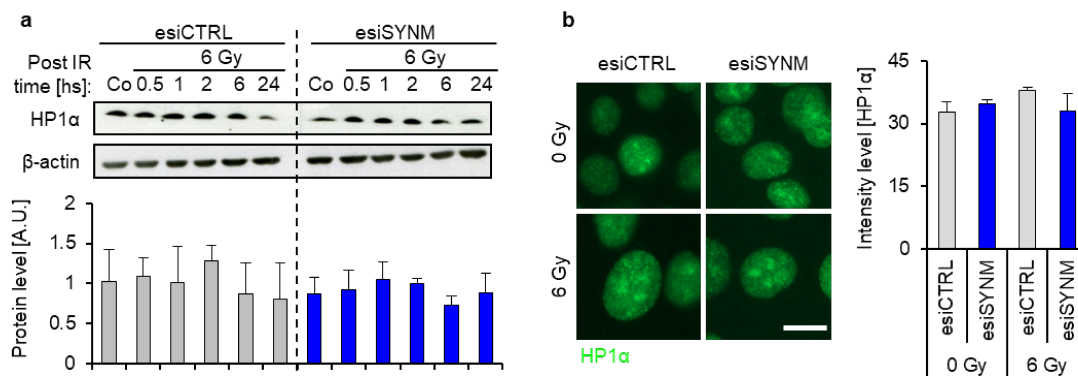


**Figure 5.16: Synemin effects on heterochromatin levels.** **a**, Immunoblots and densitometry from synemin-depleted and 6-Gy irradiated cells showing total HP1 $\alpha$  levels.  $\beta$ -actin served as loading control. Densitometries are shown under the blot. **b**, Immunofluorescence of HP1 $\alpha$  from synemin-depleted and 6-Gy irradiated cells and relative intensities for heterochromatin evaluation (bar, 10  $\mu$ m). Data are represented as mean  $\pm$  SD (n = 3; two-sided t-test).

This result suggests that synemin regulates DNA repair mechanism mainly through the phosphorylation of key DNA repair proteins leading to their recruitment to the damage sites independently of cell cycle and chromatin organization.

## 5.3 Synemin signaling in head and neck squamous cell carcinoma (HNSCC)

### 5.3.1 Regulation of kinase activity by synemin

To further unravel the molecular mechanism underlying an impaired NHEJ in synemin-deficient cells after irradiation, a broad-spectrum kinase profiling was performed. Intriguingly, significant changes were found in protein kinase activities in synemin-deficient, irradiated cells at 1 h and 24 h after X-ray exposure (Fig. 5.17a and 5.18a). Remarkably, synemin knockdown alone failed to modify protein kinase profiles (Fig 5.17a and 5.18a) indicating that the DNA repair-co-regulating function of synemin becomes essential upon genotoxic injury.

Based on the kinase profiling data, important DNA repair regulators c-Abl and several Src family members (Scr, Yes, Lck, Blk and Lyn) were identified as the top deactivated tyrosine kinases in synemin-deficient, 6-Gy X-ray irradiated cells compared to the respective controls (Fig. 5.17b and 5.18a,b). Calculating the  $-\Delta$  Effect ( $T_{24h, 6Gy} - T_{0Gy}$ ) (Fig. 5.18a) it is possible to observe the additional effects of synemin depletion on tyrosine kinases upon irradiation (Fig 5.17b and 5.18b). In contrast, serine/threonine kinases remained partly unaffected in synemin-depleted cells (Fig. 5.17b) apart from some CMGC (cyclin dependent kinases) and CAMK (calcium- and calmodulin-regulated kinases) serine/threonine kinases. Based on the prediction algorithm of Cytoscape and of the Group-based prediction system (GPS 3.0, <http://gps.biocuckoo.org/>) (Xue et al., 2008) database analysis, c-Abl was predicted to be central to components of the NHEJ and HR repair machinery. As shown before synemin consists of numerous amino acid residues which serve as putative phosphorylation substrates for serine/threonine and tyrosine kinases (Fig. 5.17c,d). Accordingly, many kinases of the kinome screen with downregulated activity are predicted to phosphorylate synemin at different sites (Fig. 5.17c,d and 5.18a,b). In order to further investigate the underlying mechanism, c-Abl total protein expression was examined, as well as c-Abl phosphorylation level at Y412 and T715 sites which are responsible for the c-Abl kinase activity and c-Abl subcellular distribution respectively. Interestingly, phosphorylation at both Y412 and T715 residues was significantly reduced upon synemin knockdown in irradiated cells relative to controls 6 h and 24 h after X-rays exposure, while the level of total c-Abl protein remained unchanged (Fig. 5.19a,b). Moreover, synemin overexpression revealed a stabilized and not radiation-inducible Y412 phosphorylation relative to mCherry controls indicative of a dependence of c-Abl activity on synemin (Fig. 5.19c).

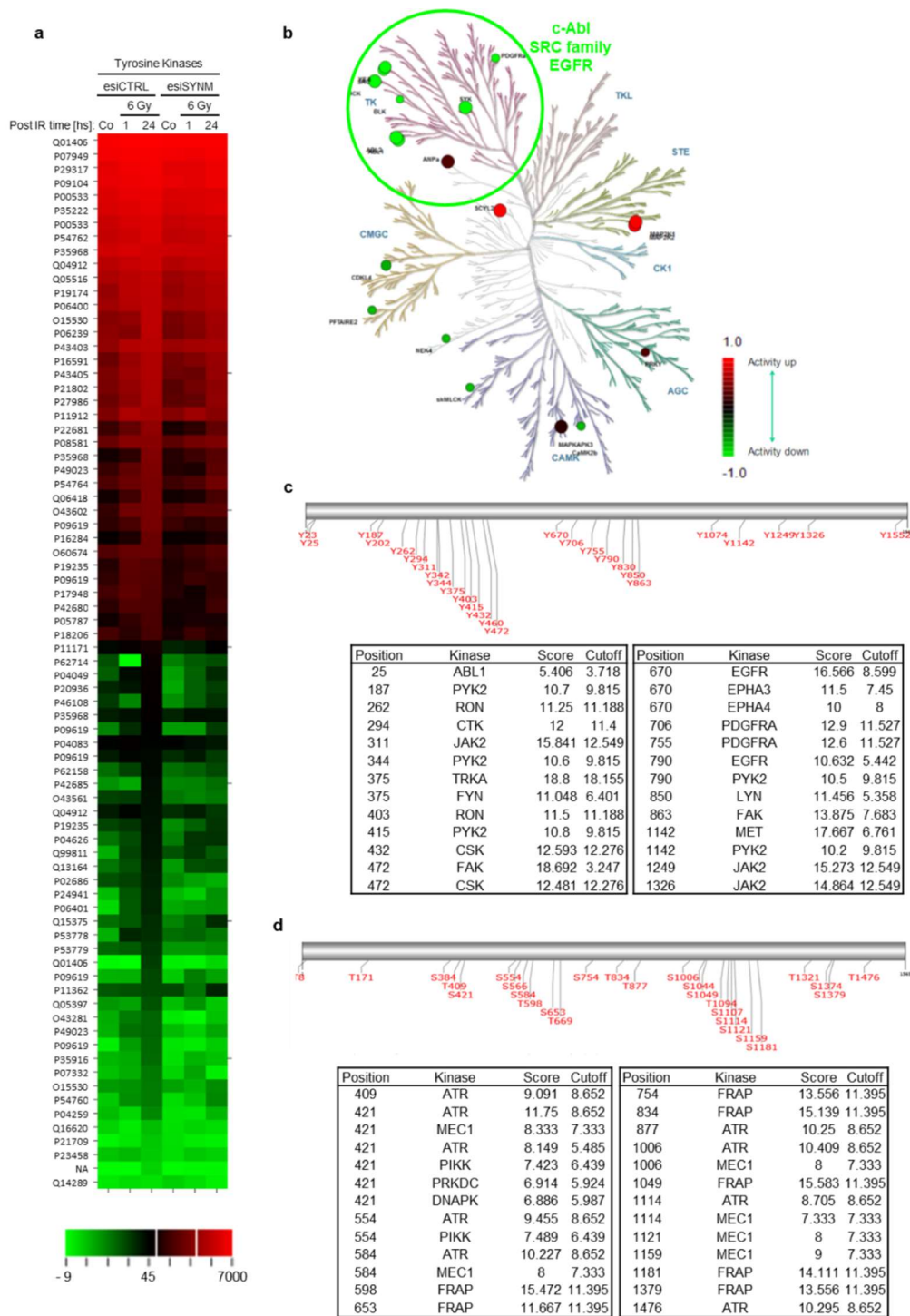


**Figure 5.17: Synemin regulates tyrosine kinase activity, in particular c-Abl kinase.** **a**, Heatmap of phosphorylated peptides by tyrosine kinases of control and synemin knockdown samples before and after 1 and 24 h X-ray treatment (n = 3). **b**, Kinase family tree of down and up regulated kinases 24 h post irradiation and synemin knockdown. The green circle shows the tyrosine kinases. **c**, Predicted phosphorylation sites (Y) of synemin and the corresponding kinases with a prediction score greater than 5 using GPS database (GPS 3.0, <http://gps.biocuckoo.org/>). **d**, Predicted sites of synemin phosphorylation at Serine (S) and Threonine (T) residues by PIKK kinases. The table shows the amino acid position and corresponding kinases with a prediction score greater than 5 using GPS database (GPS 3.0, <http://gps.biocuckoo.org/>).

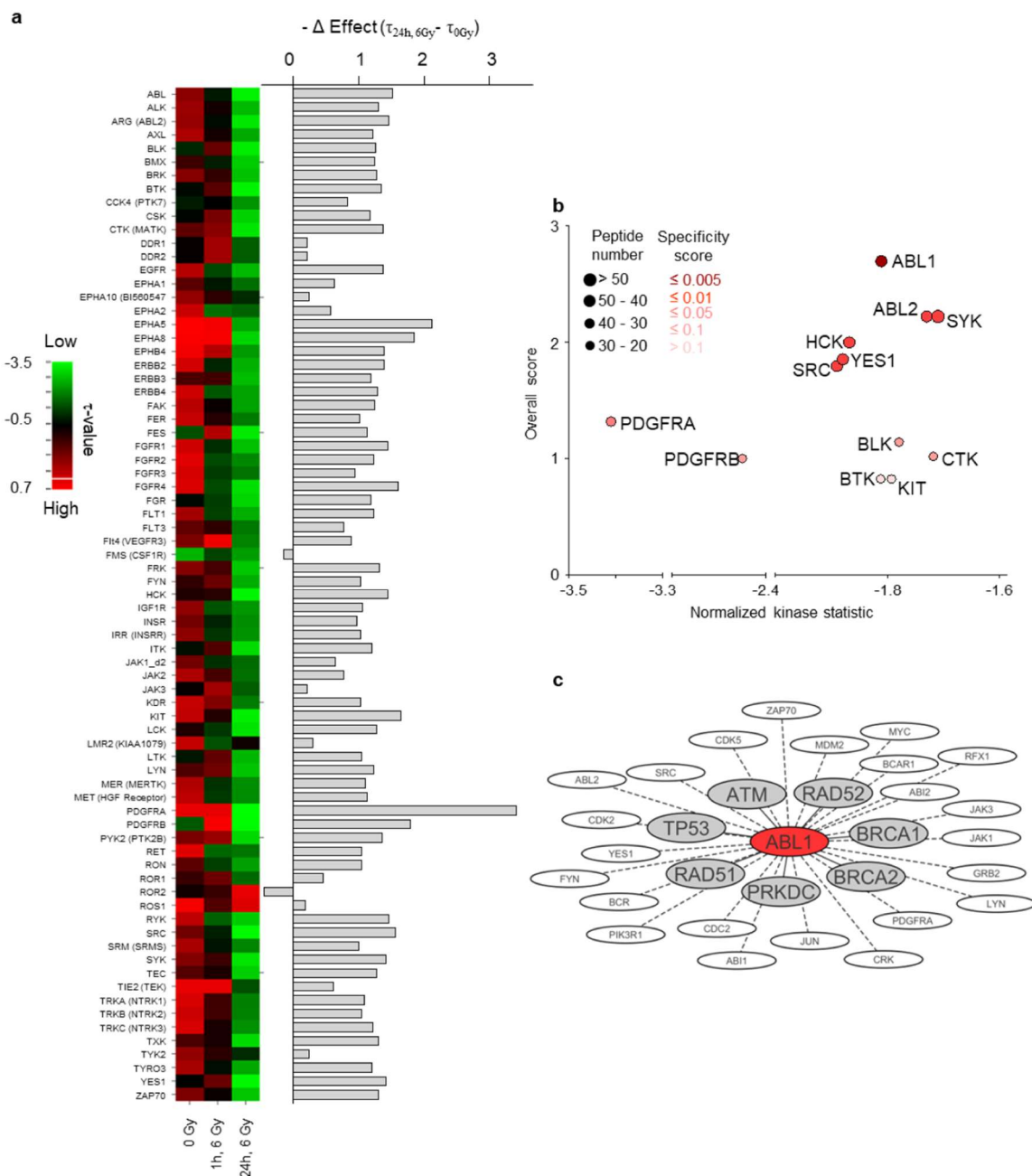


**Figure 5.18: Synemin regulates c-Abl kinase activity.** **a**, Heatmap of tyrosine kinase activities in cells depleted of synemin and exposed to 6-Gy X-ray irradiation including  $-\Delta \text{Effect} (\tau_{24h, 6Gy} - \tau_{0Gy})$  (subtraction of values obtained from synemin-depleted cells 24 h post 6 Gy X-ray irradiation from non-irradiated, synemin-depleted cells). Kinase activity profiles were generated by PamGene Technology. **b**, Top affected tyrosine kinases in synemin-depleted cell cultures 24 h post 6 Gy X-ray irradiation. X-axis indicates the  $\tau$  value for each kinase ( $\tau < 0$  indicates reduced kinase activity relative to control). The colors of the dots indicate the specificity score. The size of the dots indicates the number of peptides. The Y-axis shows the overall score. **c**, c-Abl interactome of DNA repair proteins calculated by Cytoscape.

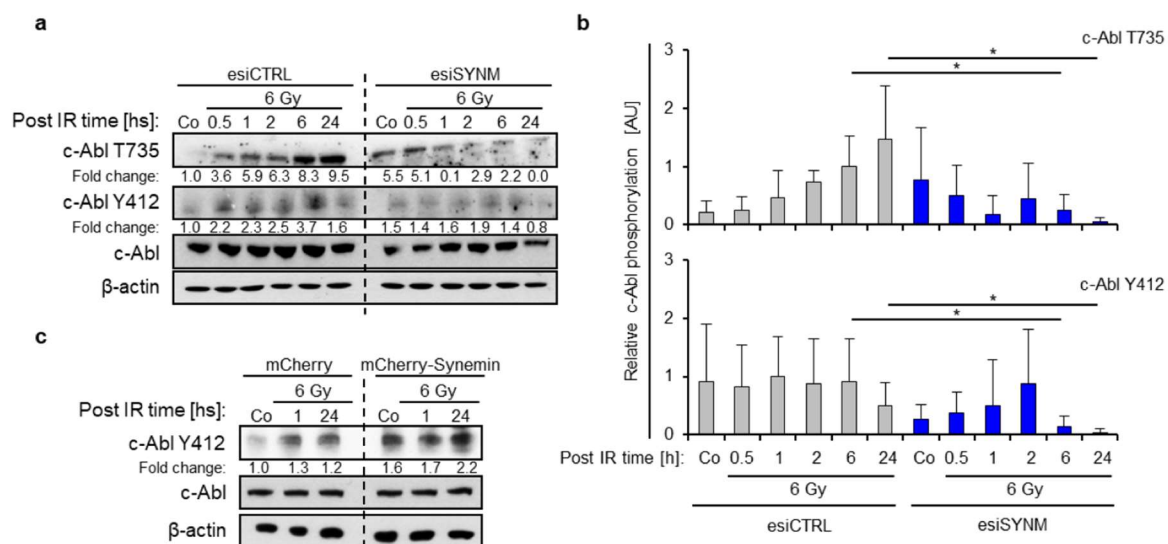


**Figure 5.19: Synemin regulates c-Abl kinase activity.** **a**, Immunoblot of c-Abl expression and phosphorylation from whole cell lysates of synemin-depleted cells and 6-Gy irradiated **b**, together with corresponding densitometries from immunoblots showing phosphorylated forms of c-Abl ( $n = 4$ ). Phosphorylation levels were calculated relative to the total amount of c-Abl. **c**, Immunoblot of c-Abl expression and phosphorylation from whole cell lysates of mCherry-Synemin transfectants at different time points post 6 Gy X-ray irradiation ( $n = 3$ ).  $\beta$ -actin served as loading control. Data are represented as mean  $\pm$  SD (two-sided t-test; \* $P < 0.05$ ).

Altogether, synemin seems to have a significant role in the regulation of c-Abl kinase activity and its localization, which could potentially associate with the regulation of DNA damage repair.

### 5.3.2 Synemin as upstream protein of c-Abl and DNA-PKcs

Previous reports indicated DNA-PKcs and ATM as potential regulators of c-Abl function (Tang et al., 2012). As it has been shown above synemin plays a critical role in the regulation of c-Abl activity, however, the understanding of interconnections between synemin, c-Abl and DNA-PKcs requires further investigations.

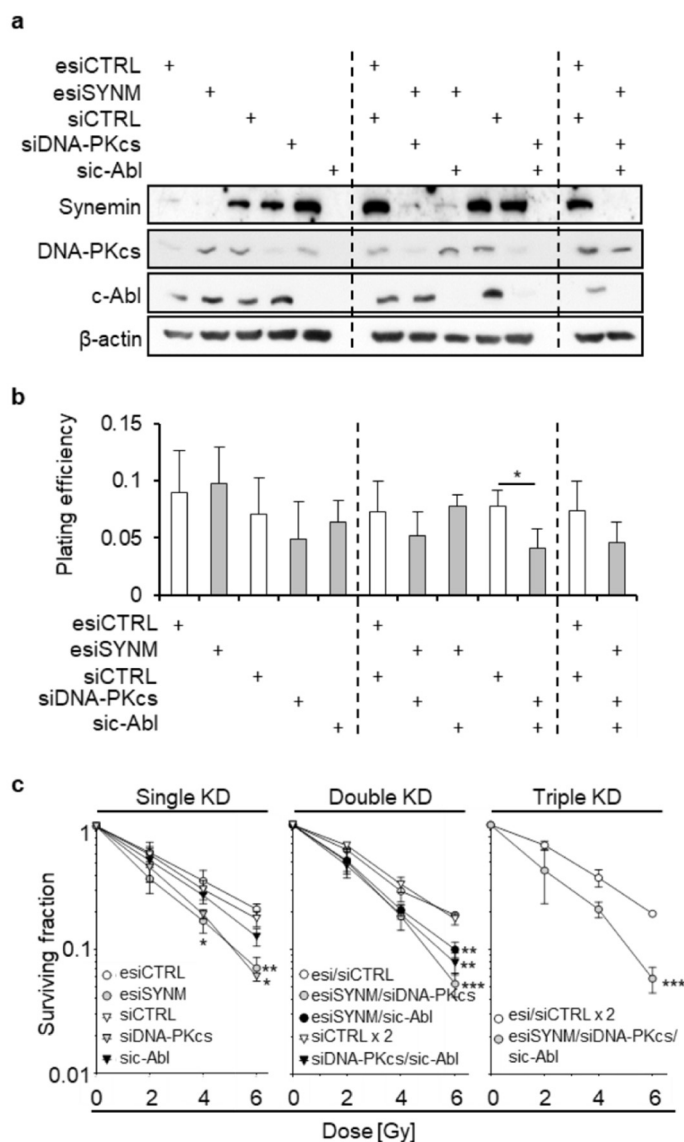


**Figure 5.20: Synemin/DNA-PKcs/c-Abl co-control radiation survival.** **a**, Knockdown efficiencies of single, double or triple esi/siRNA transfections.  $\beta$ -actin served as loading control. **b**, Plating efficiency of SAS cells upon single, double or triple knockdown of synemin, DNA-PKcs and c-Abl. **c**, 3D clonogenic radiation survival upon single, double and triple silencing of synemin, DNA-PKcs and c-Abl. Data are represented as mean  $\pm$  SD ( $n = 3$ ; two-sided t-test; \* $P < 0.05$ , \*\* $P < 0.01$ , \*\*\* $P < 0.001$ ).



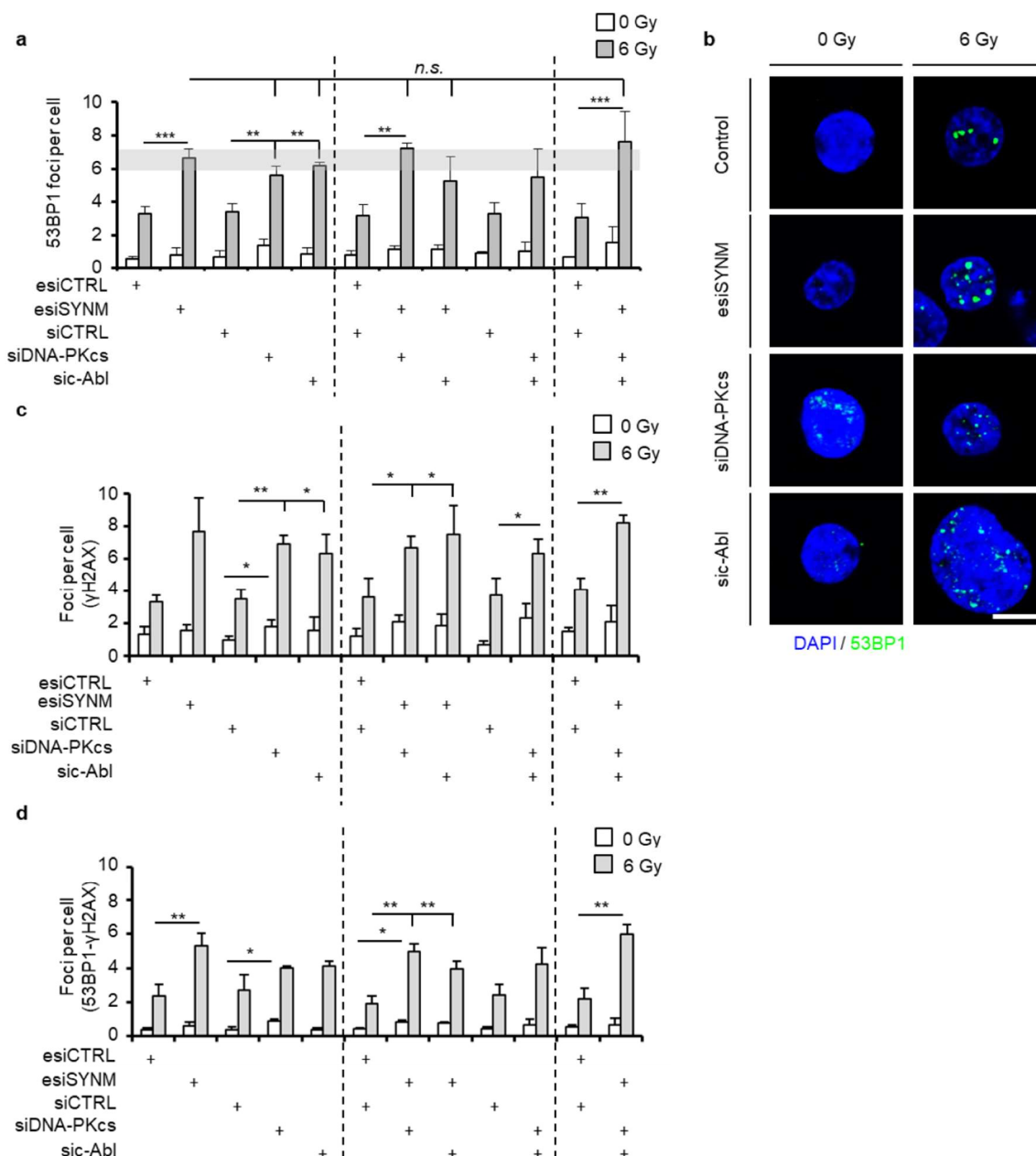


**Figure 5.21: Synemin/DNA-PKcs/c-Abl co-control DSB repair.** **a**, Residual 53BP1 foci per cell upon single, double or triple knockdown of synemin, DNA-PKcs and c-Abl in 6-Gy X-ray irradiated cells. Transfection with single or double non-specific siRNA was used as controls. **b**, Exemplary immunofluorescence images of residual 53BP1 foci (co-staining with DAPI (nucleus)). **c**,  $\gamma$ H2AX and **d**, 53BP1- $\gamma$ H2AX colocalized foci after single, double and triple knockdowns exposed to sham or 6 Gy X-rays. Data are represented as mean  $\pm$  SD ( $n = 3$ ; two-sided t-test; \* $P < 0.05$ , \*\* $P < 0.01$ , \*\*\* $P < 0.001$ ).

To this end, single, double and triple knockdown of synemin, c-Abl and DNA-PKcs (Fig. 5.20a) was performed, which revealed no significant effect on the basal survival, except for the combined DNA-PKcs/c-Abl silencing (Fig. 5.20b). Intriguingly, single synemin and DNA-PKcs but not c-Abl knockdown significantly enhanced cellular radiosensitivity upon irradiation compared to the control cells (Fig. 5.20c). Double knockdowns of synemin/DNA-PKcs, DNA-PKcs/c-Abl and synemin/c-Abl, as well as the triple synemin/DNA-PKcs/c-Abl knockdown,

demonstrated similar radiosensitizing effects as a single knockdown, indicating that all tested targets represent a part of one signaling pathway (Fig. 5.20c).

To further underpin the role of synemin/c-Abl/DNA-PKcs interaction, residual 53BP1 foci numbers relative controls were evaluated (Fig. 5.21a,b). The number of residual 53BP1 foci were similarly increased in the single, double and triple knockdowns as compared to the controls (Fig. 5.21a,b). From these data, two observations could be drawn out: (i) synemin impacts on the functionality of c-Abl and DNA-PKcs in DSB repair and (ii) synemin, c-Abl and DNA-PKcs are components of the same signaling pathway. Consistently, analysis of the number of residual  $\gamma$ H2AX and 53BP1/ $\gamma$ H2AX foci showed similar results (Fig. 5.21c,d) to the 53BP1 numbers. In conclusion, the molecular functions of DNA-PKcs and c-Abl in the DNA damage response depended on synemin.

### 5.3.3 Synemin forms a complex together with c-Abl and DNA-PKcs

To investigate a direct interaction between synemin, DNA-PKcs and c-Abl, immunoprecipitation assays with endogenous synemin and synemin conjugated with mCherry were performed. Strikingly, c-Abl and DNA-PKcs exhibited binding to synemin and synemin binding to c-Abl in reverse immunoprecipitations relative to IgG and mCherry controls (Fig. 5.22a-c). Interestingly, upon X-ray exposure, the interaction between synemin and c-Abl as well as DNA-PKcs was slightly decreased (Fig. 5.22a-c). To validate the result from immunoprecipitation and identify the subcellular interaction site between synemin and the 2 kinases, a proximity ligation assay (PLA) was performed in non-irradiated and 6 Gy X-ray treated SAS cells. In both cases, the interaction of c-Abl/synemin and DNA-PKcs S2056/synemin was detected in un- and -irradiated cells (Fig. 5.22d,e). From the PLA assay it is possible to conclude that synemin binds to c-Abl mainly in the cytoplasm, whereas DNA-PKcs S2056/synemin interaction occurs mainly in the nucleus. Taken together, synemin was able to form a protein complex together with c-Abl and DNA-PKcs independently.

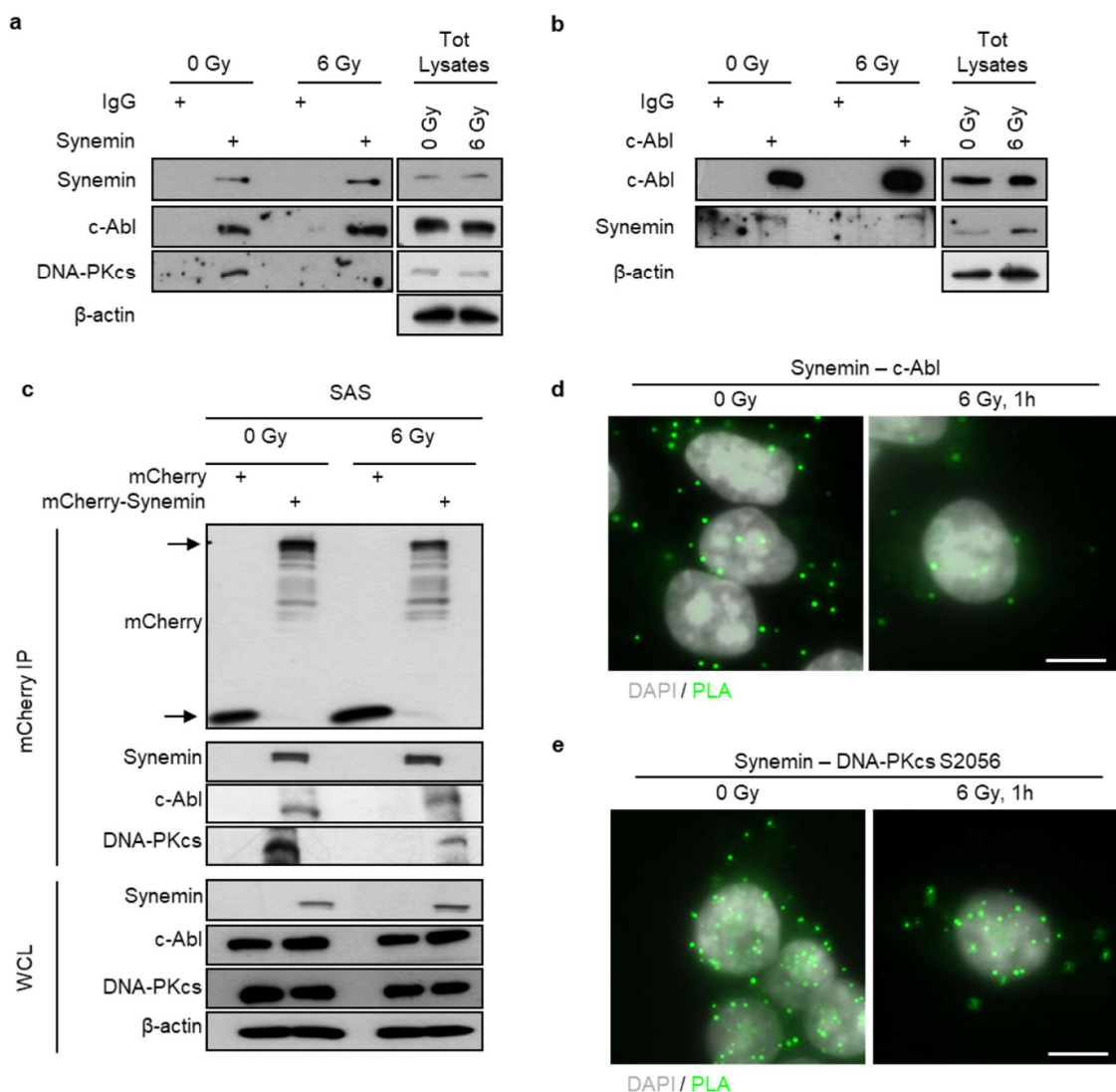


**Figure 5.22: c-Abl and DNA-PKcs forms a complex together with synemin.** **a**, Immunoprecipitation (IP) of synemin 1 h post 6 Gy X-rays ( $n = 3$ ). Immunoblotting shows expression of synemin, c-Abl and DNA-PKcs. **b**, IP of c-Abl 1 h post 6 Gy X-rays ( $n = 3$ ). Immunoblotting shows expression of synemin and c-Abl. **c**, Western blots on immunoprecipitates from 6-Gy irradiated mCherry-SAS and mCherry-Synemin-SAS cells at 1 h post irradiation ( $n = 3$ ).  $\beta$ -actin served as loading control. **d**, Interaction of synemin and c-Abl or **e**, DNA-PKcs S2056 in unirradiated and irradiated cells defined by proximity ligation assay ( $n = 3$ ) (bar, 10  $\mu$ m).

### 5.3.4 Synemin function is regulated by ATM kinase activity

In order to understand whether the interaction between synemin and c-Abl/DNA-PKcs is dependent on the kinase activity of these two proteins as well as ATM, a kinase essentially involved in c-Abl and DNA-PKcs activation, c-Abl, DNA-PKcs and ATM, were pharmacologically inhibited using imatinib (c-Abl), NU7026 (DNA-PKcs), KU55933 (ATM) prior to immunoprecipitation of synemin (Fig. 5.23a). Astonishingly, declined and absent binding of c-Abl under ATM inhibition was found in unirradiated as well as under DNA-PKcs and ATM inhibition in irradiated cells, respectively (Fig. 5.23a). DNA-PKcs, however, showed increasing dissocia-

tion from synemin upon DNA-PKcs and ATMi (Fig. 5.23a, lane 2, 3, 4). In irradiated cells, DNA-PKcs generally bound less to synemin (Fig. 5.23a), an interaction completely lost upon DNA-PKcs and ATM inhibition (Fig. 5.23a).

To corroborate the effect of ATM on synemin, SKX, an ATM deficient squamous cell carcinoma cell line owing to the overexpression of miR-421 (Mansour et al., 2013) was used. Interestingly, the result of immunoprecipitation of synemin from SKX cells demonstrated that ATM does not affect c-Abl/synemin, but instead perturbed DNA-PKcs/synemin interaction (Fig. 5.23c). This result is partly in line with the previous observations in SAS cells treated with c-Abl, ATM and DNA-PKcs inhibitors. Interestingly, SKX cells expressed higher levels of synemin and c-Abl relative to SAS cells suggesting an activation of the by-pass mechanism due to ATM dysfunctionality. In further investigations, mCherry-Synemin-overexpressing SAS cells were treated with ATMi and irradiation. The numbers of radiogenic 53BP1 and DNA-PKcs S2056 foci were significantly decreased upon ATMi-treatment of SAS cells 1 h after irradiation as compared to the DMSO-treated mCherry controls (Fig. 5.22b). At 24 h after irradiation, 53BP1 and DNA-PKcs S2056 foci numbers were significantly elevated due to the ATM inhibition which was similar to the mCherry empty vector (Fig. 5.23b). From these results, it is possible to conclude that synemin contributes to the regulation of the DNA repair via the ATM-dependent recruitment of 53BP1 and DNA-PKcs to the DSB site.

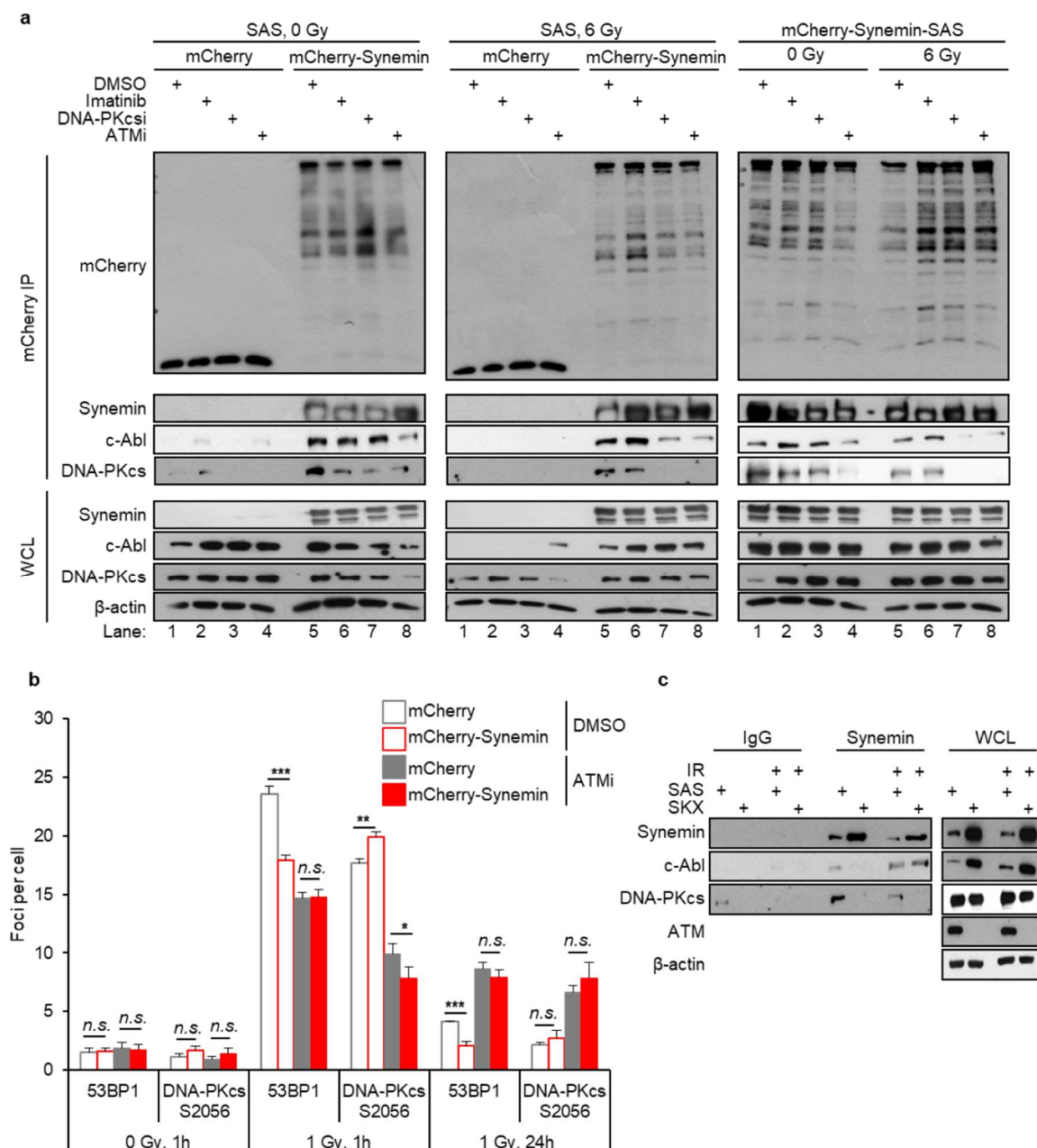


**Figure 5.23: c-Abl and DNA-PKcs interaction with synemin depends on ATM kinase activity. a**, IP of SAS cells expressing mCherry and mCherry-Synemin. Cells were treated with Imatinib, DNA-PKcsi or ATMi and exposed to sham or 6 Gy X-rays. Western blots on immunoprecipitates from mCherry-Synemin-SAS cells after a 1 h pretreatment with imatinib, DNA-PKcsi or ATMi alone or in combination with 6 Gy X-rays. **b**, 53BP1 and DNA-PKcs S2056 foci upon ATMi treatment at different time points post 1 Gy X-rays in mCherry- and mCherry-Synemin transfectants. **c**, Western blots on immunoprecipitates from SAS and SKX cells 1 h after 6 Gy X-rays exposure. Data are represented as mean  $\pm$  SD ( $n = 3$ ; two-sided t-test; \* $P < 0.05$ , \*\* $P < 0.01$ , \*\*\* $P < 0.001$ ; n.s., not significant ( $P \geq 0.05$ )).

### 5.3.5 Synemin tail is phosphorylated by ATM kinase and it is essential for synemin function

To determine the functional site of synemin, which essentially contributes to its function in DNA damage repair, two synemin constructs were designed: (i) deletion of coil-coil linker and tail domains; (ii) deletion of head and coil-coil linker domains (Fig. 5.24a,b). Plasmids containing DNA expressing synemin variants were transfected into SAS cells, and 53BP1 and DNA-PKcs S2056 foci were microscopically counted. For foci assay evaluating 53BP1 and DNA-PKcs S2056, it was observed that the number of foci in cells expressing only the synemin tail (Synemin\_Tail) was comparable to the cells with wild type synemin (Fig. 5.24c). In contrast, the construct expressing synemin head demonstrated similar effects as the mCherry control plasmid (Fig. 5.24c). These data suggest that only the tail of synemin mediates the interactions between synemin and DNA repair proteins.

Taking the prediction from the GSP database into account that only serine amino acid residues at the tail, but not at the head or coil-linker domains of synemin, are phosphorylatable by ATM (Fig. 5.24a), the residual 53BP1 foci in SAS cells expressing the different synemin constructs upon ATM inhibition were evaluated (Fig. 5.24d). Similar to the previously shown result, the Synemin\_Tail construct showed the same effect as mCherry-Synemin wildtype. As ATM kinase is inhibited, the numbers of residual foci are similar among wildtype and mutated constructs as well as mCherry control. Taken together, these results suggested that the synemin tail domain has a critical role in the DNA repair process. In addition, the GSP database indicated that only S421, S554, S1114, S1159 AA residues at the synemin tail, but none at the head or coil-linker domains of synemin can be phosphorylated by ATM (Fig. 5.25a). To characterize the influence of these phosphorylation sites within the synemin tail on DNA repair, further synemin constructs containing either tail AAs 301 to 961 (mCherry-Synemin\_301-961) or tail AAs 962 to 1565 (mCherry-Synemin\_962-1565) were generated (Fig. 5.25a). Using these constructs, 53BP1 foci upon X-ray irradiation were evaluated. A significant increase of 53BP1 foci upon expression of mCherry-Synemin\_962-1565, but not mCherry-Synemin\_301-961 was found, indicating a potential function of S1114 and S1159 in DNA repair (Fig. 5.25a-c). To further prove the functionality of these serine residues, point mutations at the phosphorylation site of S1114 (mCherry-Synemin\_S1114A) and S1159 (mCherry-Synemin\_S1159A) were introduced (Fig. 25a). 53BP1 foci quantification upon overexpression of these constructs revealed that the function of synemin was left unaffected when the S1159 was mutated, but a loss of function of synemin was observed when S1114 was altered to alanine (Fig. 5.25b,c). These data suggest that the S1114 AA residue in the synemin tail is specifically required for the DNA repair function of synemin. Interestingly, this serine is surrounded by glutamines (Q) indicating that the AA residue sequence from 1113 to 1115 is QSQ, for which a higher specificity for ATM phosphorylation has been demonstrated.

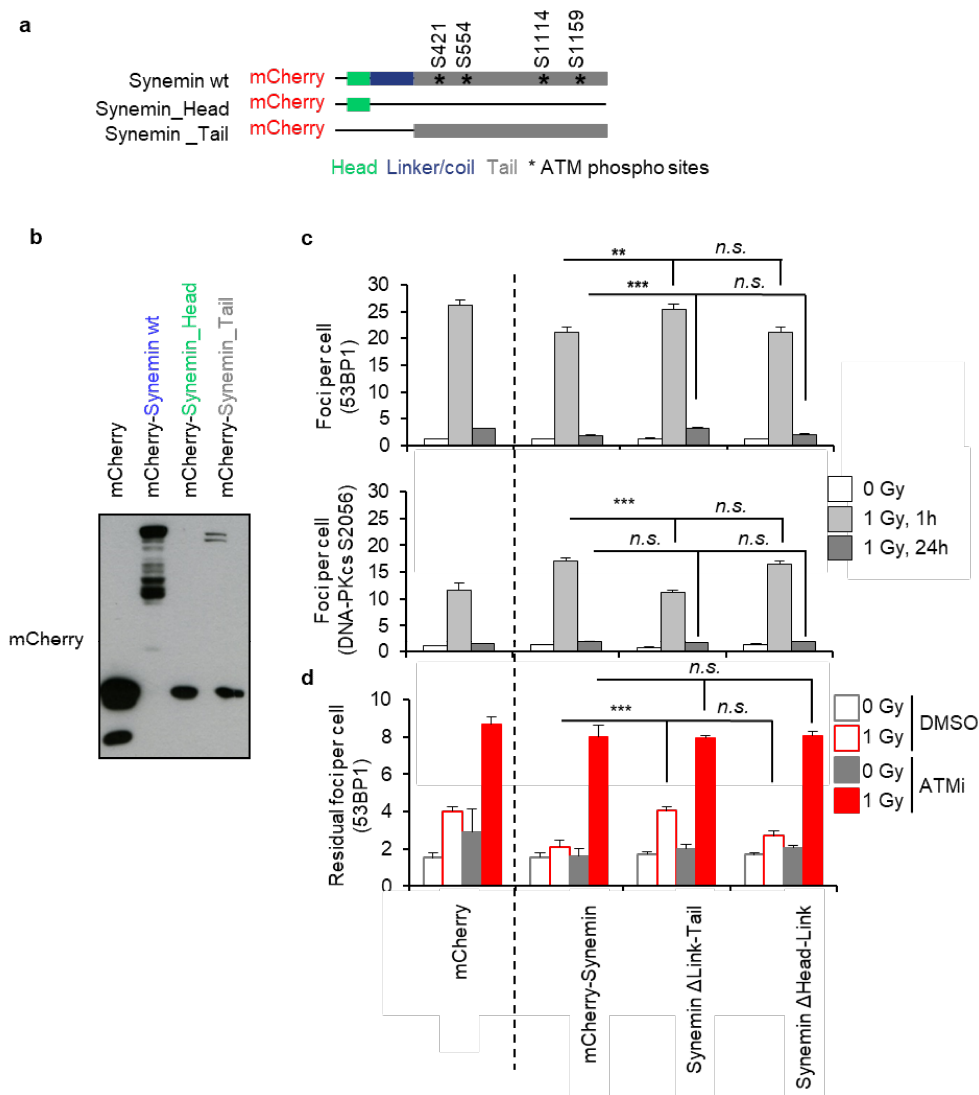


**Figure 5.24: c-Abl and DNA-PKcs interaction with synemin depends on ATM kinase activity.** **a**, Design of different synemin constructs. **b**, Immunoblotting of SAS cells transfected with different mCherry-Synemin plasmid constructs. **c**, 53BP1 and DNA-PKcs S2056 foci kinetics in 1-Gy X-ray irradiated transfectants expressing mCherry-Synemin wildtype, mCherry-Synemin  $\Delta$ Link-Tail, or mCherry-Synemin  $\Delta$ Head-Linker (mCherry was used as control). **d**, Residual 53BP1 foci upon treatment with ATMi and 1 Gy X-rays in SAS cells expressing mCherry-Synemin wildtype, mCherry-Synemin  $\Delta$ Link-Tail, or mCherry-Synemin  $\Delta$ Head-Linker (mCherry was used as control). Data are represented as mean  $\pm$  SD ( $n = 3$ ; two-sided t-test; \*\* $P < 0.01$ , \*\*\* $P < 0.001$ ; n.s., not significant ( $P \geq 0.05$ )).

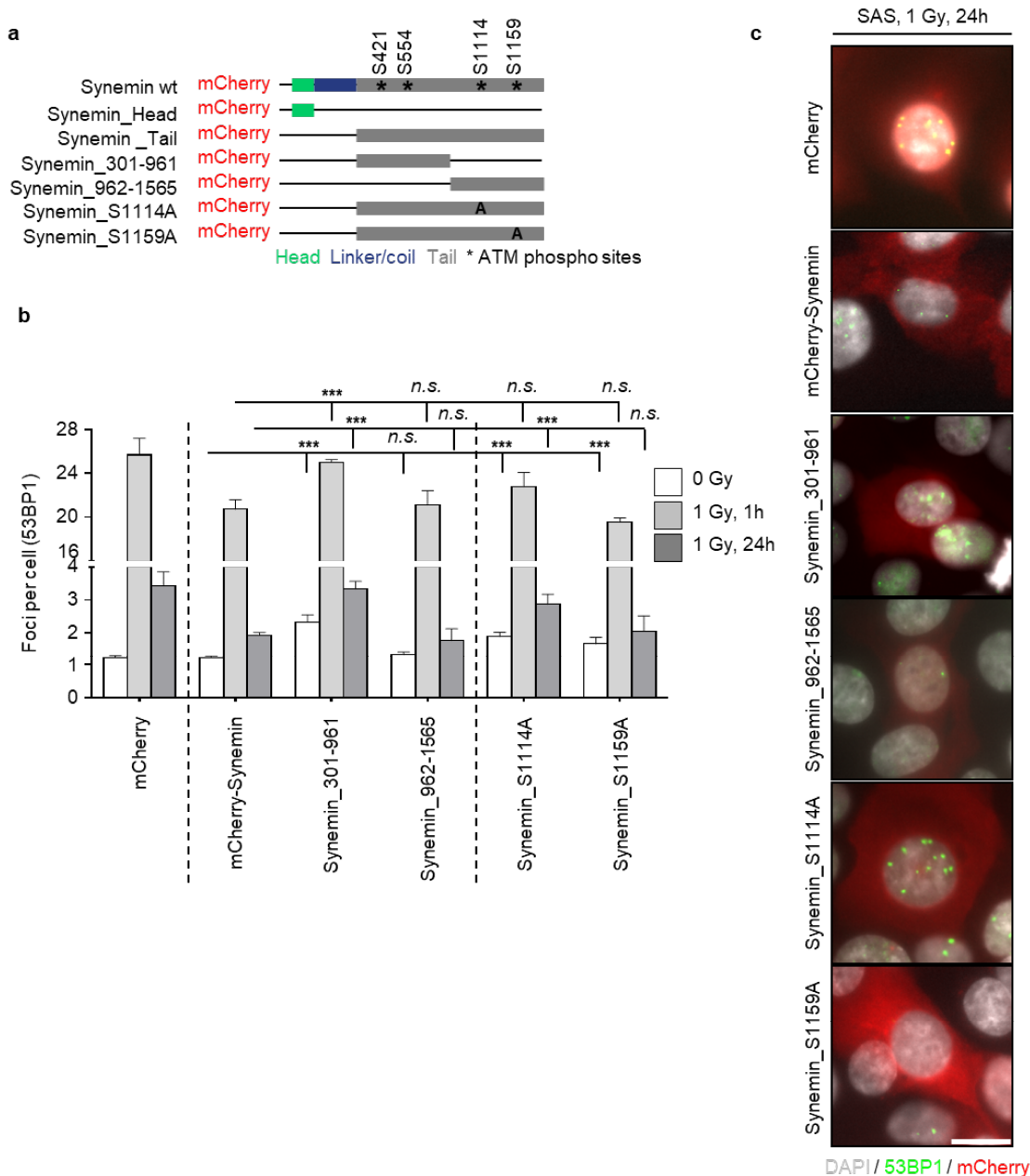


**Figure 5.25: Synemin depends DNA repair function depends on S1114 phosphorylation site.** **a**, Design of different synemin constructs. **b**, 53BP1 foci kinetics in 1-Gy X-ray irradiated transfectants expressing mCherry-Synemin wildtype, mCherry-Synemin\_301-961, mCherry-Synemin\_962-1565, mCherry-Synemin\_S1114A, and mCherry-Synemin\_S1159A (mCherry was used as control) and **c**, corresponding representative immunofluorescence images (bar, 20  $\mu$ m). Data are represented as mean  $\pm$  SD ( $n = 3$ ; two-sided t-test; \*\*\* $P < 0.001$ ; n.s., not significant ( $P \geq 0.05$ )).



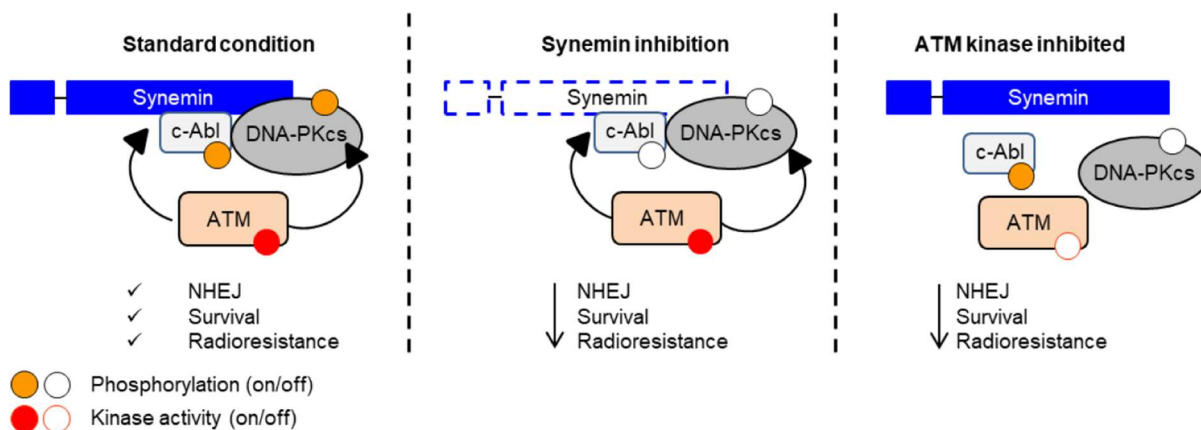


**Figure 5.26: Synemin's mechanism.** Under physiological condition, synemin interacts with c-Abl and DNA-PKcs in an ATM kinase-dependent manner. This interaction controls non-homologous end joining (NHEJ), cell survival and resistance to radiation. Upon synemin silencing, phosphorylation of c-Abl and DNA-PKcs is perturbed eliciting dysfunctionality of NHEJ and reduction of cell survival and radioresistance. A similar phenotype with lessened NHEJ and survival provoked by pharmacological inhibition of the ATM kinase activity presents with a dispersed synemin/c-Abl/DNA-PKcs protein complex.

Taken together, this study showed that an ATM-dependent interaction of synemin with c-Abl and DNA-PKcs controls NHEJ, as well as cell survival and resistance to radiation. Synemin silencing perturbed c-Abl/DNA-PKcs phosphorylation and reduced cell survival and radioresistance by modulating the functionality of NHEJ. Similarly, pharmacological inhibition of ATM kinase activity hindered the complex formation of synemin/c-Abl/DNA-PKcs, reducing NHEJ and enhancing radiosensitization of HNSCC (Fig. 5.26).

## 6 Discussion

Reduction of treatment resistance remains one of the major challenges for improving cancer patient survival. To safeguard genomic stability and cell survival, cells employ multiple complex DNA repair machineries. While the application of DNA-damaging agents such as radiation and chemotherapeutics are the standard approaches for cancer treatment, an addition of molecular targeted drugs seems to be beneficial. For instance, the combination of EGFR or integrins treatment with radiation on cancer cells demonstrated a more efficacious eradication of various subpopulations of therapy-sensitive and -resistant malignant cells (Harari and Huang, 2001; Iris Eke et al., 2010; Eke et al., 2015; Dickreuter et al., 2016; Zscheppang et al., 2016). Recent work has demonstrated that the two main DNA repair processes (i.e. HR and NHEJ) are more than just nuclear events because they are critically co-regulated by extracellular and cytoplasmic cues (Pickup et al., 2014; Mahajan and Mahajan, 2015). Numerous transmembrane growth factors, adhesion receptors, cytoplasmic protein kinases, and adapter proteins coalesce at focal adhesions and serve as essential and powerful hubs for pro-survival resistance-mediating and DNA repair-modifying signal transduction (Cabodi et al., 2010; I. Eke et al., 2010; Vehlow and Cordes, 2013; Eke et al., 2015; Seguin et al., 2015; Williams et al., 2015; Dickreuter et al., 2016; Tang et al., 2016; Christmann et al., 2017; He et al., 2019). To gain deeper insight into the functions of focal adhesion proteins (FAP) in therapy resistance of HNSCC cancer cells, we employed a 3D high-throughput RNAi-based screen (3DHT-RNAi-S) and identified a previously uncharacterized function of an IF protein, synemin, in radiochemosensitivity and DNA damage repair of HNSCC cells.

In the present work, it is shown that (1) the 3DHT-RNAi-S is a consistent and robust platform for the identification of novel targets; (2) the inhibition of synemin significantly increases the number of radiogenic DSB and elicits radiosensitization; (3) synemin expression and dynamics change upon irradiation; (4) synemin affects NHEJ, but not HR and Alt-EJ, through the regulation of two key DNA repair proteins: DNA-PKcs and Ku70; (5) synemin inhibition leads to deregulated tyrosine kinase activities post X-ray exposure; (6) synemin regulates c-Abl tyrosine kinase activity post X-ray exposure; (7) synemin is an upstream protein of DNA-PKcs and c-Abl kinases; (8) synemin forms a complex with DNA-PKcs and c-Abl

in an ATM-dependent manner; (9) synemin's function in DNA repair is limited to the tail domain, more specifically to the serine located at the 1114 position.

## **6.1 The 3DHT-RNAi-S demonstrates as a consistent and robust platform for the identification of novel targets**

The 3DHT-RNAi-S provided a consistent and extensive set of data (Fig. 2a,b and 3). Previously, it has been reported that FAPs such as  $\beta$ 1 integrin, LIMS1, FAK and FHL2 contribute to cancer cell therapy resistance (Eke et al., 2012; Hehlhans et al., 2012; Rossow et al., 2015; Zienert et al., 2015). Moreover, preclinical studies reported radio-sensitization of tumor cells and reduces their survival upon inhibition of FAPs (e.g.  $\beta$ 1 integrin, AKT, FAK) (Park et al., 2008; Eke et al., 2012b). Here, several novel candidates were identified. For example, silencing of Moesin and KIF-11 diminished basal clonogenicity. Moesin has a function to connect the major cytoskeleton structures to the plasma membrane. Thus, the inhibition of moesin could disrupt the adhesion of ECM to plasma membranes leading to the impairment in colony formation. On the other hand, KIF-11 is a motor protein required for the generation of the bipolar spindle during mitosis. Lack of the essential protein prohibits single cells to form colonies. In combination with X-ray irradiation, the main identified candidates of which silencing significantly enhanced cellular radiosensitivity were Parvin  $\beta$ , GRB7, Vinculin, Sorbin and SH3 domain containing 2 (SORBS2), and integrin  $\alpha$ 1, while SLC3A2 and CSRP1 reduced cellular radiosensitivity. Parvin  $\beta$  is overexpressed in colorectal cancer, and it correlates with tumor progression (Bravou et al., 2015). This correlation is also true for ovarian serous carcinomas, where high expression of Parvin  $\beta$  was observed in the primary tumors as well as in solid metastasis (Davidson et al., 2013). GRB7 was shown to promote cancer cell survival and invasion in triple-negative breast cancers and cervical cancers (Ramsey et al., 2011; Giricz et al., 2012; Zhao et al., 2017). Vinculin expression level was reported to be associated with an increased tumor cell proliferation and progression in prostate and pancreatic cancers (Ruiz et al., 2011; WANG et al., 2012). In the case of Integrin  $\alpha$ 1, although yet to be studied comprehensively, it has been recently identified as a pre-malignant biomarker that contributes to therapy resistance and metastasis in pancreatic cancer (Gharibi et al., 2017). In contrast, suppression of SLC3A2 was recently reported to protect ovarian cancer cells from chemotherapeutics (Cui et al., 2018).

Concurrent to the clonogenic survival assay, residual 53BP1-GFP foci were assessed as a readout for DSB repair capacity in unirradiated and 6-Gy irradiated 3D UTSCC15-53BP1-GFP cell cultures upon knockdown of the 117 FAPs. Silencing of various FAPs caused a gain of 53BP1-GFP foci relative to controls upon X-ray treatment. FAPs that could be novel determinants of DSB repair showing a significant increase in residual 53BP1-GFP foci are indicated as follows: integrin  $\alpha$ V,  $\alpha$ 7,  $\alpha$ 8,  $\alpha$ 11 and  $\beta$ 8 subunits, KEAP1, LDB3,

TGFB1, and SDCBP. Christmann and colleagues reported that integrin  $\alpha$ V $\beta$ 3 silencing chemosensitized glioma cells by suppression of HR repair capacity. KEAP1 is known to regulate DNA repair through the interaction with PALB2, a key protein for the repair of radiogenic DSB during HR (Pauty et al., 2014). KEAP1 regulates PALB2 during oxidative stress and in normal conditions PALB2 favors the sub-nuclear localization of BRCA2 and RAD51 upon exposure to genotoxic stress (Pauty et al., 2014). Silencing of integrin  $\alpha$ 1 and  $\alpha$ 7, endoglin, SDCBP, KEAP1, synemin, and talin 1 concertedly enhanced radiosensitivity and numbers of residual DSB foci. It was reported that when negatively regulated in ovarian cancer, endoglin contributed to enhanced sensitivity towards chemotherapeutics to which an increased induction of DNA damage may be related (Ziebarth et al., 2013; Chen et al., 2014). The impairment of FAPs that solely led to compromised clonogenic survival (e.g. vinculin, parvin  $\beta$ , and NDEL1) suggests the link between radiosensitization effect and alternative mechanisms other than DNA damage repair.

These results suggest that the perturbed functions of some FAPs significantly impacts both radiation survival and DSB repair. Moreover, we note that our 3D-HT-RNAi-S is a robust screening platform for the identification of novel potential regulators of cellular radiation survival and DSB repair.

## **6.2 The inhibition of synemin significantly increases DSB numbers and cellular radiosensitivity**

After the screen, the top candidate proteins were filtered using OncoPrint and Cytoscape software to evaluate their expression and interactome with DNA repair proteins. Proteins such as  $\alpha$ 1 integrin and synemin were selected as top candidates due to their novelty in cancer research. In fact, few publications in the cancer field regarding these two proteins were found. After the validations in different types of HNSCC, synemin resulted in a stronger and more promising candidate than  $\alpha$ 1 integrin.

The type IV IF protein synemin is crucial for various cell functions and the formation of organs such as heart and bones (Banwell, 2001; García-Pelagio et al., 2018). The molecular function of synemin in cancers can differ depending on tumor entities. In glioma cells, synemin is overexpressed and associated with enhanced cancer cell proliferation and survival (Pitre et al., 2012). Likewise, synemin promotes proliferation and motility of astrocytoma cells (Pan et al., 2008; Skalli et al., 2013). In HNSCC, synemin demonstrated an upregulation compared to the corresponding normal tissues similar to gliomas and astrocytomas. Moreover, synemin was amplified in several squamous cell carcinomas such as HPV negative HNSCC, lung squamous cell carcinomas (LUSCC), and cervix squamous cell carcinomas (CESCC) (Network, 2015). Contrarily, in one study of breast cancer cells, it was shown that

down-regulation of synemin expression through hypermethylation of the SYN gene led to an acquired migrating and highly metastatic phenotype (Noetzel et al., 2010).

The effect of synemin inhibition on radioresistance was evaluated in a panel of ten 3D-grown HNSCC cell lines. Synemin depletion affected neither the basal clonogenic survival of the ten HNSCC cell lines nor the spontaneous 53BP1 foci number at 0 Gy. In contrast, X-ray exposure of synemin knockdown cells showed significantly enhanced radiosensitivity and elicited significant elevated residual foci numbers in HNSCC cell lines. This suggests that the effect of synemin on DNA repair and radiosensitivity is induced upon genotoxic stress. In line with these results, synemin overexpression led to a higher clonogenic radiation survival as well as a significantly lower number of residual 53BP1 foci relative to controls. Cisplatin, a common chemotherapeutic for HNSCC patients was, therefore, used to further address the function of synemin upon genotoxic stress. Similarly, higher levels of residual 53BP1 foci were observed upon synemin knockdown. Interestingly, Skalli and coworkers observed that synemin inhibition led to a reduced clonogenicity and proliferation in glioblastoma cells.

Hence, the intermediate filament and focal adhesion protein, synemin, was selected based on its novelty for imparting co-regulation of cellular radiosensitivity and DSB repair in HNSCC.

### 6.3 Synemin expression and dynamics change upon irradiation

Subcellular distribution of synemin remains to be understood and it may be dependent on tissue type and tumor entity. In fact, synemin has been identified in focal adhesion localized at the cell membrane. Synemin, as an IF, is also part of the cytoskeleton and, therefore, is an active protein in the cytosol. In HNSCC, synemin is localized cytoplasmically with a slight perinuclear accumulation and a sparing of the cell membrane in HNSCC cell lines. Upon exposure to X-rays, synemin expression levels increased, accompanied by a changed subcellular localization from a wide cytoplasmic to more perinuclear distribution. Interestingly, synemin reorganized around the nucleus, forming filament-like structures. This reorganization could be related to the involvement of IFs in a variety of mechanisms in cellular stress response, such as tissue repair, heat shock, antimicrobial defense, and apoptosis (Marceau et al., 2007; Toivola et al., 2010; Geisler and Leube, 2016).

The function of synemin distribution around the nucleus is not clear, but it may be linked to its scaffolding function. In fact, synemin has been identified as a scaffolding protein for PKA in heart tissue (Russell et al., 2006). A few hours post irradiation, it was possible to observe that synemin formed a strong and stable network in the cytoplasm, in contrast to the un-irradiated cells which did not show an organized synemin in the cytoskeleton. From the chromatin fractionation assay, synemin partially interacted with chromatin, and this interaction increased at 1 h post irradiation. This observation is in line with the recruitment of syne-

min in the perinuclear area. Hence, synemin surrounding the nucleus might have a direct role in DNA repair mechanisms, serving as a scaffold for DNA repair molecules.

Collectively, these results suggest that synemin, also through its inducibility and perinuclear accumulation, plays an essential role in cell survival after genotoxic injury by, for example, X-rays and cisplatin, as well as in DSB repair.

#### **6.4 Synemin affects the NHEJ, but not the HR and Alt-EJ, through the regulation of two key DNA repair proteins: DNA-PKcs and Ku70**

An initial piece of evidence regarding the association between a FAP and DNA repair was reported by Hoyt and colleagues. Culturing of murine lung endothelial cells in collagen type IV or laminin supplementing medium activated integrins, by which bleomycin-induced DNA breaks were inhibited. Thus, the activation of integrins appears to be protective against genotoxic damage (Hoyt et al., 1997), indicating that FAP-mediated adhesion to ECM is a crucial factor for DSB repair.

In the present work, a significantly increased number of residual radiation-induced DSBs was observed upon synemin inhibition in HNSCC cell cultures. In addition, a functional analysis of DNA DSB repair by NHEJ and HR reporter assay (Bennardo et al., 2008) was performed. The analysis from the reporter assay revealed a significantly decreased NHEJ activity of ~50 % upon synemin inhibition. After radiation exposure to synemin-inhibited cells, changes in phosphorylation and expression of some DNA repair proteins of NHEJ such as DNA-PKcs autophosphorylated at serine 2056 (pDNA-PKcs S2056) and Ku70 expression were observed, suggesting an important role in DNA damage repair of synemin. To verify this result, foci assay of 53BP1,  $\gamma$ H2AX, and DNA-PKcs S2056 was carried out. Expectedly, residual foci numbers as well as foci kinetics were strongly affected by the absence of synemin.

Generally, it is not clear whether the reduction of 50% in protein expression or phosphorylation has an effect on DSB repair. If it is assumed that repair proteins in the cell are strongly expressed; perhaps only a complete turn off of the expression or the inhibition of activity leads to an actual impairment of repair. Still, the observable reductions of the DNA repair proteins analyzed in this work seem to highly affect not only residual foci number, but also the kinetics of the recruited proteins such as 53BP1, DNA-PKcs S2056, and  $\gamma$ H2AX.

The decreased number of pDNA-PKcs S2056 foci suggests that synemin inhibition may lead to impaired recruitment of DNA-PKcs at the damage sites, and the broken ends, therefore, cannot be processed and ligated. Nonetheless, an investigation of the expression

of downstream proteins in NHEJ (e.g., Artemis, XRCC4, XLF, and the ligase IV) could provide a deeper insight into the synemin function in NHEJ.

In contrast to NHEJ, the analysis of HR activity by the reporter assay, however, did not reveal any changes upon synemin knockdown and radiation exposure. Because single strand break (SSB) repair and Alt-EJ are crucial pathways in radiation-induced DNA damage repair, the function of synemin in these DNA repair pathways was investigated by determining PARP-1-dependent Alt-EJ expression. PARP-1 protein levels remained unchanged upon synemin inhibition and radiation exposure, indicating that synemin is involved in DNA repair merely via NHEJ.

A strategy to obtain radiosensitizing effects could be the combined treatment with a clinically available PARP inhibitor — Olaparib and synemin inhibition. Under certain conditions, SSBs are converted to DSB during replication and subsequently repaired mainly via HR (Helleday et al., 2005; Tutt et al., 2005). Because synemin inhibition affects NHEJ, it can be assumed that the combined treatment with synemin and Olaparib might result in the impairment of NHEJ, Alt-EJ, and SSB, diminishing the DNA damage capacity of HNSCC cells. Thus, cells possess solely HR to rectify damage induced by radiation, leading to a high burden of DNA damage upon induction (SSB and DSB), and eventually cell death. Another strategy could be the implementation of CDK4/6 inhibitor LY2835219, which leads to cell cycle arrest in G0-G1 phase in HNSCC (Ku et al., 2016), in combination with synemin inhibition. This double treatment together with irradiation could further sensitize the tumor cells because G1 cells apply mainly the NHEJ machinery to repair the DSB and moreover G1 cells are known to be more radiosensitive (Hall and Giaccia, 2012). These strategies, however, require a comprehensive study to demonstrate their clinical relevance and applicability.

## **6.5 Synemin inhibition leads to a deregulated tyrosine kinase activity 24 h post X-ray exposure**

To further unravel how synemin elicits its impact on NHEJ, a broad-spectrum kinase profiling was performed. Intriguingly, significant changes were found in protein kinase activities upon irradiated synemin-depleted cell cultures after 1 h and 24 h relative to controls. Interestingly, synemin knockdown alone failed to modify protein kinase activities, implying that the DNA repair-co-regulating function of synemin becomes essential upon genotoxic injury. Synemin's inhibition effect was clearly potent 24 h post X-ray. From the kinase profiling, c-Abl was identified as the top deactivated protein kinase along with members of the Scr family such as Scr, Yes, Lck, Blk, and Lyn in synemin-depleted, 6-Gy irradiated cells compared to controls. Various detected tyrosine kinases are known to play a role in DNA repair such as c-Abl, EGFR, IGF1R, Src, Lyn, and Fyn (Mahajan and Mahajan, 2015). EGFR is a well-known tyrosine kinase involved in therapy-resistance processes, leading for example to radioresistance. This

ability could be linked to its function in the regulation of essential DSB DNA repair kinases, such as ATM and DNA-PKcs (Lee et al., 2015; Teng et al., 2015). But its task is not limited to DSB; it is also involved in mismatch repair through the regulation of PCNA and also plays a role in chromatin modulation by affecting H4 phosphorylation (Chou et al., 2014; Ortega et al., 2015). IGF1R kinase has been recognized as necessary for the translocation of Rad51, a key HR protein. Src terminates DNA damage response signaling by controlling ATR and Chk1 kinases (Fukumoto et al., 2014). Regarding Lyn, it was demonstrated that upon irradiation exposure, it forms a complex with CDK1, a key protein for cell cycle regulation (Kharbanda et al., 1996). Furthermore, Lyn activates DNA-PKcs and PKC $\delta$ , these two proteins are directly involved in DNA repair processes, and their malfunction can lead to lethal effects to the cells (Kumar et al., 1998; Yoshida et al., 2002). In contrast to tyrosine kinases, serine/threonine kinases remained partly unaffected in synemin-depleted cells apart from some CMGC (cyclin-dependent kinases) and CAMK (calcium- and calmodulin-regulated kinases) serine/threonine kinases. Altogether, these results show that synemin may indirectly regulate the DNA repair machinery through the modulation of important tyrosine kinases involved in DNA repair processes.

## **6.6 Synemin regulates c-Abl tyrosine kinase at 6 and 24 h post X-ray exposure**

The non-receptor tyrosine kinase c-Abl was identified as the top deactivated protein kinase upon synemin knockdown and irradiation. c-Abl is involved in several regulatory functions (e.g. cell proliferation, differentiation, adhesion, migration, and DNA-repair (Plattner et al., 1999; Hantschel and Superti-Furga, 2004)). Due to the pro-survival functions of c-Abl, alteration of c-Abl kinase signaling might contribute to a more aggressive tumor phenotype (Srinivasan and Plattner, 2006). Thus, c-Abl has been considered as a potential therapeutic target for cancer treatment (Ren, 2005). A number of studies have reported an intricate communication between the tyrosine c-Abl and several DNA repair proteins. In fact, the molecular function of c-Abl in DNA-repair machinery has been proposed, including DNA-PKcs, ATM, BRCA1, and RAD51 (Jin et al., 1997; Shaul and Ben-Yehoyada, 2005). The dependence of c-Abl activity on synemin was then further investigated to understand the underlying mechanisms. Firstly, c-Abl total protein expression was examined, as well as its phosphorylation sites Y412 and T715 associated with c-Abl kinase activity and the distribution of c-Abl in different cell compartments. Without changes in the c-Abl protein level, both Y412 and T715 demonstrated a significant reduction upon synemin removal in irradiated cells relative to controls over the 24-h observation period. During the DNA damage response, c-Abl dissociates from cytoplasmatic proteins, such as 14-3-3, and shuttles into the nucleus to interact with various DNA repair proteins (Yoshida et al., 2005). Despite the shuttling from the cyto-



plasm to the nucleus not being investigated, it was observed that T715 phosphorylation, which dictates the distribution of c-Abl in the cell, was affected by synemin inhibition. It is possible that the decreased T715 phosphorylation leads to an impaired redistribution of c-Abl upon synemin knockdown, which prohibits the relocation of c-Abl leading to a disruption of the kinase activity of c-Abl. This observation indicates a possible function of synemin as a cytoplasmic carrier or scaffold for c-Abl. Altogether, synemin appears to have a significant role in the regulation of c-Abl kinase activity and its localization, which could potentially associate with the regulation of DNA damage repair.

## **6.7 Synemin forms a complex with DNA-PKcs and c-Abl in an ATM-dependent manner**

While other tyrosine and serine/threonine kinases demonstrated alterations in the absence of synemin, the most intriguing observation was the identification of a protein complex composed of synemin, c-Abl, and DNA-PKcs, being critical for DSB repair and clonogenic radiation survival. Interestingly, the DNA-PKcs single knockdown and the DNA-PKcs/synemin double knockdown, but not the c-Abl single knockdown, resulted in reduced survival upon treatment and an increased residual DSB foci number. This finding suggests synemin to be hierarchically upstream of c-Abl and DNA-PKcs. Synemin, as other IFs, is overexpressed in different human malignancies, contributing to a more aggressive phenotype (Quick et al., 2015; Parlakian et al., 2016). In breast cancer, synemin expression is modified by aberrant promoter methylation and correlates with early relapse (Noetzel et al., 2010). In glioblastoma, synemin controls cell proliferation through the AKT pathway by antagonizing PP2A (Pitre et al., 2012). Contrarily, a down-regulation of synemin fails to alter the stability of the cytoskeleton in human hepatocellular carcinomas, indicating the tissue specificity and the multifunctionality of synemin (Liu et al., 2011). Synemin has been described as a bona fide IF protein according to its AA sequence, with an inability to self-assemble into IFs. The unique biophysical properties determine synemin's protein interaction abilities with either the IF proteins vimentin and desmin or other proteins for facilitating the assembly of dynamic and content-specific cytoarchitecture- and stress response-related interactomes (Bilak et al., 1998). In line with these results, c-Abl and DNA-PKcs were precipitated by synemin with/-out X-ray exposure.

Further experiments using pharmacological inhibitors for c-Abl and DNA-PKcs corroborated these findings. Application of an ATM inhibitor revealed the dependence of the synemin/c-Abl/DNA-PKcs protein complex formation on ATM kinase activity both in absence and presence of radiogenic genotoxic injury. Using the ATM deficient cell line SKX, the interaction of synemin with c-Abl was conserved, independently of the ATM status. The interrelation between DNA-PKcs and synemin, however, seemed to rely on ATM as in the SAS cell line.

In conclusion, the complex formation between synemin and DNA-PKcs relies on ATM kinase activity independently of the cell line.

### **6.8 Synemin's function in DNA repair is limited to the tail domain, more specifically to the Serine located in the 1114 position**

Due to synemin interaction with DNA-PKcs being highly dependent on ATM kinase activity, synemin may possess ATM kinase substrate. Thus, potential phosphorylation sites of synemin were investigated. Firstly, a computational prediction of phosphorylatable AA residues of synemin using the GPS database (Xue et al., 2008) was carried out. Intriguingly, the prediction from the GSP database indicated that Serine 421, 554, 1114, 1159 residues located at the synemin tail, but none at the head or coil-linker domains of synemin, are phosphorylatable by ATM. To confirm the prediction and the hypothesis regarding the ATM-dependence, cells containing different constructs of synemin (i.e., a head-linker- and a linker-tail-depleted, as well as a wildtype) were used. From the outcome, it is suggested that the tail of synemin essentially contributes to DSB repair in an ATM-dependent manner. Similarly to synemin, the intermediate filament vimentin is a target of DNA-PKcs upon genotoxic stress (Kotula et al., 2013). Vimentin is phosphorylated at serine 459 by DNA-PKcs, leading to a higher cellular adhesion and migration ability.

The role of the tail in IFs is not clearly understood, whereas the head and the coil-coil domains are necessary for filament formation. Besides the unnecessary of the tail in the formation of filament, it contains important information. Synemin's tail, compared to other IFs, is considerably larger, suggesting its function beyond typical IF activity. To characterize the role of these phosphorylation sites at the synemin tail for DNA repair, synemin constructs containing either tail AAs 301 to 961 or tail AAs 962 to 1565 were generated. The analysis of 53BP1 repair foci upon X-ray irradiation revealed a significant increase of 53BP1 foci in cells expressing the anterior, but not the posterior, part of the tail, indicating a potential engagement of S1114 and S1159 for DNA repair. To further demonstrate the functionality of these serine residues, point mutations preventing phosphorylation of those serines were introduced. Serine 1114 AA residue at the synemin tail was found to be essential for the repair of radiogenic DSBs. Interestingly, this serine is surrounded by glutamines (Q), indicating that the AA residue sequence from 1113 to 1115 is QSQ, for which a higher specificity for ATM phosphorylation has been demonstrated (Sampietro et al., 2018).

In summary, these results suggest a critical role of synemin in the radiochemoresistance of HNSCC cells through its participation in NHEJ-mediated DSB repair. Synemin seems to serve as a scaffold protein for c-Abl and DNA-PKcs that co-determines DSB repair dependent on ATM. These findings shed further light on the complexity of DSB repair by

supporting the concept of cytoarchitectural elements as key co-regulators of nuclear events such as DNA damage repair.

## 7 Summary

**Background:** Therapy resistance is a great challenge in cancer treatment. Among numerous factors, cell adhesion to extracellular matrix is a well-known determinant of radiochemoresistance. It has been shown that targeting focal adhesion proteins (FAPs), e.g.  $\beta$ 1 integrin, enhances tumor cell radio(chemo)sensitivity in various entities such as head and neck squamous cell carcinoma (HNSCC), lung carcinoma, glioblastoma, breast carcinoma and leukemia. Previous studies demonstrated a functional crosstalk between specific FAPs and DNA repair processes; however, the molecular circuitry underlying this crosstalk remains largely unsolved. Hence, this study in HNSCC aimed to identify alternative FAPs associated with DNA damage repair mechanisms and radioresistance.

**Materials and Methods:** A novel 3D High Throughput RNAi Screen (3DHT-RNAi-S) using laminin-rich extracellular matrix (IrECM) was established to determine radiation-induced residual DNA double strand breaks (DSBs; foci assay) and clonogenic radiation survival. In the screen, we used UTSCC15 HNSCC cells stably expressing the DSB marker protein 53BP1 tagged to pEGFP. Validations were performed in 10 additional HNSCC cell lines (Cal33, FaDu, SAS, UTSCC5, UTSCC8, UTSCC14, UTSCC15, UTSCC45 and XF354f12) grown in 3D IrECM. Immunofluorescence staining, immunoblotting, chromatin fractionation were utilized to evaluate protein expression, dynamics and kinetics post irradiation. Investigations of molecular mechanisms of DNA repair and radio(chemo)resistance employed DSB repair reporter assays for non-homologous end joining (NHEJ) and homologous recombination (HR), cell cycle analysis, chromatin fractionation levels evaluation and kinase activity profiling (PamGene) upon protein knockdown in combination with/-out X-ray exposure. Foci assay and clonogenic survival assay were performed after single or multiple knockdowns of synemin and associated proteins such as DNA-PKcs and c-Abl. Protein-protein interactions between synemin and associated proteins were determined using immunoprecipitation and proximity ligation assay. Mutant/depletion constructs of synemin ( $\Delta$ Link-Tail,  $\Delta$ Head-Link, Synemin\_301-961, Synemin\_962-1565, S1114A and S1159A) were generated in order to identify essential synemin's sites controlling DNA repair functions.

**Results:** Among the targets found in the 3DHT-RNAi-S, synemin was one of the most promising FAP candidates to determine HNSCC cell survival and DNA damage repair. Synemin silencing radiosensitized HNSCC cells, while its exogenous overexpression induced radio-protection. Radiation induced an increased synemin/chromatin interaction and a marked accumulation of synemin in the perinuclear area. Intriguingly, synemin depletion elicited a 40% reduction in NHEJ activity without affecting HR or Alt-EJ. In line, ATM, DNA-PKcs and c-Abl phosphorylation as well as Ku70 expression strongly declined in synemin depleted and irradiated cells relative to controls, whereas an opposite effect was observed under synemin overexpression. Single, double and triple depletion of synemin, DNA-PKcs and c-Abl resulted in a similar radiosensitizing effect and DSB levels as detected upon single knockdown of synemin, describing its upstream role. In kinome analysis, tyrosine kinases showed significantly reduced activity after synemin silencing relative to controls. Furthermore, immunoprecipitation assays revealed a protein complex formed between synemin, DNA-PKcs and c-Abl under pre- and post-irradiation conditions. This protein complex dispersed when ATM was pharmacologically inhibited, implying synemin function to be dependent on ATM kinase activity. By means of the different mutation/deletion constructs of synemin, the phosphorylation site at serine 1114 located on the distal portion of synemin's tail was identified as essential protein-protein interaction site for synemin's function in DNA repair.

**Conclusions:** The established 3DHT-RNAi-S provides a robust screening platform for identifying novel targets involved in therapy resistance. Based on this screen and detailed mechanistic analyses, the intermediate filament synemin was discovered as a novel important determinant of DNA repair, tyrosine kinase activity and radiochemoresistance of HNSCC cells. These results further support the notion that DNA repair is controlled by cooperative interactions between nuclear and cytoplasmic proteins.

## 8 Zusammenfassung

**Hintergrund:** Die Therapieresistenz ist eine große Herausforderung in der Krebstherapie. Neben zahlreichen Faktoren ist die Zelladhäsion an die extrazelluläre Matrix eine bekannte Determinante der Radiochemoresistenz. Es wurde gezeigt, dass das Targeting fokaler Adhäsionsproteine (FAPs), beispielsweise das  $\beta$ 1-Integrin, die Radiosensibilität bei verschiedenen Entitäten wie Plattenepithelkarzinomen des Kopfes und Halses (HNSCC), Lungenkarzinom, Glioblastom, Brustkarzinom und Leukämie erhöht. Frühere Studien zeigen ein funktionelles Zusammenspiel von spezifischen FAPs und DNA-Reparaturprozessen. Die molekularen Mechanismen, die diesem Zusammenspiel zugrunde liegen, sind jedoch noch weitgehend unbekannt. Ziel dieser Studie in HNSCC war es, alternative FAPs zu identifizieren, die mit DNA-Reparaturmechanismen und Strahlenresistenz zusammenhängen.

**Material und Methoden:** Ein neuartiges 3D-Hochdurchsatz-RNAi-Screen (3DHT-RNAi-S) wurde unter Verwendung einer lamininreichen extrazellulären Matrix (IrECM) etabliert, um strahlungsinduzierte residuelle DNA-Doppelstrangbrüche (DSBs; Foci-Assay) und klonogenes Zellüberleben zu bestimmen. In diesem Screen wurden UTSCC15-HNSCC-Zellen, die das mit pEGFP markierte DSB-Markerprotein 53BP1 stabil exprimieren, verwendet. Validierungen wurden in 10 weiteren HNSCC-Zelllinien (Cal33, FaDu, SAS, UTSCC5, UTSCC8, UTSCC14, UTSCC15, UTSCC45 und XF354f2) durchgeführt, die in 3D-IrECM kultiviert wurden. Immunfluoreszenzfärbung, Immunoblotting und Chromatinfractionierung wurden angewendet, um Proteinexpression, Dynamik und Kinetiken nach Bestrahlung zu beleuchten. Um die molekularen Mechanismen von DNA-Reparatur und Radio(Chemo)resistenz zu untersuchen, wurden DSB-Repair-Reporter-Assays für nicht-homologes End-Joining (NHEJ) und homologe Rekombination (HR), Zellzyklusanalyse, Auswertung der Chromatinfractionierungsniveaus und Kinase-Aktivitätsanalyse (PamGene) nach Protein-Knockdown in Kombination mit Röntgenstrahlung eingesetzt. Foci-Assay und klonogener Überlebensassay wurden nach Einzel- oder Multi-Knockdowns von Synemin und zugehörigen Proteinen wie DNA-PKcs und c-Abl durchgeführt. Protein-Protein-Wechselwirkungen zwischen Synemin und assoziierten Proteinen wurden mittels Immunpräzipitation und Proximity-Ligation-Assay bestimmt. Um essentielle Regionen in Synemin zu identifizieren, die die DNA-Reparatur regu-

lieren, wurden Konstrukte von Synemin mit unterschiedlichen Mutationen/Deletionen ( $\Delta$ Link-Tail,  $\Delta$ Head-Link, Synemin\_301-961, Synemin\_962-1565, S1114A und S1159A) hergestellt.

**Ergebnisse:** Unter den im 3DHT-RNAi-S untersuchten Proteinen war Synemin einer der vielversprechendsten FAP-Kandidaten zur Bestimmung des Überlebens von HNSCC-Zellen und der Reparatur von DNA-Schäden. Das Ausschalten der Synemin-Expression radiosensibilisierte HNSCC-Zellen, während die exogene Überexpression eine Radioprotektion induzierte. Die Strahlung führte zu einer erhöhten Synemin/Chromatin-Wechselwirkung und einer deutlichen Akkumulierung von Synemin im perinukleären Bereich. Interessanterweise führte das Ausschalten von Synemin zu einer Verringerung der NHEJ-Aktivität um 40%, ohne dass dies Auswirkungen auf HR oder Alt-EJ hatte. In der Folge sank die Phosphorylierung von ATM, DNA-PKcs und c-Abl sowie die Ku70-Expression in Synemin-defizienten und bestrahlten Zellen im Vergleich zu den Kontrollen stark ab, während bei Synemin-Überexpression ein gegenteiliger Effekt zu beobachten war. Einzel-, Doppel- und Dreifachdepletion von Synemin, DNA-PKcs und c-Abl führte zu ähnlichem Ausmaß an Strahlungssensibilisierung und DSB-Anzahl im Vergleich zum Einzel-Knockdown von Synemin, was dessen übergeordnete Rolle zeigt. In der Kinomanalyse zeigten Tyrosinkinasen im Vergleich zu den Kontrollen eine signifikant verminderte Aktivität nach Synemin silencing. Darüber hinaus identifizierten Immunpräzipitationsassays einen Proteinkomplex zwischen Synemin, DNA-PKcs und c-Abl vor und nach Bestrahlung. Dieser Proteinkomplex wurde aufgespalten, als ATM pharmakologisch inhibiert wurde. Dies deutet an, dass die Synemin-Funktion von der ATM-Kinaseaktivität abhängt. Unter Verwendung unterschiedlich mutierter Konstrukte von Synemin wurde die Phosphorylierungsstelle an Serin 1114 am distalen Teil des Synemin-Schwanzes als essentielle Protein-Protein-Interaktionsstelle identifiziert, welche Synemins Funktion in der DNA-Reparatur kontrolliert.

**Schlussfolgerungen:** Der etablierte 3DHT-RNAi-S bietet eine robuste Screening-Plattform zur Identifizierung neuartiger Zielproteine, die an der Therapieresistenz beteiligt sind. Basierend auf Screening und detaillierten mechanistischen Analysen wurde das Intermediärfilamentprotein Synemin als eine neue wichtige Determinante von DNA-Reparatur, Tyrosinkinaseaktivität und Radioresistenz von HNSCC-Zellen entdeckt. Diese Ergebnisse stützen zudem die Hypothese, dass die DNA-Reparatur durch kooperative Wechselwirkungen zwischen nuklearen und zytoplasmatischen Proteinen kontrolliert wird.

## 9 Figure legends

Figure 2.1: Comparison of 2D and 3D cell culture conditions .....	5
Figure 2.2: Integrins and FAPs contribute to cancer radio- and drug-resistance by mediating cell adhesion to the extracellular matrix.....	6
Figure 2.3: Synemin structure and interaction sites.....	10
Figure 2.4: Synemin isoforms. Synemin is composed of three isoforms: $\alpha$ , $\beta$ , and L.....	10
Figure 2.5: Percentage of the most frequent tumor sites when cancer was the leading cause of death in Germany (2014).....	12
Figure 2.6: Ionizing radiation induces damage to macromolecules .....	15
Figure 2.7: DNA repair mechanism distributed in the cell cycle.....	17
Figure 2.8: DSB DNA repair mechanisms. The main DSB DNA repair mechanism are NHEJ, HR, and Alt-EJ .....	18
Figure 4.1: Schematic representation of the 3D colony formation assay workflow.....	40
Figure 4.2: Schematic representation of a DSB marked by $\gamma$ H2AX and 53BP1 .....	43
Figure 4.3: Foci assay workflow .....	44
Figure 4.4: Scheme of the Western blot setup .....	46
Figure 4.5: Schematic representation of the EJ5GFP and the pGC reporter plasmid.....	47
Figure 4.6: Principle of Proximity Ligation Technique .....	53
Figure 5.1: Identification of focal adhesion proteins affecting cell survival, radiosensitivity and DNA repair. Workflow of 3D high-throughput RNAi screening (3D HTP-RNAi-S).....	55
Figure 5.2: Identification of focal adhesion proteins affecting cell survival and radiosensitivity.....	56
Figure 5.3: Identification of focal adhesion proteins affecting DNA repair .....	57
Figure 5.4: Identification of focal adhesion proteins affecting cell survival, radiosensitivity and DNA repair.....	58
Figure 5.5: Top focal adhesion protein affecting cell survival. ....	59
Figure 5.6: Synemin essentially controls cellular radiosensitivity and DSB repair.....	60
Figure 5.7: Synemin essentially controls cellular radiosensitivity and DSB repair.....	61
Figure 5.8: Synemin essentially controls cellular radiosensitivity.....	62
Figure 5.9: Synemin characterization upon radiochemotherapy.....	63
Figure 5.10: Synemin distribution in a panel of 10 HNSCC cell lines .....	64
Figure 5.11: Synemin kinetics upon radiotherapy treatment.....	65
Figure 5.12: Synemin functions in non-homologous end joining.....	66
Figure 5.13: Synemin functions in non-homologous end joining.....	67
Figure 5.14: Synemin functions in non-homologous end joining.....	69



Figure 5.15: Synemin effects on cell cycle .....	70
Figure 5.16: Synemin effects on heterochromatin levels .....	71
Figure 5.17: Synemin regulates tyrosine kinase activity, in particular c-Abl kinase .....	73
Figure 5.18: Synemin regulates c-Abl kinase activity .....	74
Figure 5.19: Synemin regulates c-Abl kinase activity .....	75
Figure 5.20: Synemin/DNA-PKcs/c-Abl co-control radiation survival.....	76
Figure 5.21: Synemin/DNA-PKcs/c-Abl co-control DSB repair .....	77
Figure 5.22: c-Abl and DNA-PKcs forms a complex together with synemin .....	79
Figure 5.23: c-Abl and DNA-PKcs interaction with synemin depends on ATM kinase activity .....	81
Figure 5.24: c-Abl and DNA-PKcs interaction with synemin depends on ATM kinase activity .....	83
Figure 5.25: Synemin depends DNA repair function depends on S1114 phosphorylation site .....	84
Figure 5.26: Synemin's mechanism .....	85

## 10 Tables

Table 2.1: IF superfamily classification. IFs can be categorized depending on the tissue of origin or intracellular localization .....	8
Table 4.1. Devices used for the biochemical, molecular-biological and cell culture experiments .....	23
Table 4.2. Materials used for the biochemical, molecular-biological and cell culture experiments.....	25
Table 4.3. Endoribonuclease-prepared small interfering (esi)RNAs or small interfering (si)RNAs used to silence the indicated genes .....	26
Table 4.4. Inhibitors and chemotherapeutics used for <i>in vitro</i> experiments .....	26
Table 4.5. Plasmids used for cloning, overexpression, flow cytometry, fluorescence microscopy and immunoprecipitation. ....	27
Table 4.6. Primers used for the amplification and flanking of SYN1 (synemin gene) with the indicated restriction sites. Respective sequences are shown.....	28
Table 4.7. Composition of media used to culture bacteria .....	29
Table 4.8. Method kits used for biochemical applications .....	29
Table 4.9. Primary antibodies used for Western blot, immunoprecipitation and immunofluorescence	30
Table 4.10. Secondary antibodies used for Western blot, immunoprecipitation, immunofluorescence or immunohistochemical applications .....	31
Table 4.11. Solutions used for cell biological applications. The detailed composition for each solution is shown .....	32
Table 4.12. Solutions used for protein-biochemical and molecular-biological applications. The composition for each solution is shown.....	33
Table 4.13. Solutions used for immunofluorescence and immunohistological applications. The composition for each solution is shown.....	35
Table 4.14. Further solutions and chemicals used for biochemical, molecular-biological or <i>in vitro</i> applications.....	36
Table 4.15. PC programs for data analysis and presentation. ....	36
Table 4.16. HNSCC cells and origin.....	37
Table 4.17. Pipetting scheme for esiRNA and siRNA transfection in 6-well plates and 100 mm dishes .....	38
Table 4.18. Cell numbers and corresponding incubation periods used for the colony formation assays .....	40
Table 4.19. List of focal adhesion proteins selected for the screen library according to the Integrin Adhesome described by Horton et al., 2015 .....	41
Table 4.20. Composition of stacking and separation gels used for SDS PAGE .....	45

Table 4.21. PCR protocol used to amplify genes of interest and add flanking restriction sites ..... 50

Table 4.22. Protocol for restriction digest of PCR-products flanked with restriction sites and desired expression vectors..... 51

Table 4.23. Protocol for ligation of PCR-products flanked with restriction sites and desired expression vectors ..... 51

Table 4.24. Pipetting scheme for plasmid transfection in 6-well plates and 100 mm dishes ..... 52

## 11 Bibliography

- Anon. 2017. Intermediate Filaments. *Cell Biol*:613–622 DOI: 10.1016/B978-0-323-34126-4.00035-9.
- Ban ath JP, MacPhail SH, Olive PL. 2004. Radiation Sensitivity, H2AX Phosphorylation, and Kinetics of Repair of DNA Strand Breaks in Irradiated Cervical Cancer Cell Lines. *Cancer Res*, 64(19):7144–7149 DOI: 10.1158/0008-5472.CAN-04-1433.
- Banwell BL. 2001. Intermediate filament-related myopathies. *Pediatr Neurol*, 24(4):257–63.
- Begg AC, Stewart FA, Vens C. 2011. Strategies to improve radiotherapy with targeted drugs. *Nat Rev Cancer*, 11(4):239–253 DOI: 10.1038/nrc3007.
- Bellin RM, Sernett SW, Becker B, Ip W, Huiatt TW, Robson RM. 1999. Molecular characteristics and interactions of the intermediate filament protein synemin. Interactions with alpha-actinin may anchor synemin- containing heterofilaments. *JBiolChem*, 274(41):29493–29499 DOI: 10.1074/JBC.274.41.29493.
- Bennardo N, Cheng A, Huang N, Stark JM. 2008. Alternative-NHEJ Is a Mechanistically Distinct Pathway of Mammalian Chromosome Break Repair. In: Haber JE (ed) *PLoS Genet*, 4(6):e1000110 DOI: 10.1371/journal.pgen.1000110.
- Le Beyec J, Xu R, Lee S-Y, Nelson CM, Rizki A, Alcaraz J, Bissell MJ. 2007. Cell shape regulates global histone acetylation in human mammary epithelial cells. *Exp Cell Res*, 313(14):3066–3075 DOI: 10.1016/J.YEXCR.2007.04.022.
- Bilak SR, Sernett SW, Bilak MM, Bellin RM, Stromer MH, Huiatt TW, Robson RM. 1998. Properties of the novel intermediate filament protein synemin and its identification in mammalian muscle. *Arch Biochem Biophys*, 355(1):63–76 DOI: 10.1006/abbi.1998.0702.
- Bissell MJ, Kenny PA, Radisky DC. 2005. Microenvironmental regulators of tissue structure and function also regulate tumor induction and progression: the role of extracellular

- matrix and its degrading enzymes. *Cold Spring Harb Symp Quant Biol*, 70:343–56 DOI: 10.1101/sqb.2005.70.013.
- Bosman FT, Stamenkovic I. 2003. Functional structure and composition of the extracellular matrix. *J Pathol*, 200(4):423–428 DOI: 10.1002/path.1437.
- Bouvard D, Pouwels J, De Franceschi N, Ivaska J. 2013. Integrin inactivators: balancing cellular functions in vitro and in vivo. *Nat Rev Mol Cell Biol*, 14(7):430–442 DOI: 10.1038/nrm3599.
- Braakhuis BJM, Bloemena E, Leemans CR, Brakenhoff RH. 2010. Molecular analysis of surgical margins in head and neck cancer: More than a marginal issue. *Oral Oncol*, 46(7):485–491 DOI: 10.1016/J.ORALONCOLOGY.2010.01.019.
- Brakebusch C, Fässler R. 2005.  $\beta$ 1 integrin function in vivo: Adhesion, migration and more. Springer Science + Business Media, Inc. Manufactured in The Netherlands [accessed: 04/27/2019] URL: <https://link.springer.com/content/pdf/10.1007%2Fs10555-005-5132-5.pdf>.
- Bravou V, Antonacopoulou A, Papanikolaou S, Nikou S, Lilis I, Giannopoulou E, Kalofonos HP. 2015. Focal Adhesion Proteins  $\alpha$ - and  $\beta$ -Parvin are Overexpressed in Human Colorectal Cancer and Correlate with Tumor Progression. *Cancer Invest*, 33(8):387–397 DOI: 10.3109/07357907.2015.1047508.
- Breen AP, Murphy JA. 1995. Reactions of oxyl radicals with DNA. *Free Radic Biol Med*, 18(6):1033–1077.
- Bristow RG, Hill RP. 2008. Hypoxia, DNA repair and genetic instability. *Nat Rev Cancer*, 8(3):180–192 DOI: 10.1038/nrc2344.
- Cabodi S, del Pilar Camacho-Leal M, Di Stefano P, Defilippi P. 2010. Integrin signalling adaptors: not only figurants in the cancer story. *Nat Rev Cancer*, 10(12):858–70 DOI: 10.1038/nrc2967.
- Calderwood DA, Campbell ID, Critchley DR. 2013. Talins and kindlins: partners in integrin-mediated adhesion. *Nat Rev Mol Cell Biol*, 14(8):503–517 DOI: 10.1038/nrm3624.
- Ceccaldi R, Rondinelli B, D'Andrea AD. 2016. Repair Pathway Choices and Consequences at the Double-Strand Break. *Trends Cell Biol*, 26(1):52–64 DOI: 10.1016/j.tcb.2015.07.009.
- Chang HHY, Pannunzio NR, Adachi N, Lieber MR. 2017. Non-homologous DNA end joining and alternative pathways to double-strand break repair. *Nat Rev Mol Cell Biol*,

18(8):495–506 DOI: 10.1038/nrm.2017.48.

- Chaturvedi P, Chocolatewala N. 2009. Role of human papilloma virus in the oral carcinogenesis: An Indian perspective. *J Cancer Res Ther*, 5(2):71 DOI: 10.4103/0973-1482.52788.
- Chen X-P, Chen Y-G, Lan J-Y, Shen Z-J. 2014. MicroRNA-370 suppresses proliferation and promotes endometrioid ovarian cancer chemosensitivity to cDDP by negatively regulating ENG. *Cancer Lett*, 353(2):201–210 DOI: 10.1016/J.CANLET.2014.07.026.
- Chou R-H, Wang Y-N, Hsieh Y-H, Li L-Y, Xia W, Chang W-C, Chang L-C, Cheng C-C, Lai C-C, Hsu JL, Chang W-J, Chiang S-Y, Lee H-J, Liao H-W, Chuang P-H, Chen H-Y, Wang H-L, Kuo S-C, Chen C-H, Yu Y-L, Hung M-C. 2014. EGFR Modulates DNA Synthesis and Repair through Tyr Phosphorylation of Histone H4. *Dev Cell*, 30(2):224–237 DOI: 10.1016/j.devcel.2014.06.008.
- Christmann M, Diesler K, Majhen D, Steigerwald C, Berte N, Freund H, Stojanović N, Kaina B, Osmak M, Ambriović-Ristov A, Tomicic MT. 2017. Integrin alphaVbeta3 silencing sensitizes malignant glioma cells to temozolomide by suppression of homologous recombination repair. *Oncotarget*, 8(17):27754–27771 DOI: 10.18632/oncotarget.10897.
- Ciccia A, Elledge SJ. 2010. The DNA Damage Response: Making it safe to play with knives. *Mol Cell*, 40(2):179 DOI: 10.1016/J.MOLCEL.2010.09.019.
- Colevas AD, Yom SS, Pfister DG, Spencer S, Adelstein D, Adkins D, Brizel DM, Burtness B, Busse PM, Caudell JJ, Cmelak AJ, Eisele DW, Fenton M, Foote RL, Gilbert J, Gillison ML, Haddad RI, Hicks WL, Hitchcock YJ, Jimeno A, Leizman D, Maghami E, Mell LK, Mittal BB, Pinto HA, Ridge JA, Rocco J, Rodriguez CP, Shah JP, Weber RS, Wittek M, Worden F, Zhen W, Burns JL, Darlow SD. 2018. NCCN Guidelines Insights: Head and Neck Cancers, Version 1.2018. *J Natl Compr Canc Netw*, 16(5):479–490 DOI: 10.6004/jnccn.2018.0026.
- Cordes N, Blaese MA, Plasswilm L, Rodemann HP, Van Beuningen D. 2003. Fibronectin and laminin increase resistance to ionizing radiation and the cytotoxic drug Ukrain® in human tumour and normal cells in vitro. *Int J Radiat Biol*, 79(9):709–720 DOI: 10.1080/09553000310001610240.
- Cordes N, Gurtner K, Belka C. 2013. Verbesserte Behandlungschancen durch molekulares Targeting in der Radioonkologie. *Onkologe*, 19(10):848–857 DOI: 10.1007/s00761-013-2498-9.
- Cordes N, Meineke V. 2003. Cell adhesion-mediated radioresistance (CAM-RR).

- Extracellular matrix-dependent improvement of cell survival in human tumor and normal cells in vitro. *Strahlenther Onkol*, 179(5):337–44 DOI: 10.1007/s00066-003-1074-4.
- Cordes N, Seidler J, Durzok R, Geinitz H, Brakebusch C. 2006. B1-Integrin-Mediated Signaling Essentially Contributes To Cell Survival After Radiation-Induced Genotoxic Injury. *Oncogene*, 25(9):1378–1390 DOI: 10.1038/sj.onc.1209164.
- Coulombe PA, Ma L, Yamada S, Wawersik M. 2001. Intermediate filaments at a glance. [accessed: 05/30/2019] URL: <http://jcs.biologists.org>.
- Criswell S, O'Brien T, Skalli O. 2018. Presence of intermediate filament protein synemin in select sarcomas. *J Histotechnol*, 41(2):40–48 DOI: 10.1080/01478885.2018.1438757.
- Criswell S, Taylor M, Kenwright K, Skalli O. 2019. The intermediate filament protein synemin (SYNM) was found to be more widespread in CD117 + gastrointestinal stromal cell tumors (GIST) than the CD34 transmembrane phosphoglycoprotein: an immunohistochemical study. *J Histotechnol*:1–7 DOI: 10.1080/01478885.2019.1576829.
- Cui Y, Qin L, Tian D, Wang T, Fan L, Zhang P, Wang Z. 2018. ZEB1 Promotes Chemoresistance to Cisplatin in Ovarian Cancer Cells by Suppressing SLC3A2. *Chemotherapy*, 63(5):262–271 DOI: 10.1159/000493864.
- Curado MP, Hashibe M. 2009. Recent changes in the epidemiology of head and neck cancer. *Curr Opin Oncol*, 21(3):194–200 DOI: 10.1097/CCO.0b013e32832a68ca.
- Daley JM, Sung P. 2014. 53BP1, BRCA1, and the choice between recombination and end joining at DNA double-strand breaks. *Mol Cell Biol*, 34(8):1380–1388 DOI: 10.1128/MCB.01639-13.
- Damiano JS, Cress AE, Hazlehurst LA, Shtil AA, Dalton WS. 1999. Cell adhesion mediated drug resistance (CAM-DR): role of integrins and resistance to apoptosis in human myeloma cell lines. *Blood*, 93(5):1658–67 [accessed: 04/27/2019] URL: <http://www.ncbi.nlm.nih.gov/pubmed/10029595>.
- Davidson B, Holth A, Nguyen MTP, Tropé CG, Wu C. 2013. Migfilin,  $\alpha$ -parvin and  $\beta$ -parvin are differentially expressed in ovarian serous carcinoma effusions, primary tumors and solid metastases. *Gynecol Oncol*, 128(2):364–370 DOI: 10.1016/J.YGYNO.2012.10.015.
- Dickreuter E, Eke I, Krause M, Borgmann K, van Vugt MA, Cordes N. 2016. Targeting of  $\beta$ 1 integrins impairs DNA repair for radiosensitization of head and neck cancer cells. *Oncogene*, 35(11):1353–62 DOI: 10.1038/onc.2015.212.

- Eke I, Cordes N. 2011a. Dual targeting of EGFR and focal adhesion kinase in 3D grown HNSCC cell cultures. *Radiother Oncol*, 99(3):279–286 DOI: 10.1016/j.radonc.2011.06.006.
- Eke I, Cordes N. 2015. Focal adhesion signaling and therapy resistance in cancer. *Semin Cancer Biol*, 31:65–75 DOI: 10.1016/j.semcancer.2014.07.009.
- Eke I, Cordes N. 2011b. Radiobiology goes 3D: How ECM and cell morphology impact on cell survival after irradiation. *Radiother Oncol*, 99(3):271–278 DOI: 10.1016/j.radonc.2011.06.007.
- Eke I, Deuse Y, Hehlhans S, Gurtner K, Krause M, Baumann M, Shevchenko A, Sandfort V, Cordes N. 2012.  $\beta$  1 Integrin/FAK/cortactin signaling is essential for human head and neck cancer resistance to radiotherapy. *J Clin Invest*, 122(4):1529–1540 DOI: 10.1172/JCI61350.
- Eke Iris, Koch U, Hehlhans S, Sandfort V, Stanchi F, Zips D, Baumann M, Shevchenko A, Pilarsky C, Haase M, Baretton GB, Calleja V, Larijani B, Fässler R, Cordes N. 2010. PINCH1 regulates Akt1 activation and enhances radioresistance by inhibiting PP1alpha. *J Clin Invest*, 120(7):2516–27 DOI: 10.1172/JCI41078.
- Eke I, Leonhardt F, Storch K, Hehlhans S, Cordes N. 2009. The small molecule inhibitor QLT0267 radiosensitizes squamous cell carcinoma cells of the head and neck. *PLoS One*, 4(7) DOI: 10.1371/journal.pone.0006434.
- Eke I, Schneider L, Förster C, Zips D, Kunz-Schughart LA, Cordes N. 2013. EGFR/JIP-4/JNK2 signaling attenuates cetuximab-mediated radiosensitization of squamous cell carcinoma cells. *Cancer Res*, 73(1):297–306 DOI: 10.1158/0008-5472.CAN-12-2021.
- Eke I, Storch K, Krause M, Cordes N. 2013. Cetuximab attenuates its cytotoxic and radiosensitizing potential by inducing fibronectin biosynthesis. *Cancer Res*, 73(19):5869–79 DOI: 10.1158/0008-5472.CAN-13-0344.
- Eke I, Zscheppang K, Dickreuter E, Hickmann L, Mazzeo E, Unger K, Krause M, Cordes N. 2015. Simultaneous  $\beta$ 1 integrin-EGFR targeting and radiosensitization of human head and neck cancer. *J Natl Cancer Inst*, 107(2):1–11 DOI: 10.1093/jnci/dju419.
- Elbashir SM, Harborth J, Lendeckel W, Yalcin A, Weber K, Tuschl T. 2001. Duplexes of 21  $\pm$  nucleotide RNAs mediate RNA interference in cultured mammalian cells. *Nature*, 411(6836):494–498 DOI: 10.1038/35078107.
- ENCODE Project Consortium TEP. 2012. An integrated encyclopedia of DNA elements in



- the human genome. *Nature*, 489(7414):57–74 DOI: 10.1038/nature11247.
- Ferlay J, Soerjomataram I, Dikshit R, Eser S, Mathers C, Rebelo M, Parkin DM, Forman D, Bray F. 2015. Cancer incidence and mortality worldwide: Sources, methods and major patterns in GLOBOCAN 2012. *Int J Cancer*, 136(5):E359–E386 DOI: 10.1002/ijc.29210.
- Fletcher DA, Dyche Mullins R. Cell mechanics and the cytoskeleton REVIEW INSIGHT. DOI: 10.1038/nature08908.
- Frantz C, Stewart KM, Weaver VM. 2010. The extracellular matrix at a glance. *J Cell Sci*, 123(123):4195–4200 DOI: 10.1242/jcs.023820.
- Fukumoto Y, Morii M, Miura T, Kubota S, Ishibashi K, Honda T, Okamoto A, Yamaguchi Noritaka, Iwama A, Nakayama Y, Yamaguchi Naoto. 2014. Src Family Kinases Promote Silencing of ATR-Chk1 Signaling in Termination of DNA Damage Checkpoint \*. DOI: 10.1074/jbc.M113.533752.
- Gahmberg CG, Fagerholm SC, Nurmi SM, Chavakis T, Marchesan S, Grönholm M. 2009. Regulation of integrin activity and signalling. *Biochim Biophys Acta - Gen Subj*, 1790(6):431–444 DOI: 10.1016/J.BBAGEN.2009.03.007.
- Galluzzi L, Vitale I, Abrams JM, Alnemri ES, Baehrecke EH, Blagosklonny M V, Dawson TM, Dawson VL, El-Deiry WS, Fulda S, Gottlieb E, Green DR, Hengartner MO, Kepp O, Knight RA, Kumar S, Lipton SA, Lu X, Madeo F, Malorni W, Mehlen P, Nuñez G, Peter ME, Piacentini M, Rubinsztein DC, Shi Y, Simon H-U, Vandenabeele P, White E, Yuan J, Zhivotovsky B, Melino G, Kroemer G. 2012. Molecular definitions of cell death subroutines: recommendations of the Nomenclature Committee on Cell Death 2012. *Cell Death Differ*, 19(1):107–120 DOI: 10.1038/cdd.2011.96.
- Ganci F, Sacconi A, Manciooco V, Spriano G, Fontemaggi G, Carlini P, Blandino G. 2015. Radioresistance in Head and Neck Squamous Cell Carcinoma — Possible Molecular Markers for Local Recurrence and New Putative Therapeutic Strategies. *Contemp Issues Head Neck Cancer Manag*:3–34 DOI: 10.5772/60081.
- Ganguly KK, Pal S, Moulik S, Chatterjee A. 2013. Integrins and metastasis. *Cell Adh Migr*, 7(3):251–61 DOI: 10.4161/cam.23840.
- García-Pelagio KP, Buo AM, Chen L, Moorner M, Stains JP, Bloch RJ. 2019. The mechanical role of a cytoskeletal protein, Synemin, in bone, heart and skeletal muscle ARTICLES YOU MAY BE INTERESTED IN. , 2090:50008 DOI: 10.1063/1.5095923.
- García-Pelagio KP, Chen L, Joca HC, Ward C, Jonathan Lederer W, Bloch RJ. 2018.

- Absence of synemin in mice causes structural and functional abnormalities in heart. *J Mol Cell Cardiol*, 114:354–363 DOI: 10.1016/j.yjmcc.2017.12.005.
- Geisler F, Leube R. 2016. Epithelial Intermediate Filaments: Guardians against Microbial Infection? *Cells*, 5(3):29 DOI: 10.3390/cells5030029.
- Gharibi A, La Kim S, Molnar J, Brambilla D, Adamian Y, Hoover M, Hong J, Lin J, Wolfenden L, Kelber JA. 2017. ITGA1 is a pre-malignant biomarker that promotes therapy resistance and metastatic potential in pancreatic cancer. *Sci Rep*, 7(1):10060 DOI: 10.1038/s41598-017-09946-z.
- Giricz O, Calvo V, Pero SC, Krag DN, Sparano JA, Kenny PA. 2012. GRB7 is required for triple-negative breast cancer cell invasion and survival. *Breast Cancer Res Treat*, 133(2):607–615 DOI: 10.1007/s10549-011-1822-6.
- Glukhova MA, Streuli CH. 2013. How integrins control breast biology This review comes from a themed issue on Cell adhesion and migration. *Curr Opin Cell Biol*, 25:633–641 DOI: 10.1016/j.ceb.2013.06.010.
- Goodarzi AA, Jeggo PA. 2013. The Repair and Signaling Responses to DNA Double-Strand Breaks. *Adv Genet*, 82:1–45 DOI: 10.1016/B978-0-12-407676-1.00001-9.
- Greenlee RT, Hill-Harmon MB, Murray T, Thun M. 2001. Cancer Statistics, 2001. *CA Cancer J Clin*, 51(1):15–36 DOI: 10.3322/canjclin.51.1.15.
- Guérette D, Khan PA, Savard PE, Vincent M. 2007. Molecular evolution of type VI intermediate filament proteins. *BMC Evol Biol*, 7(1):164 DOI: 10.1186/1471-2148-7-164.
- Guo W, Giancotti FG. 2004. Integrin signalling during tumour progression. *Nat Rev Mol Cell Biol*, 5(10):816–826 DOI: 10.1038/nrm1490.
- Haddad RI, Shin DM. 2008. Recent Advances in Head and Neck Cancer. *N Engl J Med*, 359(11):1143–1154 DOI: 10.1056/NEJMra0707975.
- Hall EJ, Giaccia AJ. 2012. *Radiobiology for the Radiologist*. 7th ed. Mitchell CW (ed) Lippincott Williams & Wilkins, Philadelphia.
- Hanahan D, Weinberg RA. 2011. Hallmarks of cancer: The next generation. *Cell*, 144(5):646–674 DOI: 10.1016/j.cell.2011.02.013.
- Hantschel O, Superti-Furga G. 2004. Regulation of the c-Abl and Bcr–Abl Tyrosine Kinases. *Nat Rev Mol Cell Biol*, 5(1):33–44 DOI: 10.1038/nrm1280.
- Harari PM, Huang S-M. 2001. Head and neck cancer as a clinical model for molecular

- targeting of therapy: combining EGFR blockade with radiation. *Int J Radiat Oncol*, 49(2):427–433 DOI: 10.1016/S0360-3016(00)01488-7.
- He L, Wang X, Liu K, Wu X, Yang X, Song G, Zhang B, Zhong L. 2019. Integrative PDGF/PDGFR and focal adhesion pathways are downregulated in ERCC1-defective non-small cell lung cancer undergoing sodium glycididazole-sensitized cisplatin treatment. *Gene*, 691:70–76 DOI: 10.1016/j.gene.2018.12.028.
- Hehlgans S, Eke I, Cordes N. 2012. Targeting FAK radiosensitizes 3-dimensional grown human HNSCC cells through reduced Akt1 and MEK1/2 signaling. *Int J Radiat Oncol Biol Phys*, 83(5):e669-76 DOI: 10.1016/j.ijrobp.2012.01.065.
- Hehlgans S, Haase M, Cordes N. 2007. Signalling via integrins: Implications for cell survival and anticancer strategies. *Biochim Biophys Acta - Rev Cancer*, 1775(1):163–180 DOI: 10.1016/j.bbcan.2006.09.001.
- Helleday T, Bryant HE, Schultz N. 2005. Poly(ADP-ribose) Polymerase (PARP-1) in Homologous Recombination and as a Target for Cancer Therapy. *Cell Cycle*, 4(9):1176–1178 DOI: 10.4161/cc.4.9.2031.
- Herrmann H, Aebi U. 2016. Intermediate Filaments: Structure and Assembly. *Cold Spring Harb Perspect Biol*, 8(11):a018242 DOI: 10.1101/cshperspect.a018242.
- Hopfner K-P, Karcher A, Craig L, Woo TT, Carney JP, Tainer JA. 2001. Structural Biochemistry and Interaction Architecture of the DNA Double-Strand Break Repair Mre11 Nuclease and Rad50-ATPase. *Cell*, 105(4):473–485 DOI: 10.1016/S0092-8674(01)00335-X.
- Horton ER, Byron A, Askari Janet a., Ng DHJ, Millon-Frémillon A, Robertson J, Koper EJ, Paul NR, Warwood S, Knight D, Humphries JD, Humphries MJ. 2015. Definition of a consensus integrin adhesome and its dynamics during adhesion complex assembly and disassembly. *Nat Cell Biol*, 17(12):1577–1587 DOI: 10.1038/ncb3257.
- Horton ER, Byron A, Askari Janet A., Ng DHJ, Millon-Frémillon A, Robertson J, Koper EJ, Paul NR, Warwood S, Knight D, Humphries JD, Humphries MJ. 2015. Definition of a consensus integrin adhesome and its dynamics during adhesion complex assembly and disassembly. *Nat Cell Biol*, 17(12):1577–1587 DOI: 10.1038/ncb3257.
- Hoyt DG, Rizzo M, Gerritsen ME, Pitt BR, Lazo JS. 1997. Integrin activation protects pulmonary endothelial cells from the genotoxic effects of bleomycin. *Am J Physiol*, 273(3 Pt 1):L612-7 DOI: 10.1152/ajplung.1997.273.3.L612.

- Hynes RO. 2002. Integrins: Bidirectional, Allosteric Signaling Machines. *Cell*, 110(6):673–687 DOI: 10.1016/S0092-8674(02)00971-6.
- Iyama T, Wilson DM. 2013. DNA repair mechanisms in dividing and non-dividing cells. *DNA Repair (Amst)*, 12(8):620–636 DOI: 10.1016/J.DNAREP.2013.04.015.
- Jin S, Kharbanda S, Mayer B, Kufe D, Weaver DT, Ku BO. 1997. and c-Abl at the kinase homology region of DNA-dependent protein kinase catalytic subunit, *J. Biol Chem*, 272:24763–24766 DOI: 10.1074/jbc.272.40.24763.
- Jing R, Pizzolato G, Robson RM, Gabbiani G, Skalli O. 2005. Intermediate filament protein synemin is present in human reactive and malignant astrocytes and associates with ruffled membranes in astrocytoma cells. *Glia*, 50(2):107–120 DOI: 10.1002/glia.20158.
- Joiner M, van der Kogel AJ. 2009. *Basic clinical radiobiology*. 4th ed. Hodder Arnold, London, UK.
- Kalluri R. 2003. Basement membranes: structure, assembly and role in tumour angiogenesis. *Nat Rev Cancer*, 3(6):422–433 DOI: 10.1038/nrc1094.
- Kaminagakura E, Werneck da Cunha I, Soares FA, Nishimoto IN, Kowalski LP. 2011. CCND1 amplification and protein overexpression in oral squamous cell carcinoma of young patients. *Head Neck*, 33(10):1413–1419 DOI: 10.1002/hed.21618.
- Kass EM, Jasin M. 2010. Collaboration and competition between DNA double-strand break repair pathways. *FEBS Lett*, 584(17):3703–3708 DOI: 10.1016/j.febslet.2010.07.057.
- Khanamiryan L, Li Z, Paulin D, Xue Z. 2008. Self-Assembly Incompetence of Synemin Is Related to the Property of Its Head and Rod Domains †. *Biochemistry*, 47(36):9531–9539 DOI: 10.1021/bi800912w.
- Kharbanda S, Saleem A, Yuan Z-M, Kraeft S, Weichselbaum R, Chen LB, Kufe D. 1996. Nuclear Signaling Induced by Ionizing Radiation Involves Colocalization of the Activated p56/p53lyn Tyrosine Kinase with p34cdc21. [accessed: 04/30/2019] URL: <http://cancerres.aacrjournals.org/content/canres/56/16/3617.full.pdf>.
- Kim VN. 2005. Small RNAs: classification, biogenesis, and function. *Mol Cells*, 19(1):1–15 DOI: 806 [pii].
- Kinner A, Wu W, Staudt C, Iliakis G. 2008. -H2AX in recognition and signaling of DNA double-strand breaks in the context of chromatin. *Nucleic Acids Res*, 36(17):5678–5694 DOI: 10.1093/nar/gkn550.

- Koch CA, Agyei R, Galicia S, Metalnikov P, O'Donnell P, Starostine A, Weinfeld M, Durocher D. 2004. Xrcc4 physically links DNA end processing by polynucleotide kinase to DNA ligation by DNA ligase IV. *EMBO J*, 23(19):3874–3885 DOI: 10.1038/sj.emboj.7600375.
- Koch Institute R, Centre for Cancer Registry Data G. 2009. Cancer in Germany 2009/2010. [accessed: 04/27/2019] URL: [http://www.krebsdaten.de/Krebs/EN/Content/Publications/Cancer\\_in\\_Germany/cancer\\_chapters\\_2009\\_2010/cancer\\_c56.pdf?\\_\\_blob=publicationFile](http://www.krebsdaten.de/Krebs/EN/Content/Publications/Cancer_in_Germany/cancer_chapters_2009_2010/cancer_c56.pdf?__blob=publicationFile).
- van der Kogel A. 2009. Basic Clinical Radiobiology Fourth Edition. 4th ed. Joiner M, van der Kogel A (eds) CRC Press, London DOI: 10.1201/b13224.
- Konings AWT. 1987. Role of Membrane Lipid Composition in Radiation- Induced Death of Mammalian Cells. In: Prostaglandin and Lipid Metabolism in Radiation Injury. Springer US, Boston, MA, pp. 29–43 DOI: 10.1007/978-1-4684-5457-4\_2.
- Kopenhagen P, Dickreuter E, Cordes N. 2016. Head and neck cancer cell radiosensitization upon dual targeting of c-Abl and beta1-integrin. *Radiother Oncol*, 124(3):370–378 DOI: 10.1016/j.radonc.2017.05.011.
- Kotula E, Faigle W, Berthault N, Dingli F, Loew D, Sun JS, Dutreix M, Quanz M. 2013. DNA-PK target identification reveals novel links between DNA repair signaling and cytoskeletal regulation. *PLoS One*, 8(11) DOI: 10.1371/journal.pone.0080313.
- Krajewska M, Heijink AM, Bisselink YJWM, Seinstra RI, Silljé HHW, de Vries EGE, van Vugt MATM. 2013. Forced activation of Cdk1 via wee1 inhibition impairs homologous recombination. *Oncogene*, 32(24):3001–3008 DOI: 10.1038/onc.2012.296.
- Krejci L, Altmannova V, Spirek M, Zhao X. 2012. Homologous recombination and its regulation. *Nucleic Acids Res*, 40(13):5795–5818 DOI: 10.1093/nar/gks270.
- Ku BM, Koh J, Bae Y-H, Sun J-M, Lee S-H, Ahn JS, Park K, Ahn M-J. 2016. Abstract 2837: The CDK4/6 inhibitor has potent activity in combination with mTOR inhibitor in head and neck squamous cell carcinoma. *Cancer Res*, 76(14 Supplement):2837–2837 DOI: 10.1158/1538-7445.am2016-2837.
- Kumar S, Pandey P, Bharti A, Jin S, Weichselbaum R, Weaver D, Kufe D, Kharbanda S. 1998. Regulation of DNA-dependent protein kinase by the Lyn tyrosine kinase. *J Biol Chem*, 273(40):25654–8 DOI: 10.1074/JBC.273.40.25654.
- Kumta US, Tappel AL. 1961. Radiation Damage to Proteins. *Nature*, 191(4795):1304–1305 DOI: 10.1038/1911304a0.

- Kuriakose M, Sankaranarayanan M, Nair MK, Cherian T, Sugar AW, Scully C, Prime SS. 1992. Comparison of oral squamous cell carcinoma in younger and older patients in India. *Eur J Cancer B Oral Oncol*, 28B(2):113–20 [accessed: 04/28/2019] URL: <http://www.ncbi.nlm.nih.gov/pubmed/1306728>.
- Labat-Robert J. 2003. Age-dependent remodeling of connective tissue: role of fibronectin and laminin. *Pathol Biol*, 51(10):563–568 DOI: 10.1016/J.PATBIO.2003.09.006.
- Langer CJ. 2008. Targeted therapy in head and neck cancer. *Cancer*, 112(12):2635–2645 DOI: 10.1002/cncr.23521.
- Larsen M, Artym V V, Green JA, Yamada KM. 2006. The matrix reorganized: extracellular matrix remodeling and integrin signaling. *Curr Opin Cell Biol*, 18(5):463–471 DOI: 10.1016/J.CEB.2006.08.009.
- Lee H-J, Lan L, Peng G, Chang W-C, Hsu M-C, Wang Y-N, Cheng C-C, Wei L, Nakajima S, Chang S-S, Liao H-W, Chen C-H, Lavin M, Ang KK, Lin S-Y, Hung M-C. 2015. Tyrosine 370 phosphorylation of ATM positively regulates DNA damage response. *Cell Res*, 25(2):225–236 DOI: 10.1038/cr.2015.8.
- Lelièvre SA. 2009. Contributions of extracellular matrix signaling and tissue architecture to nuclear mechanisms and spatial organization of gene expression control. *Biochim Biophys Acta - Gen Subj*, 1790(9):925–935 DOI: 10.1016/J.BBAGEN.2009.03.013.
- Leube RE, Moch M, Windoffer R. 2015. Intermediate filaments and the regulation of focal adhesion. *Curr Opin Cell Biol*, 32:13–20 DOI: 10.1016/j.ceb.2014.09.011.
- Levy-Lahad E, Friedman E. 2007. Cancer risks among BRCA1 and BRCA2 mutation carriers. *Br J Cancer*, 96(1):11–15 DOI: 10.1038/sj.bjc.6603535.
- Lieber MR. 2010. The Mechanism of Double-Strand DNA Break Repair by the Nonhomologous DNA End-Joining Pathway. *Annu Rev Biochem*, 79(1):181–211 DOI: 10.1146/annurev.biochem.052308.093131.
- Liu Y-H, Cheng C-C, Lai Y-S, Chao W-T, Pei R-J, Hsu Y-H, Ho C-C. 2011. Synemin down-regulation in human hepatocellular carcinoma does not destabilize cytoskeletons in vivo. *Biochem Biophys Res Commun*, 404(1):488–93 DOI: 10.1016/j.bbrc.2010.12.008.
- Llewellyn C., Johnson N., Warnakulasuriya KAA. 2001. Risk factors for squamous cell carcinoma of the oral cavity in young people — a comprehensive literature review. *Oral Oncol*, 37(5):401–418 DOI: 10.1016/S1368-8375(00)00135-4.
- Löbrich M, Jeggo PA. 2005. Harmonising the response to DSBs: a new string in the ATM

- bow. DNA Repair (Amst), 4(7):749–759 DOI: 10.1016/J.DNAREP.2004.12.008.
- Löbrich M, Shibata A, Beucher A, Fisher A, Ensminger M, Goodarzi AA, Barton O, Jeggo PA. 2010.  $\gamma$ H2AX foci analysis for monitoring DNA double-strand break repair: Strengths, limitations and optimization. *Cell Cycle*, 9(4):662–669 DOI: 10.4161/cc.9.4.10764.
- Lowery J, Kuczmarski ER, Herrmann H, Goldman RD. 2015. Intermediate Filaments Play a Pivotal Role in Regulating Cell Architecture and Function. *J Biol Chem*, 290(28):17145–53 DOI: 10.1074/jbc.R115.640359.
- Luo B-H, Springer TA. 2006. Integrin structures and conformational signaling. *Curr Opin Cell Biol*, 18(5):579–586 DOI: 10.1016/J.CEB.2006.08.005.
- Mahajan K, Mahajan NP. 2015. Cross talk of tyrosine kinases with the DNA damage signaling pathways. *Nucleic Acids Res*, 43(22):10588–10601 DOI: 10.1093/nar/gkv1166.
- Mansour WY, Bogdanova N V., Kasten-Pisula U, Rieckmann T, Köcher S, Borgmann K, Baumann M, Krause M, Petersen C, Hu H, Gatti RA, Dikomey E, Dörk T, Dahm-Daphi J. 2013. Aberrant overexpression of miR-421 downregulates ATM and leads to a pronounced DSB repair defect and clinical hypersensitivity in SKX squamous cell carcinoma. *Radiother Oncol*, 106(1):147–154 DOI: 10.1016/j.radonc.2012.10.020.
- Marceau N, Schutte B, Gilbert S, Loranger A, Henfling MER, Broers JLV, Mathew J, Ramaekers FCS. 2007. Dual roles of intermediate filaments in apoptosis. *Exp Cell Res*, 313(10):2265–2281 DOI: 10.1016/j.yexcr.2007.03.038.
- Marelli UK, Rechenmacher F, Sobahi TRA, Mas-Moruno C, Kessler H. 2013. Tumor Targeting via Integrin Ligands. *Front Oncol*, 3:222 DOI: 10.3389/fonc.2013.00222.
- Miyamoto S, Teramoto H, Coso OA, Gutkind JS, Burbelo PD, Akiyama SK, Yamada KM. 1995. Integrin function: molecular hierarchies of cytoskeletal and signaling molecules. *J Cell Biol*, 131(3):791–805 DOI: 10.1083/JCB.131.3.791.
- Mladenov E, Magin S, Soni A, Iliakis G. 2016. DNA double-strand-break repair in higher eukaryotes and its role in genomic instability and cancer: Cell cycle and proliferation-dependent regulation. *Semin Cancer Biol*, 37–38:51–64 DOI: 10.1016/j.semcancer.2016.03.003.
- Moding EJ, Kastan MB, Kirsch DG. 2013. Strategies for optimizing the response of cancer and normal tissues to radiation. *Nat Rev Drug Discov*, 12(7):526–42 DOI: 10.1038/nrd4003.

- Mott JD, Werb Z. 2004. Regulation of matrix biology by matrix metalloproteinases. *Curr Opin Cell Biol*, 16(5):558–564 DOI: 10.1016/J.CEB.2004.07.010.
- Network TCGA. 2015. Comprehensive genomic characterization of head and neck squamous cell carcinomas. *Nature*, 517(7536):576–582 DOI: 10.1038/nature14129.
- Noetzel E, Rose M, Sevinc E, Hilgers R-D, Hartmann A, Naami A, Knüchel R, Dahl E. 2010. Intermediate filament dynamics and breast cancer: aberrant promoter methylation of the Synemin gene is associated with early tumor relapse. *Oncogene*, 29(34):4814–25 DOI: 10.1038/onc.2010.229.
- Ortega J, Li JY, Lee S, Tong D, Gu L, Li G-M. 2015. Phosphorylation of PCNA by EGFR inhibits mismatch repair and promotes misincorporation during DNA synthesis. *Proc Natl Acad Sci*, 112(18):5667–5672 DOI: 10.1073/pnas.1417711112.
- Oxvig C, Lu C, Springer TA. 1999. Conformational changes in tertiary structure near the ligand binding site of an integrin I domain. *Proc Natl Acad Sci U S A*, 96(5):2215–20 DOI: 10.1073/PNAS.96.5.2215.
- Pan Y, Jing R, Pitre A, Williams BJ, Skalli O. 2008. Intermediate filament protein synemin contributes to the migratory properties of astrocytoma cells by influencing the dynamics of the actin cytoskeleton. *FASEB J*, 22(9):3196–3206 DOI: 10.1096/fj.08-106187.
- Park CC, Zhang HJ, Yao ES, Park CJ, Bissell MJ. 2008. 1 Integrin Inhibition Dramatically Enhances Radiotherapy Efficacy in Human Breast Cancer Xenografts. *Cancer Res*, 68(11):4398–4405 DOI: 10.1158/0008-5472.CAN-07-6390.
- Parlakian A, Paulin D, Izmiryan A, Xue Z, Li Z. 2016. Intermediate filaments in peripheral nervous system: Their expression, dysfunction and diseases. *Rev Neurol (Paris)*, 172(10):607–613 DOI: 10.1016/j.neurol.2016.07.015.
- Paull TT, Gellert M. 1999. Nbs1 potentiates ATP-driven DNA unwinding and endonuclease cleavage by the Mre11/Rad50 complex. *Genes Dev*, 13(10):1276–88 [accessed: 04/28/2019] URL: <http://www.ncbi.nlm.nih.gov/pubmed/10346816>.
- Pauty J, Rodrigue A, Couturier A, Buisson R, Masson J-Y. 2014. Exploring the roles of PALB2 at the crossroads of DNA repair and cancer. *Biochem J*, 460(3):331–42 DOI: 10.1042/BJ20140208.
- Petersen OW, Rønnov-Jessen L, Howlett AR, Bissell MJ. 1992. Interaction with basement membrane serves to rapidly distinguish growth and differentiation pattern of normal and malignant human breast epithelial cells. *Proc Natl Acad Sci U S A*, 89(19):9064–8 DOI:



10.1073/PNAS.89.19.9064.

- Pickup MW, Mouw JK, Weaver VM. 2014. The extracellular matrix modulates the hallmarks of cancer. *EMBO Rep*, 15(12):1243–1253 DOI: 10.15252/embr.201439246.
- Pierce AJ, Johnson RD, Thompson LH, Jasin M. 1999. XRCC3 promotes homology-directed repair of DNA damage in mammalian cells. *Science*, 286(5401):2633–2638.
- Pitre A, Davis N, Paul M, Orr AW, Skalli O. 2012. Synemin promotes AKT-dependent glioblastoma cell proliferation by antagonizing PP2A. *Mol Biol Cell*, 23(7):1243–1253 DOI: 10.1091/mbc.E11-08-0685.
- Plattner R, Kadlec L, Demali KA, Kazlauskas A, Pendergast AM. 1999. c-Abl is activated by growth factors and Src family kinases and has a role in the cellular response to PDGF. *J Biol Chem*, 274(18):12400–12411 DOI: 10.1074/jbc.274.18.12400.
- Pollard JM, Gatti RA. 2009. Clinical Radiation Sensitivity With DNA Repair Disorders: An Overview. *Int J Radiat Oncol Biol Phys*, 74(5):1323–1331 DOI: 10.1016/j.ijrobp.2009.02.057.
- Puck TT, Marcus PI. 1956. Action of x-rays on mammalian cells. *J Exp Med*, 103(5):653–66.
- Quick Q, Paul M, Skalli O. 2015. Roles and Potential Clinical Applications of Intermediate Filament Proteins in Brain Tumors. *Semin Pediatr Neurol*, 22(1):40–48 DOI: 10.1016/j.spen.2014.12.005.
- Ramsey B, Bai T, Hanlon Newell A, Troxell M, Park B, Olson S, Keenan E, Luoh S-W. 2011. GRB7 protein over-expression and clinical outcome in breast cancer. *Breast Cancer Res Treat*, 127(3):659–669 DOI: 10.1007/s10549-010-1010-0.
- Rathmell WK, Chu G. 1994. Involvement of the Ku autoantigen in the cellular response to DNA double-strand breaks. *Proc Natl Acad Sci U S A*, 91(16):7623–7 DOI: 10.1073/PNAS.91.16.7623.
- Ray Chaudhuri A, Nussenzweig A. 2017. The multifaceted roles of PARP1 in DNA repair and chromatin remodelling. *Nat Rev Mol Cell Biol*, 18(10):610–621 DOI: 10.1038/nrm.2017.53.
- Ren R. 2005. Mechanisms of BCR–ABL in the pathogenesis of chronic myelogenous leukaemia. *Nat Rev Cancer*, 5(3):172–183 DOI: 10.1038/nrc1567.
- Roos WP, Kaina B. 2013. DNA damage-induced cell death: From specific DNA lesions to the

- DNA damage response and apoptosis. *Cancer Lett*, 332(2):237–248 DOI: 10.1016/j.canlet.2012.01.007.
- Roskelley CD, Desprez PY, Bissell MJ. 1994. Extracellular matrix-dependent tissue-specific gene expression in mammary epithelial cells requires both physical and biochemical signal transduction. *Proc Natl Acad Sci U S A*, 91(26):12378–82 DOI: 10.1073/PNAS.91.26.12378.
- Rossow L, Eke I, Dickreuter E, Cordes N. 2015. Targeting of the EGFR/ $\beta$ 1 integrin connecting proteins PINCH1 and Nck2 radiosensitizes three-dimensional SCC cell cultures. *Oncol Rep*.
- Ruiz C, Holz DR, Oeggerli M, Schneider S, Gonzales IM, Kiefer JM, Zellweger T, Bachmann A, Koivisto PA, Helin HJ, Mousses S, Barrett MT, Azorsa DO, Bubendorf L. 2011. Amplification and overexpression of vinculin are associated with increased tumour cell proliferation and progression in advanced prostate cancer. *J Pathol*, 223(4):543–552 DOI: 10.1002/path.2828.
- Russell MA, Lund LM, Haber R, McKeegan K, Cianciola N, Bond M. 2006. The intermediate filament protein, synemin, is an AKAP in the heart. *Arch Biochem Biophys*, 456(2):204–215 DOI: 10.1016/j.abb.2006.06.010.
- Sampietro D, Sámano-Sánchez H, Davey NE, Sharan M, Mészáros B, Gibson TJ, Kumar M. 2018. Conserved SQ and QS motifs in bacterial effectors suggest pathogen interplay with the ATM kinase family during infection. *bioRxiv*:364117 DOI: 10.1101/364117.
- Santuray RT, Johnson DE, Grandis JR. 2018. New Therapies in Head and Neck Cancer. *Trends in cancer*, 4(5):385–396 DOI: 10.1016/j.trecan.2018.03.006.
- Sartori AA, Lukas C, Coates J, Mistrik M, Fu S, Bartek J, Baer R, Lukas J, Jackson SP. 2007. Human CtIP promotes DNA end resection. *Nature*, 450(7169):509–514 DOI: 10.1038/nature06337.
- Savitsky K, Bar-Shira A, Gilad S, Rotman G, Ziv Y, Vanagaite L, Tagle DA, Smith S, Uziel T, Sfez S, Ashkenazi M, Pecker I, Frydman M, Harnik R, Patanjali SR, Simmons A, Clines GA, Sartiel A, Gatti RA, Chessa L, Sanal O, Lavin MF, Jaspers NG, Taylor AM, Arlett CF, Miki T, Weissman SM, Lovett M, Collins FS, Shiloh Y. 1995. A single ataxia telangiectasia gene with a product similar to PI-3 kinase. *Science*, 268(5218):1749–53 [accessed: 04/28/2019] URL: <http://www.ncbi.nlm.nih.gov/pubmed/7792600>.
- Schindelin J, Arganda-Carreras I, Frise E, Kaynig V, Longair M, Pietzsch T, Preibisch S, Rueden C, Saalfeld S, Schmid B, Tinevez J-Y, White DJ, Hartenstein V, Eliceiri K,

- Tomancak P, Cardona A. 2012. Fiji: an open-source platform for biological-image analysis. *Nat Methods*, 9(7):676–82 DOI: 10.1038/nmeth.2019.
- Schmidt LB, Tjioe KC, Assao A, Oliveira DT. 2015. Oral Squamous Cell Carcinoma in Young Population — Risk Factors, Clinical Presentation, and Prognosis. *Contemp Issues Head Neck Cancer Manag* DOI: 10.5772/60712.
- Schulte-Frohlinde D, Bothe E. 1991. The Development of Chemical Damage of DNA in Aqueous Solution. In: *The Early Effects of Radiation on DNA*. Springer Berlin Heidelberg, Berlin, Heidelberg, pp. 317–332 DOI: 10.1007/978-3-642-75148-6\_34.
- Seguin L, Desgrosellier JS, Weis SM, Cheresch DA. 2015. Integrins and cancer: Regulators of cancer stemness, metastasis, and drug resistance. *Trends Cell Biol*, 25(4):234–240 DOI: 10.1016/j.tcb.2014.12.006.
- Shattil SJ, Kim C, Ginsberg MH. 2010. The final steps of integrin activation: the end game. *Nat Rev Mol Cell Biol*, 11(4):288–300 DOI: 10.1038/nrm2871.
- Shaul Y, Ben-Yehoyada M. 2005. Role of c-Abl in the DNA damage stress response. *Cell Res*, 15(1):33–35 DOI: 10.1038/sj.cr.7290261.
- Skalli O, Wilhelmsson U, Örndahl C, Fekete B, Malmgren K, Rydenhag B, Pekny M. 2013. Astrocytoma grade IV (glioblastoma multiforme) displays 3 subtypes with unique expression profiles of intermediate filament proteins. *Hum Pathol*, 44(10):2081–2088 DOI: 10.1016/j.humpath.2013.03.013.
- Srinivasan D, Plattner R. 2006. Activation of Abl tyrosine kinases promotes invasion of aggressive breast cancer cells. *Cancer Res*, 66(11):5648–5655 DOI: 10.1158/0008-5472.CAN-06-0734.
- Storch K, Eke I, Borgmann K, Krause M, Richter C, Becker K, Schröck E, Cordes N. 2010. Three-dimensional cell growth confers radioresistance by chromatin density modification. *Cancer Res*, 70(10):3925–34 DOI: 10.1158/0008-5472.CAN-09-3848.
- Sun N, Huiatt TW, Paulin D, Li Z, Robson RM. 2010. Synemin interacts with the LIM domain protein zyxin and is essential for cell adhesion and migration. *Exp Cell Res*, 316(3):491–505 DOI: 10.1016/j.yexcr.2009.10.015.
- Takagi J. 2004. Structural basis for ligand recognition by RGD (Arg-Gly-Asp)-dependent integrins. *Biochem Soc Trans*, 32(Pt3):403–6 DOI: 10.1042/BST0320403.
- Tang J, Wang JY, Parker LL. 2012. Detection of early Abl kinase activation after ionizing radiation by using a peptide biosensor. *Chembiochem*, 13(5):665–73 DOI:

10.1002/cbic.201100763.

Tang K-J, Constanzo JD, Venkateswaran N, Melegari M, Ilcheva M, Morales JC, Skoulidis F, Heymach J V., Boothman DA, Scaglioni PP. 2016. Focal Adhesion Kinase Regulates the DNA Damage Response and Its Inhibition Radiosensitizes Mutant KRAS Lung Cancer. *Clin Cancer Res*, 22(23):5851–5863 DOI: 10.1158/1078-0432.CCR-15-2603.

Teng K, Zhang Y, Hu X, Ding Y, Gong R, Liu L. 2015. Nimotuzumab enhances radiation sensitivity of NSCLC H292 cells in vitro by blocking epidermal growth factor receptor nuclear translocation and inhibiting radiation-induced DNA damage repair. *Onco Targets Ther*, 8:809 DOI: 10.2147/OTT.S77283.

Toivola DM, Strnad P, Habtezion A, Omary MB. 2010. Intermediate filaments take the heat as stress proteins. *Trends Cell Biol*, 20(2):79–91 DOI: 10.1016/j.tcb.2009.11.004.

Toner M, O'Regan EM. 2009. Head and neck squamous cell carcinoma in the young: a spectrum or a distinct group? Part 1. *Head Neck Pathol*, 3(3):246–8 DOI: 10.1007/s12105-009-0135-0.

Tubbs A, Nussenzweig A. 2017. Endogenous DNA Damage as a Source of Genomic Instability in Cancer. *Cell*, 168(4):644–656 DOI: 10.1016/j.cell.2017.01.002.

Tutt ANJ, Lord CJ, McCabe N, Farmer H, Turner N, Martin NM, Jackson SP, Smith GCM, Ashworth A. 2005. Exploiting the DNA repair defect in BRCA mutant cells in the design of new therapeutic strategies for cancer. *Cold Spring Harb Symp Quant Biol*, 70:139–48 DOI: 10.1101/sqb.2005.70.012.

Uziel T, Lerenthal Y, Moyal L, Andegeko Y, Mittelman L, Shiloh Y. 2003. Requirement of the MRN complex for ATM activation by DNA damage. *EMBO J*, 22(20):5612–5621 DOI: 10.1093/emboj/cdg541.

Vehlow A, Cordes N. 2013. Invasion as target for therapy of glioblastoma multiforme. *Biochim Biophys Acta*, 1836(2):236–44 DOI: 10.1016/j.bbcan.2013.07.001.

WANG Y, KURAMITSU Y, UENO T, SUZUKI N, YOSHINO S, IIZUKA N, ZHANG X, AKADA J, OKA M, NAKAMURA K. 2012. Proteomic differential display identifies upregulated vinculin as a possible biomarker of pancreatic cancer. *Oncol Rep*, 28(5):1845–1850 DOI: 10.3892/or.2012.2004.

WERB Z, CHIN JR. 1998. Extracellular Matrix Remodeling during Morphogenesis. *Ann N Y Acad Sci*, 857(1 MORPHOGENESIS):110–118 DOI: 10.1111/j.1749-6632.1998.tb10111.x.

- Willers H, Dahm-Daphi J, Powell SN. 2004. Repair of radiation damage to DNA. *Br J Cancer*, 90(7):1297–1301 DOI: 10.1038/sj.bjc.6601729.
- Williams GJ, Lees-Miller SP, Tainer JA. 2010. Mre11–Rad50–Nbs1 conformations and the control of sensing, signaling, and effector responses at DNA double-strand breaks. *DNA Repair (Amst)*, 9(12):1299–1306 DOI: 10.1016/J.DNAREP.2010.10.001.
- Williams KE, Bundred NJ, Landberg G, Clarke RB, Farnie G. 2015. Focal Adhesion Kinase and Wnt Signaling Regulate Human Ductal Carcinoma In Situ Stem Cell Activity and Response to Radiotherapy. *Stem Cells*, 33(2):327–341 DOI: 10.1002/stem.1843.
- Xue Y, Ren J, Gao X, Jin C, Wen L, Yao X. 2008. GPS 2.0, a Tool to Predict Kinase-specific Phosphorylation Sites in Hierarchy. *Mol Cell Proteomics*, 7(9):1598–1608 DOI: 10.1074/mcp.M700574-MCP200.
- Yamada KM, Cukierman E. 2007. Modeling Tissue Morphogenesis and Cancer in 3D. *Cell*, 130(4):601–610 DOI: 10.1016/J.CELL.2007.08.006.
- Yamada KM, Miyamoto S. 1995. Integrin transmembrane signaling and cytoskeletal control. *Curr Opin Cell Biol*, 7(5):681–689 DOI: 10.1016/0955-0674(95)80110-3.
- Yoshida K, Miki Y, Kufe D. 2002. Activation of SAPK/JNK Signaling by Protein Kinase C $\delta$  in Response to DNA Damage. *J Biol Chem*, 277(50):48372–48378 DOI: 10.1074/JBC.M205485200.
- Yoshida K, Yamaguchi T, Natsume T, Kufe D, Miki Y. 2005. JNK phosphorylation of 14-3-3 proteins regulates nuclear targeting of c-Abl in the apoptotic response to DNA damage. *Nat Cell Biol*, 7(3):278–285 DOI: 10.1038/ncb1228.
- Zhao H-B, Zhang X-F, Jia X-L, Wang H-B. 2017. Grb7 is over-expressed in cervical cancer and facilitate invasion and inhibit apoptosis in cervical cancer cells. *Pathol - Res Pract*, 213(9):1180–1184 DOI: 10.1016/J.PRP.2017.05.013.
- Ziebarth AJ, Newshean S, Steg AD, Shah MM, Katre AA, Dobbin ZC, Han H-D, Lopez-Berestein G, Sood AK, Conner M, Yang ES, Landen CN. 2013. Endoglin (CD105) Contributes to Platinum Resistance and Is A Target for Tumor-Specific Therapy in Epithelial Ovarian Cancer. *Clin Cancer Res*, 19(1):170–182 DOI: 10.1158/1078-0432.CCR-12-1045.
- Zienert E, Eke I, Aust D, Cordes N. 2015. LIM-only protein FHL2 critically determines survival and radioresistance of pancreatic cancer cells. *Cancer Lett*, 364(1) DOI: 10.1016/j.canlet.2015.04.019.

Zschenker O, Streichert T, Hehlhans S, Cordes N. 2012. Genome-Wide Gene Expression Analysis in Cancer Cells Reveals 3D Growth to Affect ECM and Processes Associated with Cell Adhesion but Not DNA Repair. In: Borgmann K (ed) PLoS One, 7(4):e34279 DOI: 10.1371/journal.pone.0034279.

Zscheppang K, Kurth I, Wachtel N, Dubrovskaja A, Kunz-Schughart LA, Cordes N. 2016. Efficacy of beta1 integrin and EGFR targeting in sphere-forming human head and neck cancer cells. J Cancer, 7(6):736–745 DOI: 10.7150/jca.14232.

## 12 Acknowledgements

I would like to express my appreciation and thanks to my advisor Prof. Dr. Nils Cordes, you have been an exceptional mentor for me. I would like to thank you for giving me the opportunity to develop my own project, for the continuous support, for motivating me and also for your patience.

I would also like to thank Prof. Dr. Georg Breier for his interest in my thesis and his willingness to serve as my committee member.

Very special thanks to Dr. Anne Vehlow, Dr. Sarah Föster and Dr. Ellen Dickreuter for encouraging my research, for your brilliant comments and suggestions. I always enjoyed working with you all.

I would especially like to thank my old and new labmates of the MCR group for the support, the discussions and all the fun we have had in the last four years. It was awesome to work with you all.

Most importantly, none of this could have happened without the support of my family and my life partner. Words cannot express how much I am grateful to my mum and dad for all of the support they gave me all those years, making me the strong person I am today. Next I would like to give a very special thanks to my beloved Treewut who was always my support and help me so much through this whole process. Of course I have to mention our little good boy, Zumo, the black lab lab, which distracted me from work and kept me in shape! Mum, dad, Tree and Zumo, I love you so much! You are the most important piece of my life!

## Curriculum vitae

### Personal information:

Name: Sara Sofia Deville  
Address: Handelallee n. 7  
01309 Dresden  
Birth: 12. April 1991 in Santa Fe (Arg)

### Studies:

2015-today Promotion at the Medizinischen Fakultät der Technischen Universität Dresden  
Doctoral thesis „The intermediate filament synemin regulates non-homologous end joining in an ATM-dependent manner“ at OncoRay – National Center for Radiation Research in Oncology, Molecular and Cellular Radiobiology, Technische Universität Dresden, Dresden  
2013-2015 Master studies at Politecnico di Milano  
2010- 2013 Bachelor studies at Politecnico di Milano  
2005-2010 Liceo linguistico Salvatore Quasimodo, Magenta, Milano, Italy  
2008-2009 Perry high school, Canton, Ohio, USA.

### Publications:

2019 “The intermediate filament Synemin promotes non-homologous end joining in an ATM-dependent manner”, *Submitted* in Cancer Research, CAN-19-1588.  
2019 “Conference report: From Radiation to Innovation in Medicine – The International Marie Sklodowska-Curie Meeting”, “*in revision*” in Radiotherapy & Oncology, CTRO\_2019\_49.



**Poster presentations and talks:**

27/02-01/03/2019 **20th International AEK Cancer Congress**

Heidelberg, Germany.

- Flash talk and poster presentation “Synemin promotes non-homologous end joining through the regulation of c-Abl and DNA-PKcs kinases in head and neck squamous cell carcinomas”.

4-5/02/2019 **1st German Cancer Research Congress (GCRC)**

Heidelberg, Germany.

- Poster presentation “Synemin promotes DNA repair through the regulation of c-Abl and DNA-PKcs kinases in an ATM dependent manner in head and neck cancers”.

12/10/2018 **International Marie Sklodowska-Curie Meeting: From Radiation to Innovation in Medicine**

Institute Curie, Paris, France.

- Poster presentation “Synemin, a novel regulator of DNA repair machinery and tyrosine kinases in head and neck cancers”

30/06-03/07/2018 **25<sup>th</sup> Biennial Congress of the European Association for Cancer Research**

Amsterdam, Netherlands.

- Poster presentation “Synemin is a novel co-regulator of non-homologous end joining in head and neck cancer cells”

23-25/05/2018 **7<sup>th</sup> French Cell Adhesion Club Symposium**

Institut de Science et d'Ingénierie Supramoléculaires, University of Strasbourg, Strasbourg, France.

- Poster presentation “The intermediate filament Synemin is key for DNA double strand break repair”

15-17/03/2018 **National Center for Radiation Research in Oncology (NCRO) Retreat**

Technische Universität Dresden, Faculty of Medicine, Dresden, Germany.

- Poster presentation “Synemin is a novel co-regulator of the non-homologous end joining pathway in head and neck cancer cells”

17-21/09/2017 **Joint 43rd ERRS and 20th GBS Conference**

Institute of Medical Radiation Biology and Institute of Cell Biology, Essen, Germany

- Poster presentation “Synemin is a novel co-regulator of the radiation-induced DNA damage response in head and neck cancer cells”

- 18-20/05/2016    **Workshop: Biomarkers for Radiation Oncology**  
Technische Universität Dresden, Faculty of Medicine, Dresden, Germany.
- Poster presentation “The role of focal adhesion proteins in DNA damage repair in head and neck cancer cells”
- 14-16/04/2016    **National Center for Radiation Research in Oncology (NCRO) Retreat**  
OncoRay, Faculty of Medicine, Technische Universität Dresden, Dresden, Germany.

---

# Anlage 1

**Technische Universität Dresden**

**Medizinische Fakultät Carl Gustav Carus**

**Promotionsordnung vom 24. Juli 2011**

## **Erklärungen zur Eröffnung des Promotionsverfahrens**

1. Hiermit versichere ich, dass ich die vorliegende Arbeit ohne unzulässige Hilfe Dritter und ohne Benutzung anderer als der angegebenen Hilfsmittel angefertigt habe; die aus fremden Quellen direkt oder indirekt übernommenen Gedanken sind als solche kenntlich gemacht.

2. Bei der Auswahl und Auswertung des Materials sowie bei der Herstellung des Manuskripts habe ich Unterstützungsleistungen von folgenden Personen erhalten:

Herr Prof. Dr. med. Nils Cordes, Frau Dr. phil. Anne Vehlow, Frau Dr. rer. nat. Ellen Dickreuter, Frau Dr. rer. nat. Sarah Förster and Frau Inga Lange

3. Weitere Personen waren an der geistigen Herstellung der vorliegenden Arbeit nicht beteiligt. Insbesondere habe ich nicht die Hilfe eines kommerziellen Promotionsberaters in Anspruch genommen. Dritte haben von mir weder unmittelbar noch mittelbar geldwerte Leistungen für Arbeiten erhalten, die im Zusammenhang mit dem Inhalt der vorgelegten Dissertation stehen.

4. Die Arbeit wurde bisher weder im Inland noch im Ausland in gleicher oder ähnlicher Form einer anderen Prüfungsbehörde vorgelegt.

5. Die Inhalte dieser Dissertation wurden in folgender Form veröffentlicht:

Deville S S, Vehlow A, Förster S, Dickreuter E, Borgmann K, Cordes N. The intermediate filament synemin regulates non-homologous end joining in an ATM-dependent manner. Unter Begutachtung bei Cancer Research.

6. Ich bestätige, dass es keine zurückliegenden erfolglosen Promotionsverfahren gab.

7. Ich bestätige, dass ich die Promotionsordnung der Medizinischen Fakultät der Technischen Universität Dresden anerkenne.

8. Ich habe die Zitierrichtlinien für Dissertationen an der Medizinischen Fakultät der Technischen Universität Dresden zur Kenntnis genommen und befolgt.

Dresden, den

---

## Anlage 2

**Hiermit bestätige ich die Einhaltung der folgenden aktuellen gesetzlichen Vorgaben im Rahmen meiner Dissertation Erklärungen zur Eröffnung des Promotionsverfahrens**

1. die Einhaltung des Gentechnikgesetzes

Alle gentechnischen Arbeiten wurden in den gentechnischen Anlagen der Sicherheitsstufe S1 mit den Aktenzeichen Az: 54-8451/248 beziehungsweise Az: 54-8451/243 durchgeführt.

2. die Einhaltung von Datenschutzbestimmungen der Medizinischen Fakultät und des Universitätsklinikums Carl Gustav Carus.

Dresden, den

## **Darstellung des Eigenanteils**

Hiermit versichere ich, Sara Sofia Deville, dass ich die vorliegende Dissertation ohne unzulässige Hilfe Dritter und ohne Benutzung anderer als der angegebenen Hilfsmittel selbstständig angefertigt habe. Die aus fremden Quellen direkt oder indirekt übernommenen Gedanken sind als solche kenntlich gemacht. Die Arbeit wurde bisher weder im Inland noch im Ausland in gleicher oder ähnlicher Form einer anderen Prüfungsbehörde vorgelegt. Die Arbeit wurde in der Gruppe „Molekulare und Zelluläre Strahlenbiologie“ am „OncoRay - Nationalen Zentrum für Strahlenforschung in der Onkologie“, Medizinische Fakultät Carl Gustav Carus, Technische Universität Dresden unter der wissenschaftlichen Leitung von Herrn Prof. Dr. Nils Cordes angefertigt. Die Promotionsordnung wird anerkannt.

Dresden, den 27<sup>th</sup> January 2020

Sara Sofia Deville